2013

Gold Oxide as a Masking Layer for Regioselective Surface Chemistry

Kevin M. Cook
Lehigh University

Gold Oxide as a Masking Layer for Regioselective Surface Chemistry

by

Kevin M. Cook

A Dissertation

Presented to the Graduate and Research Committee

of Lehigh University

in Candidacy for the Degree of

Doctor of Philosophy

in

Chemistry

Lehigh University

September 2, 2013

Approved and recommended for acceptance as a dissertation in partial fulfillment of the requirements for the degree of Doctor of Philosophy

Kevin M. Cook

Gold Oxide as a Masking Layer for Regioselective Surface Chemistry

_____

Defense Date

_____

Dr. Gregory S. Ferguson
Dissertation Director

_____

Approved Date

Committee Members:

_____

Dr. David T. Moore

_____

Dr. James E. Roberts

_____

Dr. Manoj K. Chaudhury

Copyright Permissions

The material contained in Chapters 2, 3, 4, and 5 has been published prior to submittal of this dissertation. The proper copyright permission was obtained from each journal before submittal of this document, with the publication cited at the beginning the chapter.

Acknowledgements

I am grateful to many people who supported me throughout my time pursuing my Ph.D. First and foremost, I would like to thank my advisor, Prof. Gregory Ferguson for his insight, advice, and patience throughout my graduate studies. It is difficult to express the impact his mentorship has had on me professionally and personally. During my time at Lehigh, I have grown as a scientist and professional and developed my leaderhip and teaching skills to a greater extent than I ever anticipated. Without Prof. Ferguson this dissertation would not have been possible, and I am truly endebted to him. I would like to thank my committee, Prof. Manoj Chaudhury, Prof. James Roberts, and Prof. David Moore for their help during this process, particularily, Prof. Roberts and Prof. Moore for helpful discussions over the years. Additionally, I would like to thank Lehigh University for its financial support during my time at the university.

My family and friends have been supportive and encouraging over the past five years. My fiancé, Sara, has been wonderful during this process, and true to her nature she has been especially supportive, taking care of the little things, watching our dogs, Selma and Walter, and allowing me the time and space I needed to work. My family has also been great, starting with my mother, Barbara, who always "lit a candle" for me. I would also like to thank my father, Brian Sr., and brothers, Victor, Brian Jr., and Daniel for their support. Finally, I would like to thank my friends Kevin Christy, Ed Sneizak, Ajay Wood, Chris Cummings, and Joe Malinowski, for allowing me to "nerd out" and putting up with the fact that I have lived in Pennsylvania for the past 5 years, even though their sole reward will be referring to me as Dr. Cook.

Table of Contents

List of Figures and Tables

Gold Oxide as a Masking Layer for Regioselective Surface Chemistry

Abstract

The work in this dissertation is focused on the development of methods for spatially controlling the adsorption of self-assembled monolayers (SAMs) on selected gold electrodes in an array. This research draws from synthetic organic and inorganic chemistry, electrochemistry, and surface science to provide a unique solution to the problem of directing the formation of SAMs, which are potentially useful in sensing and photovoltaic applications. To meet this need, we developed a facile electrochemical method that utilizes gold-oxide thin films as protecting layers to allow the selective placement of SAMs on specific gold electrodes. This approach is analogous to the ‘‘protection–deprotection’’ strategy used successfully by synthetic organic chemists for decades and is potentially applicable for a broad range of chemical functionality. The gold-oxide thin film can easily be added or removed, allowing convenient incorporation into the synthetic scheme. We used a combination of x-ray photoelectron spectroscopy (XPS), variable-angle spectroscopic ellipsometry (VASE) and contact-angle measurements to demonstrate that distinct monolayers can be formed on the neighboring electrodes and microelectrodes with no evidence of cross-contamination.

In order to characterize the thin oxide films used in this method, as well as to assess their lability in various chemical environments, we also developed a method for measuring their wavelength-dependent, complex refractive index (n + ik). We first measured the thickness of the thin film independently by angle-resolved XPS. Using that thickness value, we determined the values of n and k by VASE. Using this unique combination of XPS and VASE, we were able to obtain values for the complex refractive

index of an electrochemically formed thin film of gold oxide for wavelengths between 350 and 800 nm.

Exploratory studies involving silver (I)-thiolate polymers were conducted to examine their possible use as precursors to monolayer films and metallic nanoparticles. X-ray photoelectron spectroscopy (XPS) measurements suggested that these polymers adsorb onto gold surfaces from solution, but decomposition produced surfaces that were not the same as those formed by self-assembly of alkanethiols on gold bearing a submonolayer of underpotential-deposited silver. In separate studies, the silver(I)-thiolate polymers could be decomposed into nanoparticles by thermolysis or photolysis as confirmed by transmission electron microscopy (TEM) and UV/vis spectrophotometry.

Chapter 1

Formation and Characterization of Organosulfur Self-Assembled Monolayers (SAMs) on Gold and Use of Gold Oxide to Make the Formation Selective

1.1 Introduction

Since their discovery,[1-3] self-assembled monolayer (SAMs) films have been a major focus of research concentrated on the control of surface chemistry.[4] These films consist of a single oriented layer of molecules that spontaneously chemisorb to a solid surface from either the gas or solution phase. The formation of monolayer films is spontaneous due to the minimization of interfacial free energy of the substrate and stabilization within the films from van der Waals forces.[4-6] Adsorbates typically consist of a "head" group, which attaches to the substrate, a "spacer" chain and a terminal "tail" group (Figure 1.1). These adsorbates form uniform, ordered and stable monolayer films on a variety of substrates,[7-10] with a breadth of functional "head" groups specific to the particular substrate.[4,5]

Research in this area has focused not only on understanding self-assembly, but also on implementing this surface modification for use in devices.[4,5,11] Historically, the self-assembly of organosulfur (e.g., alkanethiol, dialkyl disulfide) compounds on metals such as gold has provided a convenient route for the control of surface properties that is easy to implement, adapt, and tailor.[4,5] After monolayer formation, the tail group is exposed at the surface of the monolayer, imparting its chemical properties, so control of the functionality of monolayer tail groups allows control of surface chemistry. Our

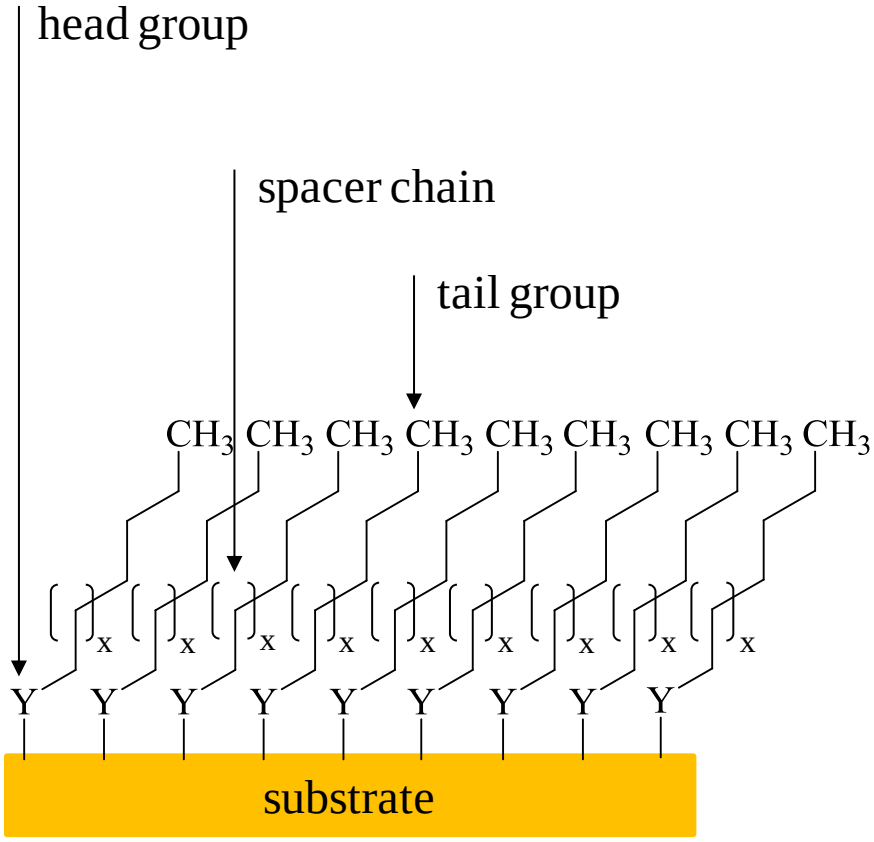

Figure 1.1. A schematic representation of a substrate surface bearing a SAM.

group has previously shown that surface chemistry can be controlled by the electrochemically directed formation of SAMs from alkyl thiosulfates. As discussed below, however, this chemistry is not compatible with all functional tail groups because of side-reactions that can occur.[12-14] The work described in this dissertation addressed this problem by using gold oxide as a masking layer to allow regioselective formation of SAMs from dialkyl disulfides. This chapter provides a review of topics relevant to the work that follows, including the formation and characterization of organosulfur SAMs formed from solution on gold, previous methods for regioselective formation of SAMs, and the chemistry of gold oxide.

1.2 Organosulfur SAMs on Gold

The molecules most commonly used as precursors for self-assembly on gold are alkanethiols and dialkyl disulfides, though others have been reported[4] and will not be discussed in this work. Both types of molecule give similar SAMs on gold, with thiolate sulfur covalently bound in three-fold hollow sites on the surface of the gold, and with alkyl chains tilting slightly relative to the surface normal (Figure 1.1).[6,10,15-18] The reaction pathways leading to SAMs from these molecules, however, are different. The formation of a SAM from an alkanethiol proceeds with the formal loss of a proton and an electron (equation 1.1),[4,6,19,20] whereas that from a dialkyl disulfide precursor involves

$$RSH + Au \rightarrow AuSR + H^+ + e^- \qquad (1.1)$$

oxidative addition of the disulfide bond (equation 1.2).[4,6,20,21]

$$RSSR + 2Au \rightarrow 2AuSR \qquad (1.2)$$

The process of assembly occurs in three stages: 1) adsorption of headgroups to the substrate, with adsorbed molecules orientied horizontally and forming "stripped phases" along the surface; 2) alignment of the chains; and 3) reorientation of terminal groups and relaxation of the layer into a crystalline state, wherein the adjacent chains are oriented as depicted in Figure 1.1.[22] At the end of the second stage, the layer is considered to be in an amorphous or glassy state with 80 – 90% of the surface sites occupied. [22] The final and longest stage requires 12 – 24 h for completion.

1.2.1 Conditions for the Spontaneous Formation of SAMs from Solution

As mentioned above and implied in Figure 1.1, a complete monolayer contains close-packed thiolate sulfur on the gold surface and alkyl chains tilted and aligned with one another. Although driven by the formation of strong covalent bonds and stabilized by the van der Waals interactions of adjacent chains, successful formation depends on experimental conditions. To create a high-quality SAM from the solution phase, important parameters include the precursor concentration, precursor chain length, the solvent, immersion time, and cleanliness of the substrate.

The concentration of the monolayer precursor must be sufficiently high, typically 1 – 10 mM, to enable the formation of a complete SAM.[4,18,21] The length of the alkyl chains has a profound effect on the ability of *n*-alkanethiols and *n*-dialkyl disulfides to form an ordered SAM on a substrate.[18,19,21] Longer alkyl chains provide greater van der Waals stabilization, resulting in higher quality and more thermodynamically stable films.[18,21,23] As a result, SAMs formed from longer chains of *n*-alkanethiols are more resistant to thermal desorption than those formed from short chains.[18,21] Monolayers

formed from thiols or disulfides with shorter (C_2 – C_9) chains are less ordered than those formed from longer (C_{10} – C_{18}) chains, as measured by grazing-angle IR, ellipsometric thickness, and contact angles.[18,19,21,24]

The choice of solvent influences the quality of SAMs because some solvent molecules (e.g., hexadecane) can intercalate into the SAM as it forms, preventing precursor molecules from reaching the substrate and completing the monolayer.[18,25] This complication can be avoided with solvents such as ethanol or THF, which cannot intercalate within the monolayer.[18,21] Depending on the solvent, the immersion time required for formation of a complete monolayer varies, but 12 – 24 h is typical.[18,21]

Although gold is inert towards chemisorption of oxygen and water, the surface of nominally clean gold substrates are still covered with a layer of physisorbed contaminants from the ambient atmosphere (e.g., water, organic materials).[18] Substrates typically have been cleaned by one of two related methods. The first is treatment with ultraviolet light in the presence of ozone (UV/O_3), which oxidizes the surface to form a layer of gold oxide.[26,27] Surface contamination is removed during oxidation or when the oxide is reduced in ethanol, providing a gold surface free of chemisorbed or strongly physisorbed material.[17,28-32] This method was examined by Rubinstein and coworkers, who used x-ray photoelectron spectroscopy (XPS) and ellipsometry to show that not only contamination could be cleaned from gold, but also that a previously formed SAM could be removed from a substrate surface.[30,31] The surface of gold becomes slightly roughened during this treatment, but is otherwise unaffected and available for monolayer formation.[31] The second cleaning method often used is electrochemical cycling of a gold electrode in a solution of 0.1 – 0.5-M H_2SO_4.[16,31,33] In this process, the electrode is repeatedly oxidized

and reduced in cycles until a clean gold surface is produced. Similar to treatment with UV/O_3, this process can remove surface contamination from a gold electrode, with or without a previously formed SAM. This method also can roughen the surface of the gold electrode, but again without affecting the quality of SAMs formed after treatment.[31]

1.2.2 Treatment of Gold and Gold Oxide with Alkanethiols and Dialkyl Disulfides

As noted above, monolayers from alkanethiols form by the spontaneous chemisorption of the thiol group on the gold surface (equation 1.1). This reaction allows variation of functional groups at the tail of the molecule.[8,34-36] Adsorption from mixtures of precursors allows the formation of mixed monolayers, giving an added degree of control over surface wetting properties.[7,18,35,37-39] Once formed, thiolate SAMs are also prone to exchange with thiols in solution.[18,35,37-39]

The spontaneous formation of SAMs on gold from dialkyl disulfides is very similar to that from alkanethiols: many of the same solvents are used, typical concentrations of precursors are the same, and the time of immersion required is only slightly longer.[1,7,21,40] The formation of SAMs from a disulfide does not proceed to as high a degree of completion as those from the corresponding thiol because as surface sites on the substrate are occupied by bound thiolate groups, the approach to the surface of the large disulfide molecules is sterically hindered.[21] As a result, methyl-terminated monolayers formed from disulfides have slightly lower contact angles than those formed from thiols, and exchange of disulfides with thiolate monolayers occurs at a very slow rate.[21] Monolayers form more readily from alkanethiols than from dialkyl disulfides, as evidenced by the preferential adsorption of thiols from mixed solutions containing both

types of molecule[7,18] Monolayers can be formed from symmetric (RSSR) or asymmetric (RSSR') disulfides, allowing for the incorporation of different molecules into a monolayer from a single precursor.[1,36,40,41] Similar to thiols, the formation of mixed monolayers from the coadsorption of different dialkyl disulfide molecules is also possible.[40,41]

As the formation of SAMs from alkanethiols is a redox process, the rate of formation of these monolayers can be accelerated *via* an applied oxidative potential.[20,42-48] This process allows the formation of a complete monolayer in minutes, rather than hours, as well as the *in situ* electrochemical monitoring of the assembly process.[20] Potential-assisted formation of SAMs from dialkyl disulfides has also been reported, though using reductive potentials.[20] Potential-assisted formation of complete SAMs from dialkyl disulfides can also be monitored electrochemically *in situ* and achieved in minutes.[20] The ability to activate selected electrodes and the decreased time required during potential-assisted SAM formation have helped to facilitate the inclusion of these monolayers in many advanced applications, such as senor arrays.[11,49]

The contrast in reactivity between alkanethiols and dialkyl disulfides with gold oxide is particularly important in this dissertation. When a gold-oxide surface is exposed to thiol, the oxide is reduced as a SAM forms (equation 1.3),[20,30,31,50-52] sometimes

$$Au_2O_3 + 6\,RSH \rightarrow 2\,AuSR + 2\,RSSR + 3\,H_2O \qquad (1.3)$$

encapsulating islands of the oxide underneath the monolayer in the process.[30] In contrast, gold oxide does not react with solutions of dialkyl disulfides.[1,20,31] This difference

presented an opportunity to use gold oxide as a masking layer for directed formation of SAMs from disulfides.

1.3 Characterization of SAMs

Early work on the characterization of SAMs confirmed the presence of these films and determined the orientation of the molecules on the substrate surface.[6,10,15-17,19] Since then, these materials have been extensively studied using a wide variety of techniques, including contact-angle goniometry,[9,18,21,23] ellipsometry,[18,20,21,23] grazing-angle IR,[15,23,24,53] x-ray diffraction (XRD),[17] high-energy electron loss spectroscopy (HREELS),[54] near edge x-ray absorption fine structure spectroscopy (NEXAFS)[55] x-ray photoelectron spectroscopy (XPS),[18,21,23,56,57] and scanning tunneling microscopy (STM).[58-62] Once the formation of SAMs was understood, some of the same methods of characterization could be employed in order to give a quick, reliable measure of the formation of SAMs, and their use in devices and technical applications could be easily monitored. The studies described in this dissertation utilized contact-angle goniometry, spectroscopic ellipsometry, and XPS to characterize SAMs, and this section provides background information for these three methods.

1.3.1 Contact-Angle Goniometry

The formation of a monolayer films provides a means for manipulating the composition, and thus interfacial free energy, of a surface. A fast and convenient measurement related to interfacial free energy is the contact angle, θ, of a static liquid droplet on the surface of a flat solid (Figure 1.2).[63] The balance of the forces at the

three-phase contact line determines the angle at which the drop meets the surface, according to Young's equation (1.4),[64] where the interfacial free energy between

$$\gamma_{lv} \cos\theta = \gamma_{sv} - \gamma_{sl} \quad (1.4)$$

the solid and liquid phases is denoted γ_{sl}, the interfacial free energy between the vapor and liquid phases (i.e., "surface tension") is denoted $\gamma_{lv,}$ and the interfacial free energy between the solid and vapor phases is denoted γ_{sv}. An advancing contact angle, θ_a is the angle that a drop makes after it has been advanced across the surface, and a receding contact angle, θ_r is the angle it makes after it has been receded across the surface.[63] The difference between these two measurements is referred to as the "contact-angle hysteresis," and can give a measure of the degree of order in a SAM.[63] Contact angles depend strongly on the type of end groups present on the SAM (e.g., methyl, hydroxyl). For instance, a SAM formed from a 1-mM solution of hexadecanethiol in ethanol has an advancing contact angle of hexadecane of 47° ± 2°,[18] whereas a SAM formed from a 1-mM solution of 18-nonadecene-1-thiol has an advancing contact angle of hexadecane of 39° ± 2°.[18]

1.3.2 Ellipsometry

Ellipsometry is an optical technique used to probe thin films and surfaces that relies on the interaction between polarized light and a material. Light may be polarized in a plane parallel to the plane of incidence ("p") or perpendicular to it ("s"). Reflection of a beam of polarized light from the surface of a material results in the loss of some of the light through transmittance, and a change in the polarization of all reflected light

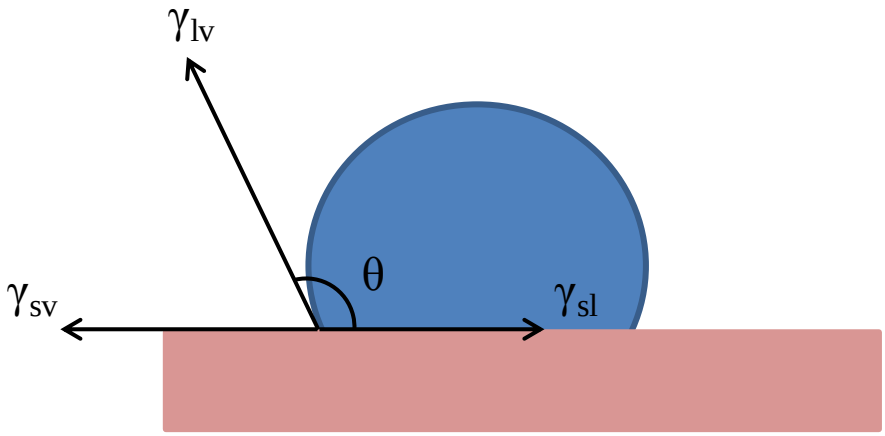

Figure 1.2. A diagram representing the balance of the forces at the three-phase contact line, where a liquid droplet meets a solid surface, that determines the contact angle.

(Figure 1.3). For a beam of light reflecting from the interface between a medium and the surface of a material, the ratio of the amplitude of the reflected wave to the amplitude of the incident wave is given by the Fresnel reflection coefficients in the p (r_p equation 1.5) and s (r_s equation 1.6) planes,[65] where the subscript

$$r_{12}^{p} = \frac{n_2\cos\theta_1 - n_1\cos\theta_2}{n_2\cos\theta_1 + n_1\cos\theta_2} \tag{1.5}$$

$$r_{12}^{s} = \frac{n_1\cos\theta_1 - n_2\cos\theta_2}{n_1\cos\theta_1 + n_2\cos\theta_2} \tag{1.6}$$

12 denotes the interface between medium 1 and medium 2, n_1 is the refractive index of medium 1, n_2 is the refractive index of medium 2, θ_1 is the angle of incidence, and θ_2 is the angle of the transmitted light. For samples with two interfaces, the total reflection coefficient can be derived from the ratio of the resultant total amplitude of the reflected wave to the amplitude of the incident wave, resulting in coefficients for the p (R^P equation 1.7) and s (R^S equation 1.8) planes,[65] where the subscript 23 denotes the

$$R^{p} = \frac{r_{12}^{p} + r_{23}^{p}\exp(-i2\beta)}{1 + r_{12}^{p} + r_{23}^{p}\exp(-i2\beta)} \tag{1.7}$$

$$R^{s} = \frac{r_{12}^{s} + r_{23}^{s}\exp(-i2\beta)}{1 + r_{12}^{s} + r_{23}^{s}\exp(-i2\beta)} \tag{1.8}$$

interface between medium 2 and medium 3, β is the film "phase thickness" (the change in the phase of the light due to the film) given by equation 1.9, and d is the film thickness.

$$\beta = 2\pi\left(\frac{d}{\lambda}\right) n_2\cos\theta_2 \tag{1.9}$$

The fundamental equation of ellipsometry (equation 1.10) defines the parameters, Ψ and

$$\frac{R_p}{R_s} = \tan(\Psi)\, e^{i\Delta} \tag{1.10}$$

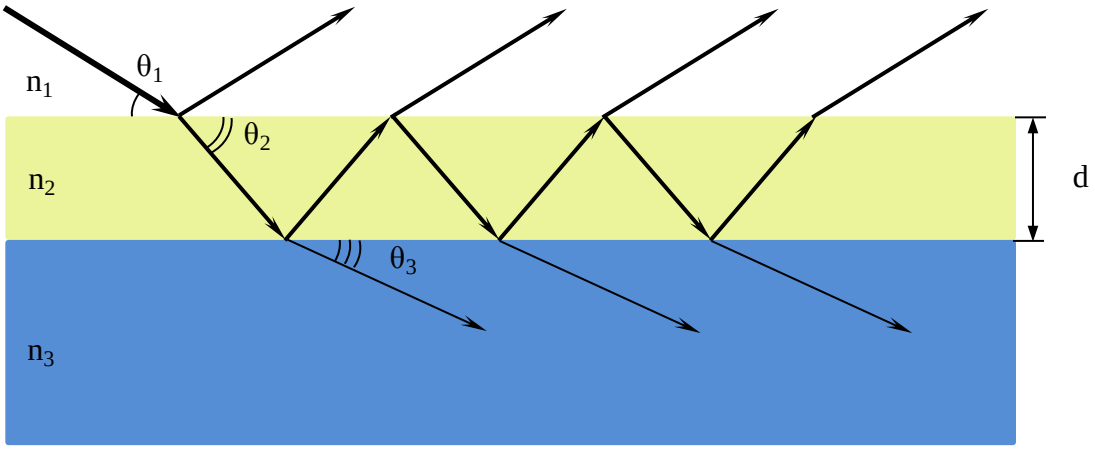

Figure 1.3. The interaction of light with a thin film (component 2) of thickness d on a substrate (component 3).

Δ, which are measured experimentally. The parameter Ψ is defined as the angle whose tangent is equal to the ratio of the magnitudes of the total reflection coefficients (equation 1.11), which gives a measure of the change in amplitude of the perpendicular and parallel

$$\tan(\Psi) = \frac{|R_p|}{|R_s|} \tag{1.11}$$

components of the wave after reflection.[65] On the other hand, Δ is defined as the change in "phase difference" between the parallel component and perpendicular components of the wave after reflection (equation 1.12),[65] where δ_1 is the phase difference of the

$$\Delta = \delta_1 - \delta_2 \tag{1.12}$$

incident wave, and δ_2 is the phase difference of the reflected wave.

In order to obtain useful film properties, such as thickness and refractive index from Ψ and Δ, a regression analysis of the optical data is required. In this dissertation, the software used for this analysis was *WVASE32™*, provided by the J.A. Woollam Company.[66] This software does the regression analysis by fitting an optical model system with variable film thickness and/or refractive index to the experimental data. To evaluate the quality of the regression match between the calculated fit and observed data, the software uses an expression called the mean-squared error (MSE), which represents a sum of the squares of the differences between the measured and calculated data, with each difference weighted by the standard deviation of that measured data point.[66] Equation 1.13 shows this expression, where N is the number of (Ψ, Δ) pairs, M is the

$$\text{MSE}=\sqrt{\frac{1}{2N-M}\sum_{i=1}^{N}\left[\left(\frac{\Psi_i^{mod}-\Psi_i^{exp}}{\sigma_{\Psi,i}^{exp}}\right)^2+\left(\frac{\Delta_i^{mod}-\Delta_i^{exp}}{\sigma_{\Delta,i}^{exp}}\right)^2\right]} \tag{1.13}$$

number of variable parameters in the model, and σ is the standard deviation of the experimental data points. The software tries to minimize the MSE through successive iterations until the MSE converges and no additional improvement is generated. The key to this analysis, however, is the choice of an accurate optical model to describe the experimental system. If an inaccurate model is applied, the software can generate unrealistic values of the physical properties of the system. For this reason, we have used spectroscopic ellipsometry in conjunction with x-ray photoelectron spectroscopy (XPS) to eliminate film thickness as a variable in our optical model to determine refractive index, and we have used known values of refractive index to calculate thickness.

1.3.3 X-ray Photoelectron Spectroscopy (XPS)

X-ray photoelectron spectroscopy is based on the photoelectric effect, wherein an incident x-ray causes the ejection of photoelectrons from core-level and valence states of atoms in a sample of interest.[67] In our Scienta ESCA-300 instrument, high energy (1486.6 eV) Al-K_α x-rays irradiate the sample surface at a set angle between 20 and 45°. The kinetic energy of emitted photoelectrons can be measured by a detector held at various angles relative to the plane of the surface, referred to as the take-off angle. The binding energy of the atomic states giving rise to photoemission can be determined using equation 1.14,[67] where h is Planck's constant, ν is the frequency of the x- ray, E_k is the

$$E_b = h\nu - E_k + \Phi \qquad (1.14)$$

kinetic energy of the emitted photoelectron, E_b is the binding energy of the state from which it was produced, and Φ is the work function of the instrument. During calibration of the instrument, the work function is determined by the measurement of a

photoemission standard, such as the 4f level of gold, for which the value of E_b is known to a high degree of accuracy. The binding energy of the emitted electron is characteristic of the energy level it vacated, and thus corresponds to a specific electronic state of a particular element. Chemical shifts in this binding energy reflect the oxidation state of the element, with higher oxidation states giving rise to more positive binding energies.

The penetration depth of x-rays is on the order of microns, but detectable photoemission is only generated from atoms within a much smaller region nearer to the surface. The thickness of this region depends on the characteristic mean free path, or attenuation pathlength, λ, of photoelectrons through that material.[67] The attenuation length is a measure of the average distance travelled by a photoelectron between collisions with atoms in the sample. Each material has its own value of λ that depends on its crystal structure, density, and scattering cross-section of the constituent atoms. Approximately 63% of photoelectrons emitted at a depth of λ are scattered prior to reaching the surface, and 95% of photoelectrons from a depth of 3λ are scattered.[67] Typical values of λ are between 1 – 3 nm, so sampling depths are 3 – 10 nm for XPS measurements.[67] The angular dependence of this sampling depth, z, is given by equation 1.15, where θ is the take-off angle at which photoemission is collected. For the case of a

$$z = 3\lambda \sin\theta \tag{1.15}$$

substrate with a uniform thin overlayer of thickness z, the measured photoemission intensity, I^z, is given by equation 1.16 for the substrate, and equation 1.17 for the

$$I_s^z = I_s e^{-z/\lambda \sin\theta} \tag{1.16}$$

$$I_o^z = I_o\left(1 - e^{-z/\lambda \sin\theta}\right) \tag{1.17}$$

overlayer, where I_s is photoemission from an infinite substrate, and I_o is photoemission from an infinitely thick overlayer. It is therefore clear from these relations that the measured photoemission intensity is dependent on both the sampling depth, and the take-off angle.

Varying the take-off angle at which photoemission is collected allows the use of XPS for the depth-profiling of materials. Depth-profiling is especially important for the study of thin films on a substrate, such as those in this dissertation. For instance, when photoemission is collected at a take-off angle of 45° from a sample with a thin film overlayer, the photoemission from the underlying substrate is attenuated to a larger extent than if photoemission were collected at a take-off angle of 90° (Figure 1.4). Additionally, more photoemission is collected from the overlayer at an angle of 45°, than would be at 90°.

Data from XPS are typically first collected over a wide range of the binding-energy spectrum (a "survey spectrum") in order to determine which elements are present at a surface and to obtain their approximate amounts. For quantification, high-resolution spectra are usually collected within much smaller regions of interest. These high-resolution scans can be fit to provide quantitative data and information about chemical structure and oxidation state(s).

Commercial software allows photoemission to be fit by the insertion of component peaks with a mixture of Gaussian and Lorentzian character that is determined by the user. The user may also choose to specify the values allowed for other fitting parameters, such as component position, full-width at half maximum (fwhm) of the components, and ratios of component areas. Once a quality fit of experimental data has

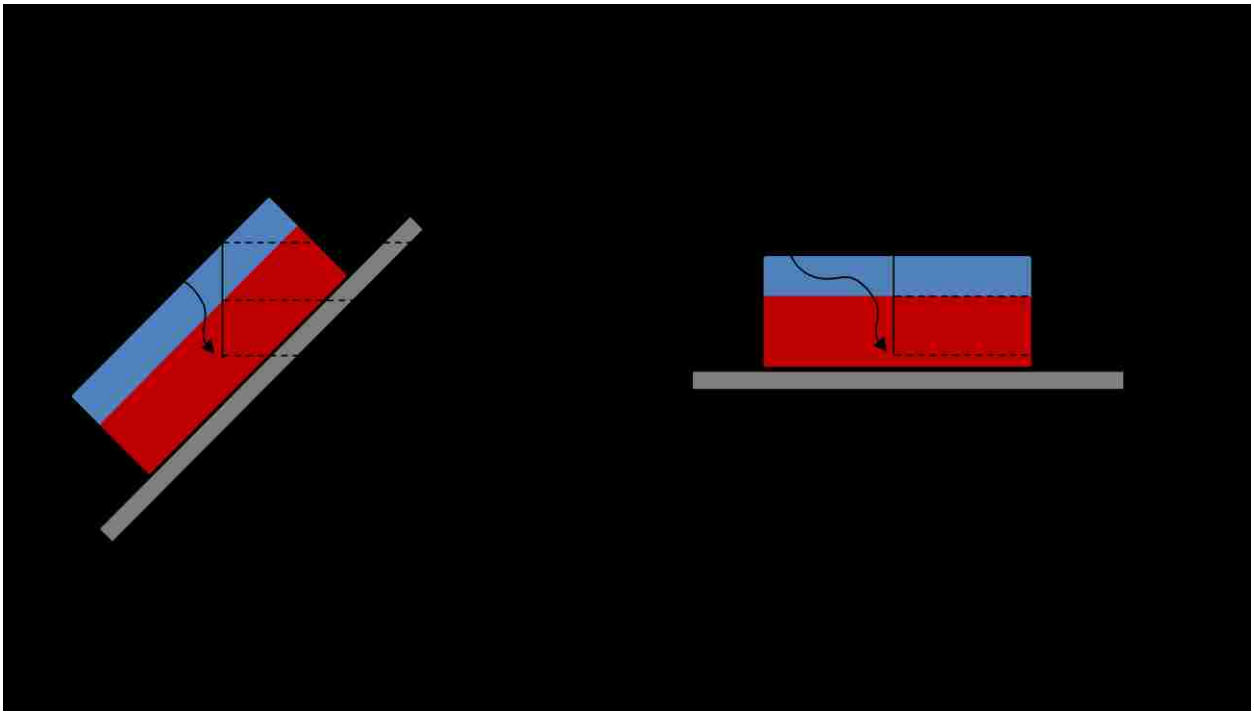

Figure 1.4. Schematic representation of the effect of take-off angle on observed ratio of intensities for a thin overlayer (I_o) and substrate (I_s).

been achieved, a quantitative analysis of the data can be performed using the integrated intensities of photoemission. It is important to note that quantitative analysis should only be performed using data taken from the same sample, on the same day, and under the same experimental conditions (i.e., take-off angle, pass energy, etc.), and after correcting for the number of scans and relative sensitivity factors for each initial electronic state to adjust the integrated photoemission intensities.

1.4 Patterned SAMs on Uniform Substrates

Producing patterned SAMs on uniform substrates can be achieved through a variety of methods, including microcontact printing and lithographic techniques (e.g. photolithography, e-beam lithography, and x-ray lithography).[4,68] In microcontact printing, a patterned stamp containing or wetted with the molecule of interest is applied to a surface for a brief period of time (5-10 s), allowing monolayer formation in the pattern present on the stamp with resolution of features down to ~ 20 nm.[69,70] Lithographic techniques involve the initial formation of a SAM across the entire substrate, followed by removal from specific areas to form a patterned surface.[68,71] Typically, resists are fabricated for this use, allowing degradation of the monolayer not protected by the applied pattern.[68] For example, electron-beam lithography can be used to generate features on a substrate with resolutions as small as ~ 10 nm.[4,72]

1.5 Directed Self-Assembly on Patterned Substrates

Directed self-assembly of molecules onto a substrate bearing a pre-existing pattern is a goal in present research due to the promise such modified surfaces hold for

use in sensors (eNoses, eTongues, etc.), photovoltaics, and microelectronics.[4] Many of these applications require a technique that allows the user to apply monolayers with different types of functionality on electrodes adjacent to one another. As mentioned above, accelerated formation of SAMs by potential-assisted chemisorption of organosulfur compounds has been studied extensively by many authors.[20,31,42,44,48] Reductive potentials can also be used to either desorb monolayers from specific electrodes, or to prevent spontaneous formation of films.[43,45,47,73-75] Sequential formation of SAMs from these techniques are potentially problematic though, as the ability of thiols from solution to interchange with thiolate monolayers can give rise to cross-contamination of neighboring electrodes.

In previous work, the Ferguson group developed a method for the site-selective formation of SAMs from alkyl thiosulfates on both macroscopic gold electrodes and microelectrodes and with the ability to introduce ω-functionality.[12,13,76] This method relied on the anodic activation of alkyl thiosulfates at selected electrodes in an array (equation 1.18), and allowed the sequential placement of SAMs of varying functionality

$$RS_2O_3^- + Au \xrightarrow{-e^-} AuSR + SO_3 \qquad (1.18)$$

without cross-contamination (Figure 1.5).[12-14,76,77] This process occurs at potentials sufficiently anodic to also cause concurrent oxidation of the gold surface which may mediate oxidation of the alkyl thiolsufates as the SAM forms.[78] This method, however, is not compatible with nucleophilic end groups because the SO_3 by-product is a strong Lewis acid and leads to side-reactions at the surface of the SAM. Monolayers formed from hydroxyl-terminated alkyl thiosulfates, for example, contained large amounts of

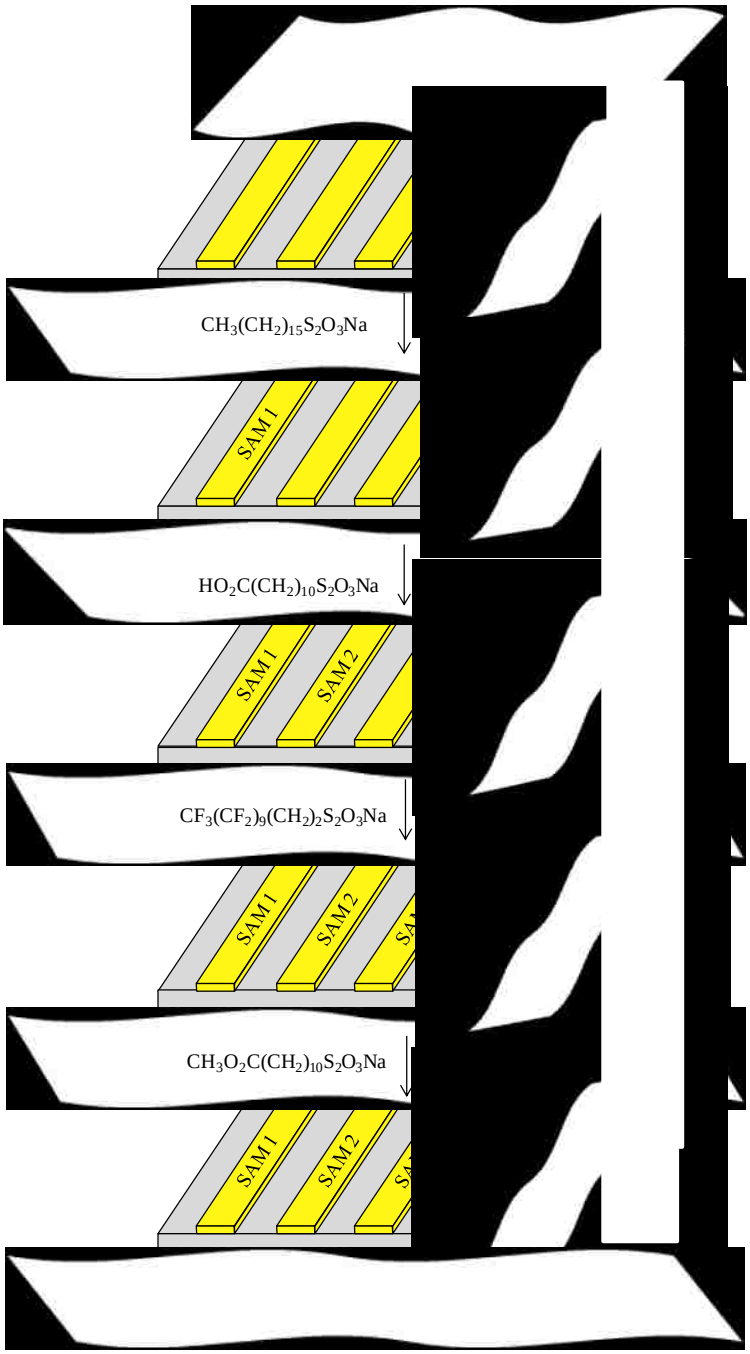

Figure 1.5. Sequential adsorption of SAMs on individually addressable gold electrodes by oxidation of alkyl thiosulfates. Reprinted (adapted) with permission from Labukas, J. P.; Ferguson, G. S., *Langmuir* **2011,** *27* (7), 3219-3223. Copyright 2011 American Chemical Society.

sulfate, resulting presumably from the reaction of SO_3 with the terminal hydroxyl groups.[13]

The work described in this dissertation was undertaken with the goal of developing an alternative method for the regioselective formation of SAMs without the limitations of the alkyl-thiosulfate system. Our approach used the fact that dialkyl disulfides spontaneously form SAMs on gold but not oxidized gold surfaces,[1,20,31] to allow regioselective formation of SAMs on selected gold electrodes. This strategy is similar to the well-established ‘‘protection–deprotection’’ approach used successfully by synthetic organic chemists for decades.

1.6 Gold Oxide

A unique characteristic of gold is that its oxides are not thermodynamically stable. Nonetheless, they are kinetically inert in air or vacuum for periods of days.[30,79,80] Therefore, gold oxides can be produced through synthetic methods such as electrochemical oxidation,[81-86] chemical treatment,[30,31,79,80,87] or UV/O_3 exposure[27,29-32,50] and studied or used. The work in this dissertation uses oxide films, formed electrochemically or by UV/O_3 exposure, as masking layers to prevent monolayer formation.

The most well-studied gold oxide is Au_2O_3, which has been characterized by XPS,[26,27,80,84,87,88] ellipsometry,[89-94] measurements of resistivity,[95] and temperature-programmed desorption (TPD),[26,27,80] as well as examined using density functional theory (DFT) calculations.[96,97] The DFT calculations predicted Au_2O_3 to be a semiconductor with a band-gap of 0.85 eV, and to crystallize in an orthorhombic structure.[97] A detailed

discussion of the XPS and ellipsometric data found in the literature for gold oxide will be presented in Chapter 2. Depending on the method of formation, this oxide may occur as an anhydrous[26,27,80] or hydrous compound, with the hydrous type most typically resulting from electrochemical oxidation (equation 1.19).[82-86,98] Hydrated Au_2O_3 is also commonly

$$2\ Au + 3\ H_2O \rightarrow Au_2O_3 + 6\ H^+ + 6\ e^- \qquad (1.19)$$

described as gold hydroxide, $Au(OH)_3$, in the literature as it is difficult to discern the differences in the oxygen species present.[82,83,85,98] Due to the ambiguity of the composition of gold-oxide films, mixed oxides of the general formula $Au_xO_y(OH)_z$ are often reported.[81-83,85] Other oxides are also known, such as gold peroxide, AuO_2, but this species is considered to be highly unstable, decomposing readily to Au_2O_3 and O_2.[98] The gold oxide formed by exposure to UV/O_3 is thought to be anhydrous Au_2O_3.[26,27,30]

Formation of gold oxides electrochemically proceeds by the initial formation of a submonolayer of OH and/or O on the metal surface, which then extends to a full monolayer.[86] Continued oxidation and film growth proceeds by interchange between metal atoms in the substrate and the OH or O species in the ad-layer, which results in the transition of these species from reversibly adsorbed to irreversibly adsorbed (kinetically).[86] Two forms (α and β) of electrochemically formed gold oxide have been reported in the literature.[82-85] A thin, compact (α) oxide, which –based on XPS[81,83,84] and quartz-crystal microbalance measurements[82]– is thought to contain mostly Au (II), and a thicker, hydrous (β) oxide, which is thought to be predominately Au (III).[82-85] The α form is typically produced at potentials below 2.0 V (*vs.* reversible hydrogen electrode, RHE) under potentiostatic and potential-cycling conditions, whereas the β form is produced potentiostatically above 2.0 V or by cycling between a lower (~ 0.5 – 1.0 V)

and upper (1.8 – 2.6 V) limit using a symmetric square-wave periodic potential or linear potential cycling.[82,83,85]

1.7 Dissertation Structure

Each of the chapters in this dissertation describes a major component of research. The second chapter describes our studies of electrochemically formed gold oxide to gain an understanding of its composition, and to determine its complex refractive index over much of the visible range of wavelengths. We used these values of the refractive index in an ellipsometric study of the lability of thin films exposed to various solvents and supporting electrolytes, described in Chapter 3. That work established conditions under which the oxide film is inert over a timeframe suitable for experimentation. Chapter 4 focuses on the development of a protection-deprotection scheme for the directed formation of SAMs from dialkyl disulfides, using gold oxide as a temporary masking layer. Chapter 5 then describes the demonstration of the compatibility of this method with nucleophilic functional groups, as well as our extension of this technique to microelectrodes. In Chapter 6, exploratory work on the use of silver(I)-thiolate polymers as precursors to SAMs and nanoparticles is presented. Finally, in Chapter 7, future work is proposed for the continuation of these projects.

1.8 References

1. Nuzzo, R. G.; Allara, D. L., Adsorption of Bifunctional Organic Disulfides on Gold Surfaces. *J. Am. Chem. Soc.* **1983,** *105* (13), 4481-4483.
2. Bigelow, W. C.; Pickett, D. L.; Zisman, W. A., Oleophobic Monolayers. I. Films Adsorbed from Solution in Nonpolar Liquids. *J. Colloid Sci.* **1946,** *1*, 513-38.

3. Sagiv, J., Organized Monolayers by Adsorption. 1. Formation and Structure of Oleophobic Mixed Monolayers on Solid Surfaces. *J. Am. Chem. Soc.* **1980,** *102* (1), 92-8.
4. Love, J. C.; Estroff, L. A.; Kriebel, J. K.; Nuzzo, R. G.; Whitesides, G. M., Self-assembled Monolayers of Thiolates on Metals as a Form of Nanotechnology. *Chem. Rev.* **2005,** *105* (4), 1103-1169.
5. Ulman, A., Formation and Structure of Self-assembled Monolayers. *Chem. Rev.* **1996,** *96* (4), 1533-1554.
6. Dubois, L. H.; Nuzzo, R. G., Synthesis, Structure, and Properties of Model Organic Surfaces. *Annu. Rev. Phys. Chem.* **1992,** *43* (1), 437-463.
7. Bain, C. D.; Biebuyck, H. A.; Whitesides, G. M., Comparison of Self-assembled Monolayers on Gold: Coadsorption of Thiols and Disulfides. *Langmuir* **1989,** *5* (3), 723-727.
8. Bain, C. D.; Evall, J.; Whitesides, G. M., Formation of Monolayers by the Coadsorption of Thiols on Gold: Variation in the Head Group, Tail Group, and Solvent. *J. Am. Chem. Soc.* **1989,** *111* (18), 7155-7164.
9. Bain, C. D.; Whitesides, G. M., Correlations Between Wettability and Structure in Monolayers of Alkanethiols Adsorbed on Gold. *J. Am. Chem. Soc.* **1988,** *110* (11), 3665-3666.
10. Bourg, M. C.; Badia, A.; Lennox, R. B., Gold-sulfur Bonding in 2D and 3D Self-assembled Monolayers: XPS Characterization. *J. Phys. Chem. B* **2000,** *104* (28), 6562-6567.
11. Chaki, N. K.; Vijayamohanan, K., Self-assembled Monolayers as a Tunable Platform for Biosensor Applications. *Biosens. Bioelectron.* **2002,** *17*, 1-12.
12. Lee, M.-T.; Hsueh, C.-C.; Freund, M. S.; Ferguson, G. S., Electrochemical Self-assembly of Monolayers from Alkylthiosulfates on Gold. *Langmuir* **2003,** *19* (13), 5246-5253.
13. Labukas, J. P.; Drake, T. J. H.; Ferguson, G. S., Compatibility of ω-Functionality in the Electrochemically Directed Self-Assembly of Monolayers on Gold from Alkyl Thiosulfates. *Langmuir* **2010,** *26* (12), 9497-9505.
14. Labukas, J. P.; Ferguson, G. S., Direct Route to Well-Defined, Chemically Diverse Electrode Arrays. *Langmuir* **2011,** *27* (7), 3219-3223.
15. Dubois, L. H.; Zegarski, B. R.; Nuzzo, R. G., Molecular Ordering of Organosulfur Compounds on Au(111) and Au(100): Adsorption from Solution and in Ultrahigh Vacuum. *J. Chem. Phys.* **1993,** *98* (1), 678-688.
16. Strong, L.; Whitesides, G. M., Structures of Self-assembled Monolayer Films of Organosulfur Compounds Adsorbed on Gold Single Crystals: Electron Diffraction Studies. *Langmuir* **1988,** *4* (3), 546-558.
17. Samant, M. G.; Brown, C. A.; Gordon, J. G., Structure of an Ordered Self-assembled Monolayer of Docosyl Mercaptan on Gold(111) by Surface X-ray Diffraction. *Langmuir* **1991,** *7* (3), 437-439.
18. Bain, C. D.; Troughton, E. B.; Tao, Y.-T.; Evall, J.; Whitesides, G. M.; Nuzzo, R. G., Formation of Monolayer Films by the Spontaneous Assembly of Organic Thiols from Solution onto Gold. *J. Am. Chem. Soc.* **1989,** *111* (1), 321-335.
19. Porter, M. D.; Bright, T. B.; Allara, D. L.; Chidsey, C. E. D., Spontaneously Organized Molecular Assemblies. 4. Structural Characterization of Normal-Alkyl

Thiol Monolayers on Gold by Optical Ellipsometry, Infrared-Spectroscopy, and Electrochemistry. *J. Am. Chem. Soc.* **1987,** *109* (12), 3559-3568.
20. Ron, H.; Rubinstein, I., Self-assembled Monolayers on Oxidized Metals. 3. Alkylthiol and Dialkyl Disulfide Assembly on Gold Under Electrochemical Conditions. *J. Am. Chem. Soc.* **1998,** *120* (51), 13444-13452.
21. Biebuyck, H. A.; Bain, C. D.; Whitesides, G. M., Comparison of Organic Monolayers on Polycrystalline Gold Spontaneously Assembled from Solutions Containing Dialkyl Disulfides or Alkanethiols. *Langmuir* **1994,** *10* (6), 1825-1831.
22. Schreiber, F., Structure and growth of self-assembling monolayers. *Prog. Surf. Sci.* **2000,** *65* (5-8), 151-256.
23. Laibinis, P. E.; Whitesides, G. M.; Allara, D. L.; Tao, Y. T.; Parikh, A. N.; Nuzzo, R. G., Comparison of the Structures and Wetting Propeteries of Self-Assembled Monolayers on Normal-Alkanethiols on the Coinage Metal-Surfaces, Cu, Ag, Au. *J. Am. Chem. Soc.* **1991,** *113* (19), 7152-7167.
24. Roy, D.; Fendler, J., Reflection and Absorption Techniques for Optical Characterization of Chemically Assembled Nanomaterials. *Adv. Mater.* **2004,** *16* (6), 479-508.
25. Cook, H. D.; Ries, H., Adsorption of Radiostearic Acid and Radiostearyl Alcohol from n-Hexadecane onto Solid Surfaces. *J. Phys. Chem.* **1959,** *63* (2), 226-230.
26. King, D. E., Oxidation of Gold by Ultraviolet-light and Ozone at 25-Degrees-C. *J. Vac. Sci. Technol., A* **1995,** *13* (3), 1247-1253.
27. Krozer, A.; Rodahl, M., X-ray Photoemission Spectroscopy Study of UV/ozone Oxidation of Au Under Ultrahigh Vacuum Conditions. *J. Vac. Sci. Technol., A* **1997,** *15* (3), 1704-1709.
28. McIntyre, N. S.; Davidson, R. D.; Walzak, T. L.; Williston, R.; Westcott, M.; Pekarsky, A., Uses of Ultraviolet Ozone for Hydrocarbon Removal - Applications to Surfaces of Complex Composition or Geometry. *J. Vac. Sci. Technol., A* **1991,** *9* (3), 1355-1359.
29. Worley, C. G.; Linton, R. W., Removing Sulfur from Gold Using Ultraviolet Ozone Cleaning. *J. Vac. Sci. Technol., A* **1995,** *13* (4), 2281-2284.
30. Ron, H.; Rubinstein, I., Alkanethiol Monolayers on Preoxidized Gold - Encapsulation of Gold Oxide Under an Organic Layer. *Langmuir* **1994,** *10* (12), 4566-4573.
31. Ron, H.; Matlis, S.; Rubinstein, I., Self-assembled Monolayers on Oxidized Metals. 2. Gold Surface Oxidative Pretreatment, Monolayer Properties, and Depression Formation. *Langmuir* **1998,** *14* (5), 1116-1121.
32. Vig, J. R., UV Ozone Cleaning of Surfaces. *J. Vac. Sci. Technol., A* **1985,** *3* (3), 1027-1034.
33. Cook, K. M.; Ferguson, G. S., Gold Oxide as a Protecting Group for Regioselective Surface Chemistry. *Chem. Commun.* **2011,** *47* (46), 12550-12552.
34. Bain, C. D.; Whitesides, G. M., A Study by Contact-angle of the Acid-base Behavior of Monolayers Containing Omega-mercaptocarboxylic Acids Adsorbed on Gold - An Example of Reactive Spreading. *Langmuir* **1989,** *5* (6), 1370-1378.
35. Laibinis, P. E.; Fox, M. A.; Folkers, J. P.; Whitesides, G. M., Comparisons of Self-assembled Monolayers on Silver and Gold - Mixed Monolayers Derived

from $HS(CH_2)_{21}X$ and $HS(CH_2)_{10}Y$ (X, Y = CH3, CH2OH) Have Similar Properties. *Langmuir* **1991,** *7* (12), 3167-3173.
36. Witt, D.; Klajn, R.; Barski, P.; Grzybowski, B. A., Applications Properties and Synthesis of Omega-functionalized *n*-Alkanethiols and Disulfides - The Building Blocks of Self-assembled Monolayers. *Curr. Org. Chem.* **2004,** *8* (18), 1763-1797.
37. Bain, C. D.; Whitesides, G. M., Formation of Two-component Surfaces by the Spontaneous Assembly of Monolayers on Gold from Solutions Containing Mixtures of Organic Thiols. *J. Am. Chem. Soc.* **1988,** *110* (19), 6560-6561.
38. Folkers, J. P.; Laibinis, P. E.; Whitesides, G. M., Self-assembled Monolayers of Alkanethiols on Gold" Comparisons of Monolayers Containing Mixtures of Short-chain and Long-chain Constituents with CH_3 and CH_2OH Terminal Groups. *Langmuir* **1992,** *8* (5), 1330-1341.
39. Laibinis, P. E.; Nuzzo, R. G.; Whitesides, G. M., Structure of Monolayers Formed by Coadsorption of Two *n*-Alkanethiols of Different Chain Lengths on Gold and its Relation to Wetting. *J. Phys. Chem.* **1992,** *96* (12), 5097-5105.
40. Nuzzo, R. G.; Fusco, F. A.; Allara, D. L., Spontaneously Organized Molecular Assemblies. 3. Preparation and Properties of Solution Adsorbed Monolayers of Organic Disulfides on Gold Surfaces. *J. Am. Chem. Soc.* **1987,** *109* (8), 2358-2368.
41. Offord, D. A.; John, C. M.; Linford, M. R.; Griffin, J. H., Contact-angle Goniometry, Ellipsometry, and Time-of-flight Secondary-ion Mass-spectrometry of Gold Supported, Mixed Self-Assembled Monolayers formed from Alkyl Mercaptans. *Langmuir* **1994,** *10* (3), 883-889.
42. Abbott, N. L.; Whitesides, G. M., Potential-Dependent Wetting of Aqueous-solutions on Self-Assembled Monolayers formed from 15-(Ferrecenylcarbonyl)Pentadecanethiol on Gold. *Langmuir* **1994,** *10* (5), 1493-1497.
43. Diao, P.; Guo, M.; Hou, Q. C.; Xiang, M.; Zhang, Q., Electrochemically Partitioned Assembly of Organosulfur Monolayers and Nanoparticles. *J. Phys. Chem. B* **2006,** *110* (41), 20386-20391.
44. Diao, P.; Hou, Q. C.; Guo, M.; Xiang, M.; Zhang, Q., Effect of Substrate Potentials on the Structural Disorders of Alkanethiol Monolayers Prepared by Electrochemically Directed Assembly. *J. Electroanal. Chem.* **2006,** *597* (2), 103-110.
45. Riepl, M.; Mirsky, V. M.; Wolfbeis, O. S., Electrical Control of Alkanethiols Self-Assembly on a Gold Surface as an Approach for Preparation of Microelectrode Arrays. *Microchim. Acta* **1999,** *131* (1), 29-34.
46. Weisshaar, D. E.; Lamp, B. D.; Porter, M. D., Thermodynamically Controld Electrochemical Formation of Thiolate Monolayers at Gold - Characterization and Comparison to Self-Assembled Analogs. *J. Am. Chem. Soc.* **1992,** *114* (14), 5860-5862.
47. Mullen, T. J.; Dameron, A. A.; Weiss, P. S., Directed Assembly and Separation of Self-Assembled Monolayers via Electrochemical Processing. *J. Phys. Chem. B* **2006,** *110* (29), 14410-14417.

48. Abbott, N. L.; Gorman, C. B.; Whitesides, G. M., Active Control of Wetting Using Applied Electrical Potentials and Self-assembled Monlayers. *Langmuir* **1995,** *11* (1), 16-18.
49. Tencer, M.; Nie, H.-Y.; Berini, P., Electrochemical Differentiation and TOF-SIMS Characterization of Thiol-coated Gold Features for (Bio)chemical Sensor Applications. *J. Electrochem. Soc.* **2009,** *156* (12), J386-J392.
50. Woodward, J. T.; Walker, M. L.; Meuse, C. W.; Vanderah, D. J.; Poirier, G. E.; Plant, A. L., Effect of an Oxidized Gold Substrate on Alkanethiol Self-assembly. *Langmuir* **2000,** *16* (12), 5347-5353.
51. Sharpe, R. B. A.; Burdinski, D.; Huskens, J.; Zandvliet, H. J. W.; Reinhoudt, D. N.; Poelsema, B., Oxidized Gold as an ultrathin Etch Resist Applied in Microcontact Printing. *J. Am. Chem. Soc.* **2006,** *128* (49), 15560-15561.
52. Zheng, Z.; Yang, M.; Zhang, B., Reversible Nanopatterning on Self-assembled Monolayers on Gold. *J. Phys. Chem. C* **2008,** *112* (17), 6597-6604.
53. Bertilsson, L.; Liedberg, B., Infrared Study of Thiol Monolayer Assemblies on Gold: Preparation, Characterization, and Functionalization of Mixed Monolayers. *Langmuir* **1993,** *9* (1), 141-149.
54. Duwez, A.-S., Exploiting Electron Spectroscopies to Probe the Structure and Organization of Self-assembled Monolayers: A Review. *J. Electron Spectrosc. Relat. Phenom.* **2004,** *134* (2), 97-138.
55. Hähner, G.; Kinzler, M.; Thümmler, C.; Wöll, C.; Grunze, M. In *Structure of Self-organizing Organic Films: A Near Edge X-ray Absorption Fine Structure Investigation of Thiol Layers Adsorbed on Gold*, 38th National Symposium of the American Vacuum Society, Seattle, Washington (USA), AVS: Seattle, Washington (USA), 1992; pp 2758-2763.
56. Laibinis, P. E.; Bain, C. D.; Whitesides, G. M., Attenuation of Photoeleectrons in Monolayers of Normal-Alkanethiols Adsorbed on Copper, Silver, and Gold. *J Phys. Chem.* **1991,** *95* (18), 7017-7021.
57. Bain, C. D.; Whitesides, G. M., Attenuation Lengths of Photoelectrons in Hydrocarbon Films. *J. Phys. Chem.* **1989,** *93* (4), 1670-1673.
58. Sun, L.; Crooks, R. M., Imaging of Defects Contained within *n*-Alkylthiol Monolayers by Combination of Underpotential Deposition and Scanning Tunneling Microscopy: Kinetics of Self-Assembly. *J. Electrochem. Soc.* **1991,** *138* (8), L23-L25.
59. Fenter, P.; Eberhardt, A.; Eisenberger, P., Self-Assembly of n-Alkyl Thiols as Disulfides on Au(111). *Science* **1994,** *266* (5188), 1216-1218.
60. Poirier, G. E., Mechanism of Formation of Au Vacancy Islands in Alkanethiol Monolayers on Au(111). *Langmuir* **1997,** *13* (7), 2019-2026.
61. Sun, L.; Crooks, R. M., Indirect Visualization of Defect Structures Contained within Self-assembled Organomercaptan Monolayers: Combined use of Electrochemistry and Scanning Tunneling Microscopy. *Langmuir* **1993,** *9* (8), 1951-1954.
62. Poirier, G. E., Characterization of Organosulfur Molecular Monolayers on Au(111) using Scanning Tunneling Microscopy. *Chem. Rev.* **1997,** *97* (4), 1117-1128.

63. Adamson, A. W.; Gast, A. P., *Physical Chemistry of Surfaces*. Wiley: New York, 1997.
64. Young, T., An Essay on the Cohesion of Fluids. *Philos. Tr. R. Soc. S-A* **1805,** *95*, 65-87.
65. Tompkins, H. G.; McGahan, W. A., *Spectroscopic Ellipsometry and Reflectometry : A User's Guide*. Wiley: New York, 1999.
66. J. A. Woollam Co., I., *Guide to Using WVASE32: Spectroscopic Ellipsometry Data Acquisition and Analysis Software*. Lincoln, NE, 2008; p 677.
67. Briggs, D.; Seah, M. P., *Practical Surface Analysis : by Auger and x-ray Photoelectron Spectroscopy*. Wiley: Chichester; New York, 1983.
68. Smith, R. K.; Lewis, P. A.; Weiss, P. S., Patterning Self-assembled Monolayers. *Prog. Surf. Sci.* **2004,** *75* (1-2), 1-68.
69. Xia, Y.; Whitesides, G. M., Soft Lithography. *Angew. Chem. Int. Ed.* **1998,** *37* (5), 550-575.
70. Odom, T. W.; Love, J. C.; Wolfe, D. B.; Paul, K. E.; Whitesides, G. M., Improved Pattern Transfer in Soft Lithography Using Composite Stamps. *Langmuir* **2002,** *18* (13), 5314-5320.
71. Behm, J. M.; Lykke, K. R.; Pellin, M. J.; Hemminger, J. C., Projection Photolithography Utilizing a Schwarzschild Microscope and Self-assembled Alkanethiol Monolayers as Simple Photoresists. *Langmuir* **1996,** *12* (8), 2121-2124.
72. Gölzhäuser, A.; Geyer, W.; Stadler, V.; Eck, W.; Grunze, M.; Edinger, K.; Weimann, T.; Hinze, P. In *Nanoscale Patterning of Self-assembled Monolayers with Electrons*, Papers from the 44th international conference on electron, ion, and photon beam technology and nanofabrication, Rancho Mirage, California, (USA), AVS: Rancho Mirage, California, (USA), 2000; pp 3414-3418.
73. Widrig, C. A.; Chung, C.; Porter, M. D., The Electrochemical Desorption of n-Alkanethiol Monolayers From Polycrystalline Au and Ag Electrodes. *J. Electroanal. Chem.* **1991,** *310* (1-2), 335-359.
74. Meunier-Prest, R.; Legay, G.; Raveau, S.; Chiffot, N.; Finot, E., Potential-assisted Deposition of Mixed Alkanethiol Self-assembled Monolayers. *Electrochim. Acta* **2010,** *55* (8), 2712-2720.
75. Kumar, A.; Biebuyck, H. A.; Whitesides, G. M., Patterning Self-assembled Monolayers - Applications in Materials Science. *Langmuir* **1994,** *10* (5), 1498-1511.
76. Hsueh, C.-C.; Lee, M.-T.; Freund, M. S.; Ferguson, G. S., Electrochemically Directed Self-assembly on Gold. *Angew. Chem., Int. Ed.* **2000,** *39* (7), 1228-1230.
77. Labukas, J. P.; Ferguson, G. S., Electrochemically Directed Two-component Monolayers on Gold. *J. Mater. Res.* **2011,** *26* (2), 262-267.
78. Pillai, R. G.; Braun, M. D.; Freund, M. S., Electrochemically Assisted Self-Assembly of Alkylthiosulfates and Alkanethiols on Gold: The Role of Gold Oxide Formation and Corrosion. *Langmuir* **2010,** *26* (1), 269-276.
79. Tsai, H. C.; Hu, E.; Perng, K.; Chen, M. K.; Wu, J. C.; Chang, Y. S., Instability of Gold Oxide Au_2O_3. *Surf. Sci.* **2003,** *537* (1-3), L447-L450.
80. Saliba, N.; Parker, D. H.; Koel, B. E., Adsorption of Oxygen on Au(111) by Exposure to Ozone. *Surf. Sci.* **1998,** *410* (2-3), 270-282.

81. Tremiliosi-Filho, G.; Dall'Antonia, L. H.; Jerkiewicz, G., Growth of Surface Oxides on Gold Electrodes Under Well-defined Potential, Time and Temperature Conditions. *J. Electroanal. Chem.* **2005,** *578* (1), 1-8.
82. Xia, S. J.; Birss, V. I., A Multi-technique Study of Compact and Hydrous Au Oxide Growth in 0.1 M Sulfuric Acid Solutions. *J. Electroanal. Chem.* **2001,** *500* (1-2), 562-573.
83. Petrović, Ž.; Metikoš-Huković, M.; Babić, R.; Katić, J.; Milun, M., A Multi-technique Study of Gold Oxidation and Semiconducting Properties of the Compact Alpha-oxide Layer. *J. Electroanal. Chem.* **2009,** *629* (1-2), 43-49.
84. Dickinson, T.; Povey, A. F.; Sherwood, P. M. A., X-ray Photoelectron Spectroscopic Studies of Oxide Films on Platinum and Gold Electrodes. *J. Chem. Soc., Faraday Trans. 1* **1975,** *71* (0), 298-311.
85. Tremiliosi-Filho, G.; Dall'Antonia, L. H.; Jerkiewicz, G., Limit to Extent of Formation of the Quasi-two-dimensional Oxide State on Au Electrodes. *J. Electroanal. Chem.* **1997,** *422* (1-2), 149-159.
86. Conway, B. E., Electrochemical Oxide Film Formation at Noble-metals as a Surface-chemical Process. *Prog. in Surf. Sci.* **1995,** *49* (4), 331-452.
87. Pireaux, J. J.; Liehr, M.; Thiry, P. A.; Delrue, J. P.; Caudano, R., Electron Spectroscopic Characterization of Oxygen-adsorption on Gold Surfaces. 2. Production of Gold Oxide in DC Reactive Sputtering. *Surf. Sci.* **1984,** *141* (1), 221-232.
88. Juodkazis, K.; Juodkazytė, J.; Jasulaitienė, V.; Lukinskas, A.; Šebeka, B., XPS Studies on the Gold Oxide Surface Layer Formation. *Electrochem. Commun.* **2000,** *2* (7), 503-507.
89. Vela, M. E.; Zerbino, J. O.; Arvia, A. J., Ellipsometric Study of Hydrous Gold Oxide Layers and Gold Surfaces Resulting From their Electroreduction. *Thin Solid Films* **1993,** *233* (1-2), 82-85.
90. Sirohi, R. S.; Genshaw, M. A., Electrochemical Ellipsometric Study of Gold. *J. Electrochem. Soc.* **1969,** *116* (7), 910-914.
91. Kolb, D. M.; McIntyre, J. D., Spectrophotometric Determination of Optical Properties of an Adsorbed Oxygen Layer on Gold. *Surf. Sci.* **1971,** *28* (1), 321-334.
92. Kim, Y. T.; Collins, R. W.; Vedam, K., Fast Scanning Spectroelectrochemical Ellipsometry - Insitu Characterization of Gold Oxide. *Surf. Sci.* **1990,** *233* (3), 341-350.
93. Horkans, J.; Cahan, B. D.; Yeager, E., Electrode Potential Scanning Ellipsometric Spectroscopy - Study of Formation of Anodic Oxide Film on Noble-metals. *Surf. Sci.* **1974,** *46* (1), 1-23.
94. Ohtsuka, T., Precise Determination of Thickness and Optical-constant of Oxide Layer on Gold by 3-Parameter Ellipsometry. *Denki Kagaku* **1992,** *60* (12), 1123-1129.
95. Tabor, R. F.; Morfa, A. J.; Grieser, F.; Chan, D. Y. C.; Dagastine, R. R., Effect of Gold Oxide in Measurements of Colloidal Force. *Langmuir* **2011,** *27* (10), 6026-6030.

96. Shi, H.; Stampfl, C., First-principles Investigations of the Structure and Stability of Oxygen Adsorption and Surface Oxide Formation at Au(111). *Phys. Rev.B* **2007,** *76* (7), 14.
97. Shi, H. Q.; Asahi, R.; Stampfl, C., Properties of the Gold Oxides Au_2O_3 and Au_2O: First-principles Investigation. *Phys. Rev.B* **2007,** *75* (20), 205125.
98. Burke, L. D.; Buckley, D. T.; Morrissey, J. A., Novel View of the Electrochemisty of Gold. *Analyst* **1994,** *119* (5), 841-845.

Chapter 2

Determination of the Wavelength-dependent Refractive Index of a Thin Film of Gold Oxide

This chapter includes material that has been reproduced in part with permission from: Cook, K. M.; Ferguson, G.S.; *Journal of Physical Chemistry C* **2011**, *115(46)*, 22976-22980

2.1 Abstract

A two-step procedure is described for measuring the complex refractive index of an anodically produced oxide film on a gold electrode. Both the composition and the thickness of the oxide were determined independently using x-ray photoelectron spectroscopy. These measurements served to define the system and thereby avoid assumptions regarding the film stoichiometry that would otherwise be required. The thickness was then used to calculate values of n and k from ellipsometric data collected across the visible spectrum (350-800 nm).

2.2 Introduction

In order to develop our protection-deprotection approach, using gold oxide as a masking layer to direct the formation of SAMs from dialkyl disulfides, we needed a convenient method to monitor the presence or absence and the thickness of gold-oxide thin films. Spectroscopic ellipsometry would provide an ideal method, but requires knowledge of the wavelength-dependent refractive index of these films. This chapter describes a method for measuring these optical constants.

Gold has been valued throughout history for its scarcity and lack of chemical reactivity. A remarkable example of this chemical uniqueness is the instability of its oxide, relative to the component elements, under ordinary conditions. Thus, whereas the surfaces of the other metals (except mercury) immediately form a native oxide on contact with air, gold does not. In part for this reason, detailed characterization of thin films of other metal oxides has, in general, been more straightforward than for gold oxide(s). As discussed in Chapter 1, two forms (α and β) of electrochemically formed gold oxide have been reported in the literature.[1-3] The α form is typically produced at potentials below 2.0 V (vs. RHE) under potentiostatic and potential-cycling conditions, and the β form is produced potentiostatically above 2.0 V or by cycling between a lower (~ 0.5 – 1.0 V) and upper (1.8 – 2.6 V) limit using a symmetric square-wave periodic potential or linear potential cycling.[1-3] The thin compact (α) oxide is thought to contain mostly Au (II), while the thicker hydrous (β) oxide is thought to be predominately Au (III).[1-3]

Determination of the complex refractive index (N = n + ik) of gold-oxide thin films by ellipsometry requires that film thickness (t_{ox}) be measured independently because an accurate thickness and index cannot be determined simultaneously by ellipsometry. Approaches to solving this problem have included estimating film thicknesses by coulometric measurements,[4-6] and determining n, k, and t_{ox} simultaneously by using ultraviolet-visible specular reflection spectroscopy[7] to measure both reflectance ($\Delta R/R$) and ellipsometric parameters (Ψ, Δ).[8,9] The coulometric method involves measuring the charge associated with reduction and represented by the area under the cathodic stripping peak of the film. Assuming a uniform composition and density of the film (usually taken to be Au_2O_3), as well as the redox reaction responsible for stripping,

the coulometric measurement can be used to calculate the thickness of the film. These assumptions, however, can introduce error if the films are actually mixed oxides.[4-6,8] Reflectance measurements, on the other hand, require a linear approximation to be made: the oxide film thickness is estimated to be proportional to the change in reflectivity of a gold surface as it is oxidized. In this technique, however, the oxide and gold films must be non-absorbing in this regime in order to determine n, k, and t_{ox} simultaneously. As gold (and likely gold oxide) adsorbs light below 600 nm,[10] substantial errors occur for measurements made below 600 nm, and values for the complex refractive index are only reported for wavelengths in the range of ~600–715 nm.[7-9]

To avoid these weaknesses, we used angle-resolved x-ray photoelectron spectroscopy (XPS) to measure both the composition and the thickness of a single gold oxide thin film. We were then able to use the known thickness to determine wavelength-dependent values of the complex refractive index of the film with variable-angle spectroscopic-ellipsometry (VASE, Figure 2.1). Although the value of film thickness obtained by XPS depends on a calculated value of attenuation length of the photoelectrons, the choices for the values assumed in the calculation (the density and formula weight of Au_2O_3) could be verified by the measured elemental composition.

2.3 Results and Discussion

2.3.1 Formation and Composition of the Gold Oxide

Brief application of an anodic potential (1.2 V, 10 s) to a gold electrode immersed in aqueous sulfuric acid (0.5 M) produced a thin film of oxide on the electrode surface

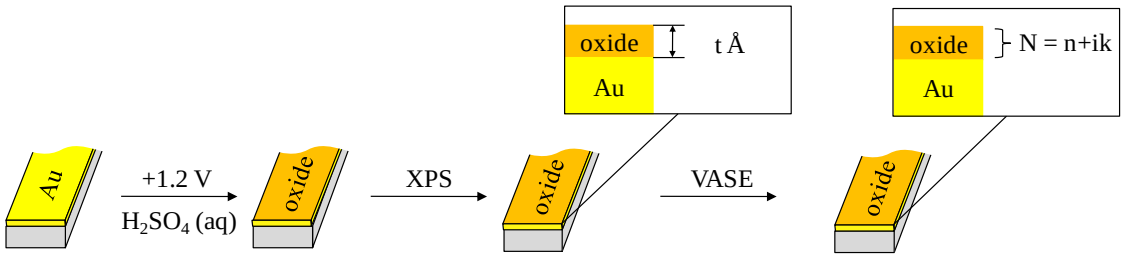

Figure 2.1. Schematic representation of the approach used to determine the complex refractive index of a thin film of gold oxide formed electrochemically on a gold substrate. The thickness of the oxide film was determined independently by angle-resolved XPS, and this thickness was then used to determine the complex refractive index by variable-angle spectroscopic ellipsometry (VASE).

(Figure 2.2).[6,7,11-13] High resolution XPS in the Au 4f region (take-off angle, 20°) confirmed the presence of the oxide film, with a broad spin-orbit doublet (fwhm, 1.3 eV) consistent with Au (III) (85.7 eV, $4f_{7/2}$; 89.4 eV, $4f_{5/2}$) and a narrower doublet (fwhm, 0.7 eV) due to the underlying elemental gold (84.0 eV, $4f_{7/2}$; 87.7 eV, $4f_{5/2}$; Figure 2.3, top).[11-15] A high resolution spectrum in the oxygen 1s region (take-off angle, 20°) contained a broad envelope that could be fit with four components at: 529.3 eV, fwhm, 0.793 eV; 530.1 eV, fwhm, 1.215 eV; 531.1 eV, fwhm, 2.073 eV; and 532.5 eV, fwhm, 1.533 eV (Figure 2.3, bottom). Similar binding energies have been attributed to a mixed oxide containing both oxo and hydroxyl species (Au_2O_3 and $Au(OH)_3$, respectively).[13-15] Nonetheless, the ratio of Au^{3+} to oxygen calculated from these spectra is 36:64, close to that expected for the oxide, Au_2O_3 (40:60).

To determine the extent to which adsorbed contamination might have contributed to the slight excess of O 1s photoemission, a control experiment was performed to sample the contaminants that may adsorb from the atmosphere. In this experiment a freshly evaporated gold electrode was exposed to the ambient laboratory atmosphere, allowing a layer of contamination to collect. The growth of this layer was monitored by ellipsometry until a constant thickness was reached (12 Å over ~48 h, Figure 2.4), after which the sample was analyzed by XPS. Ellipsometric data were collected over a wavelength range of 350 – 800 nm, and the model used to analyze the data comprised a substrate with the optical constants of the unaltered gold, and an overlayer of hexadecane, for which optical constants had been measured previously. These values of n and k for hexadecane were chosen because they are likely to be close to those of hydrocarbon

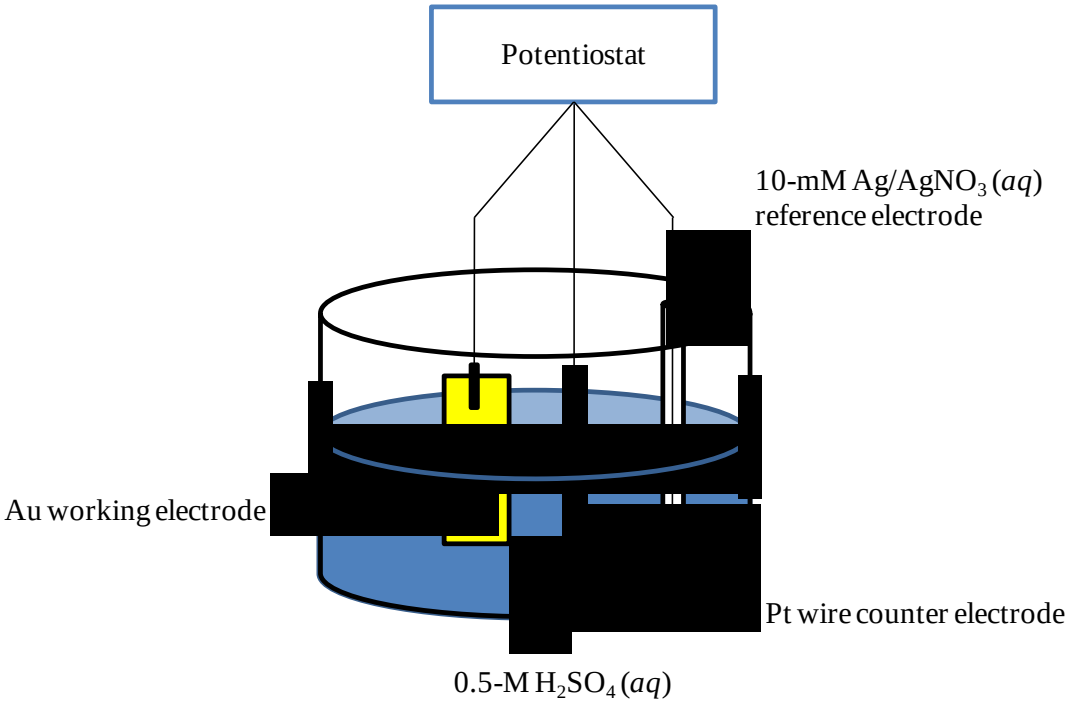

Figure 2.2. Schematic representation of an electrochemical cell used to oxidize the gold electrodes.

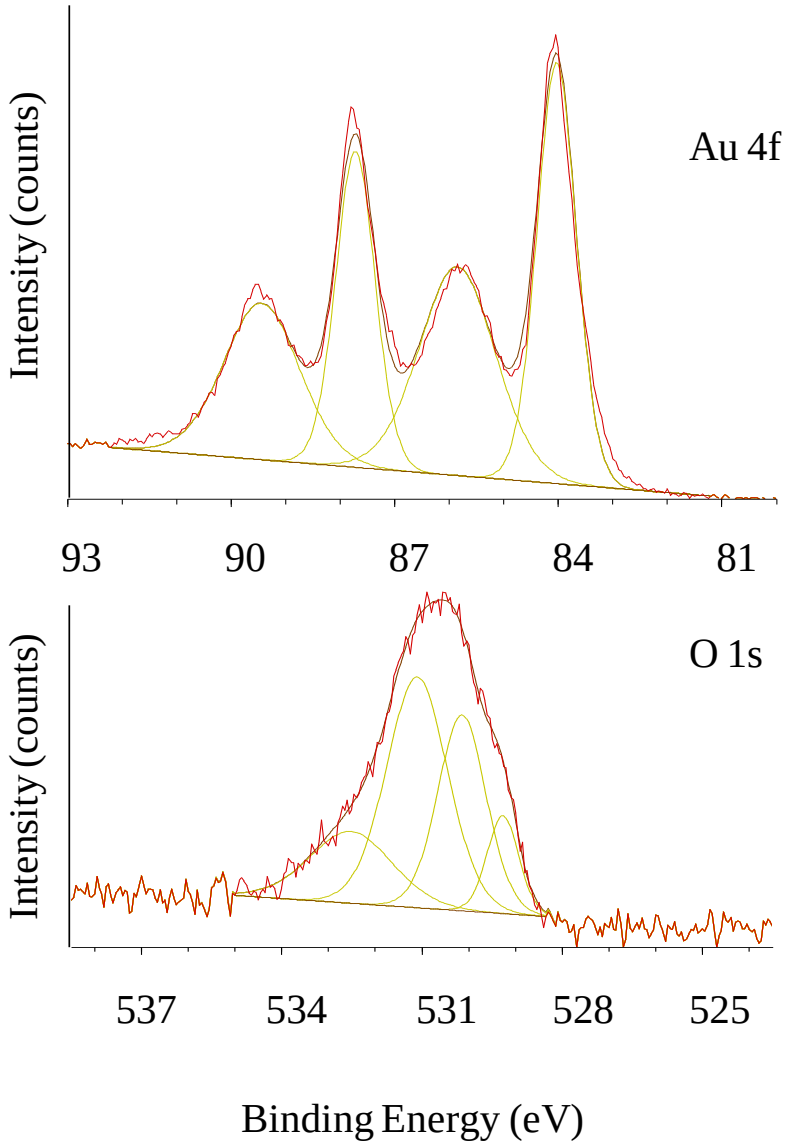

Figure 2.3. High resolution XPS spectra in the Au 4f and O 1s regions of an oxidized gold electrode.

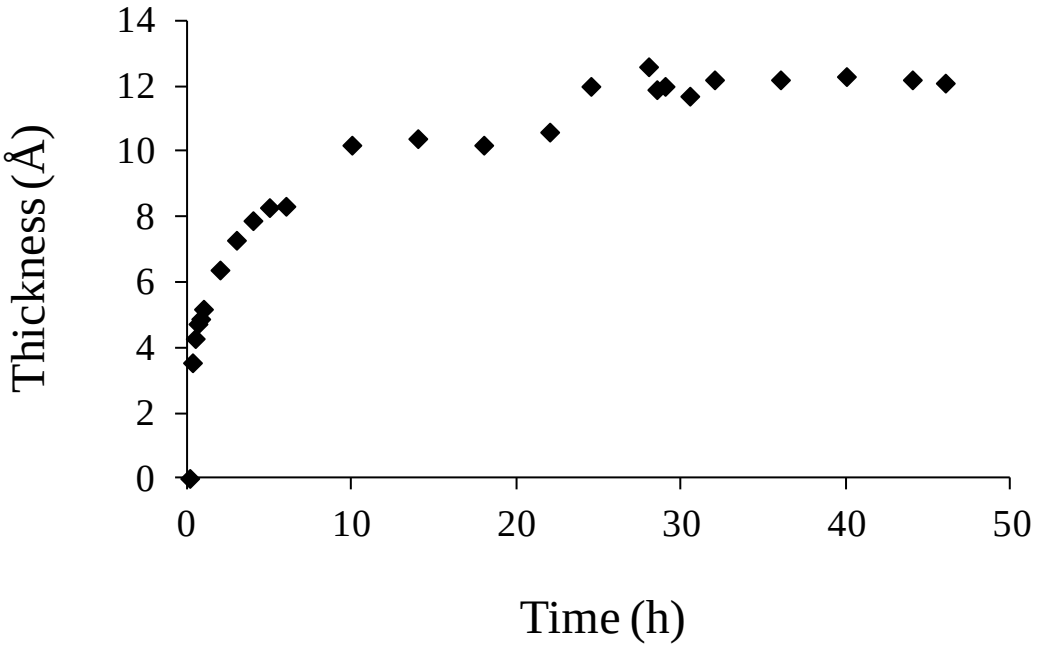

Figure 2.4. Growth in thickness of a contamination layer on a gold film over time, monitored ellipsometrically. The accuracy of ellipometric measurements of thickness is typically ±2Å.

contamination deposited from the atmosphere. A high resolution spectrum in the carbon 1s region (Figure 2.5) contained photoemission that could be fit by peaks at: 284.2 eV, fwhm, 1.155 eV; 284.9 eV, fwhm, 1.444 eV; and 287.1 eV, fwhm, 2.803 eV. A high resolution spectrum in the oxygen 1s region (Figure 2.6) contained photoemission that could be fit by peaks at: 530.5 eV, fwhm, 1.098 eV; 531.6 eV, fwhm, 1.416 eV; and 532.4 eV, fwhm 2.399 eV, which are consistent with similar measurements reported by others,[13-17] as well as similar to some of the components found in the fit of our gold-oxide spectrum. The sum of photoemission intensities from these peaks was ~ 20% of the total Au 4f photoemission, compared to that for our oxide spectra (~ 65% of the total Au 4f photoemission from the metal and the oxide). It is likely then, that contamination contributed to the intensity of the O 1s peaks at 530.1, 531.1 and 532.5 eV, and thereby decreased the Au:O ratio below that expected for Au_2O_3. Compared to the two forms (α and β) of electrochemically formed gold oxide reported in the literature, our results indicate a hydrous Au (III) oxide formed over a timeframe (10 s) and at a potential (1.2 V) at which a compact $Au(OH)_2$ or AuO is normally reported to be produced.[1-3]

2.3.2 Determination of Oxide Thickness

Angle-resolved XPS provided an independent estimate of the thickness of the electrochemically produced oxide film. High-resolution spectra in the Au 4f region were collected at take-off angles from 60° and 90° (between the detector and the plane of the sample) in 5-degree increments because the estimated attenuation length used in the analysis is most accurate in this regime (Figure 2.7).[18] The thickness of a thin overlayer on a thick substrate can be estimated fitting only attenuation of the photoemission from

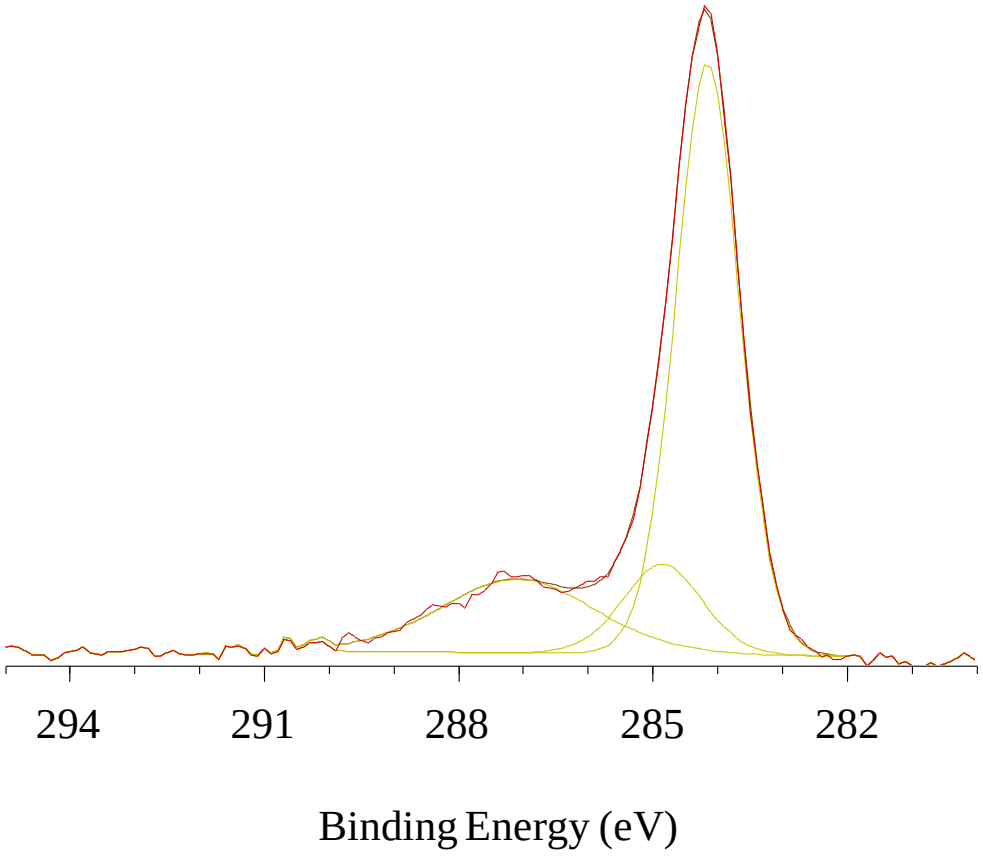

Figure 2.5. High resolution XPS spectrum in the C 1s region of contamination on a gold electrode.

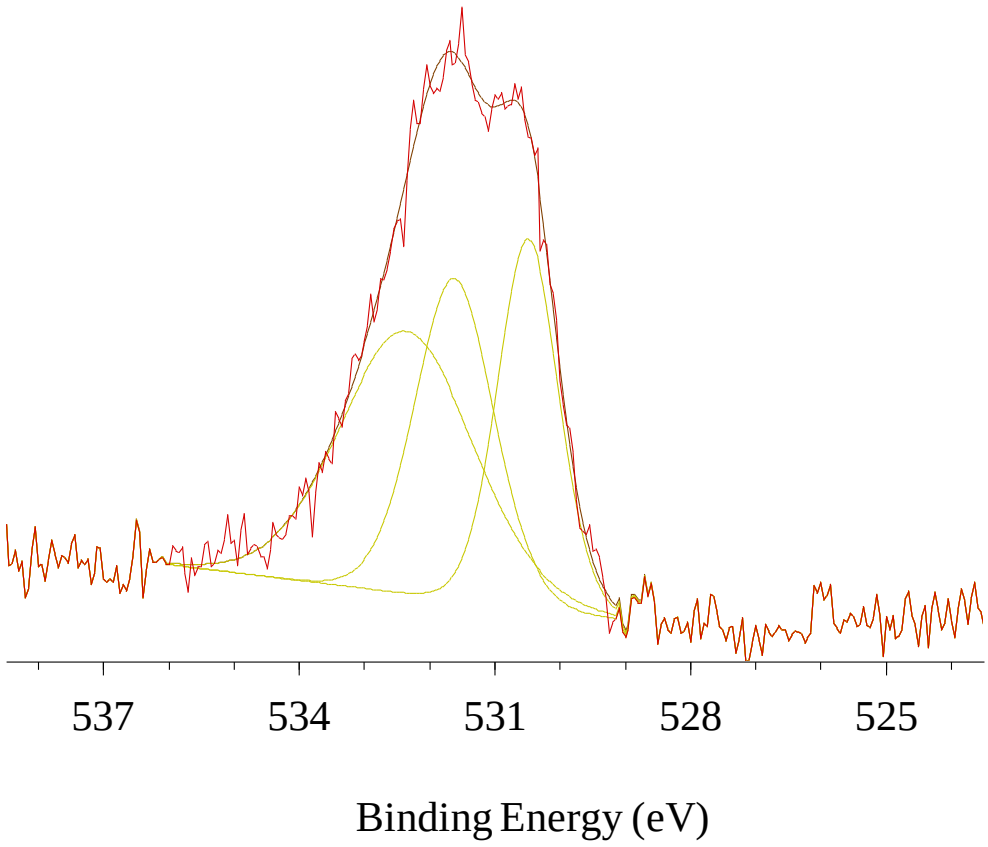

Figure 2.6. High resolution XPS spectrum in the O 1s region of contamination on a gold electrode.

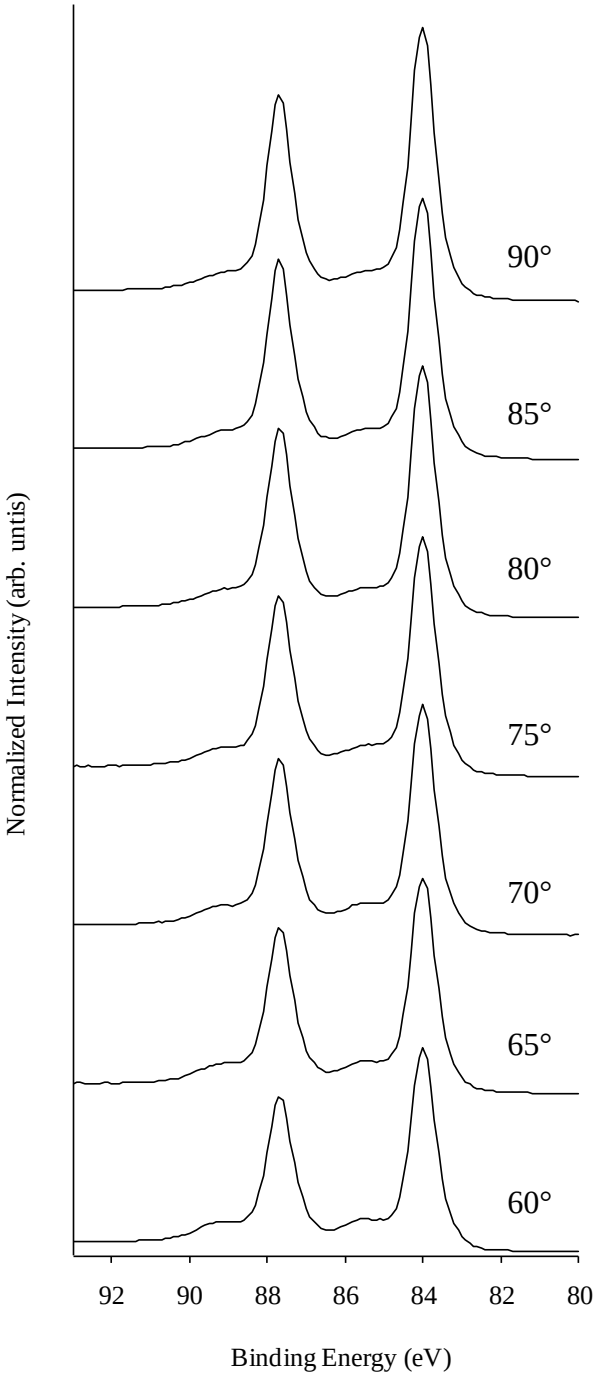

Figure 2.7. High resolution XPS spectra in the Au 4f region of an oxidized gold electrode with take-off angles between 60 and 90°.

the underlying substrate, or by using the ratio of photoemission intensities from both the overlayer and the substrate. We have analyzed our data using both methods and offer a comparison. Equation 2.1 describes the attenuated photoemission from the substrate (I_s)

$$\ln (I_s/I_\infty) = -t_{ox}/(\lambda_{ox} \sin \theta) \qquad (2.1)$$

as a function of take-off angle, where I_s refers specifically to the intensity of the Au $4f_{7/2}$ peak for the substrate measured through the oxide, I_∞ is the intensity of that peak for an infinite slab clean gold, λ_{ox} is the attenuation length for a gold 4f photoelectron through the oxide overlayer, θ is the take-off angle, and t_{ox} is the thickness of the oxide film. The constant, I_∞, was determined experimentally on the same electrode after sputtering with Ar ions to remove the oxide.[19] The attenuation length for gold oxide (λ_{ox}) was estimated using the NIST electron effective-attenuation-length database,[18] which gave a practical attenuation length of 18 Å (see experimental section). A plot of $\ln(I_s/I_\infty)$ *versus* $1/(\lambda_{ox} \sin \theta)$ gave a straight line for take-off angles between 60 and 80°, but deviated from linearity at higher angles. The slope of the best-fit line including all the data indicated an oxide thickness of 21 Å (Figure 2.8). This result is almost certainly an overestimation of the oxide thickness, due to an inherent weakness of the approach: photoemission from the Au substrate bearing an oxide will be attenuated not only by the oxide, but also by a thin layer of contamination on the oxide surface. Subsequent sputtering within the UHV chamber to produce the bare gold substrate removes both the oxide and the contamination. As a result, the measured ratio of I_s/I_∞ is smaller than it should be, leading to an overestimation of the oxide thickness. The deviation from linearity at high take-off angles is consistent with the presence of pinholes in the oxide layer, which could give rise to enhanced photoemission intensity due to the substrate (I_s) at high take-off

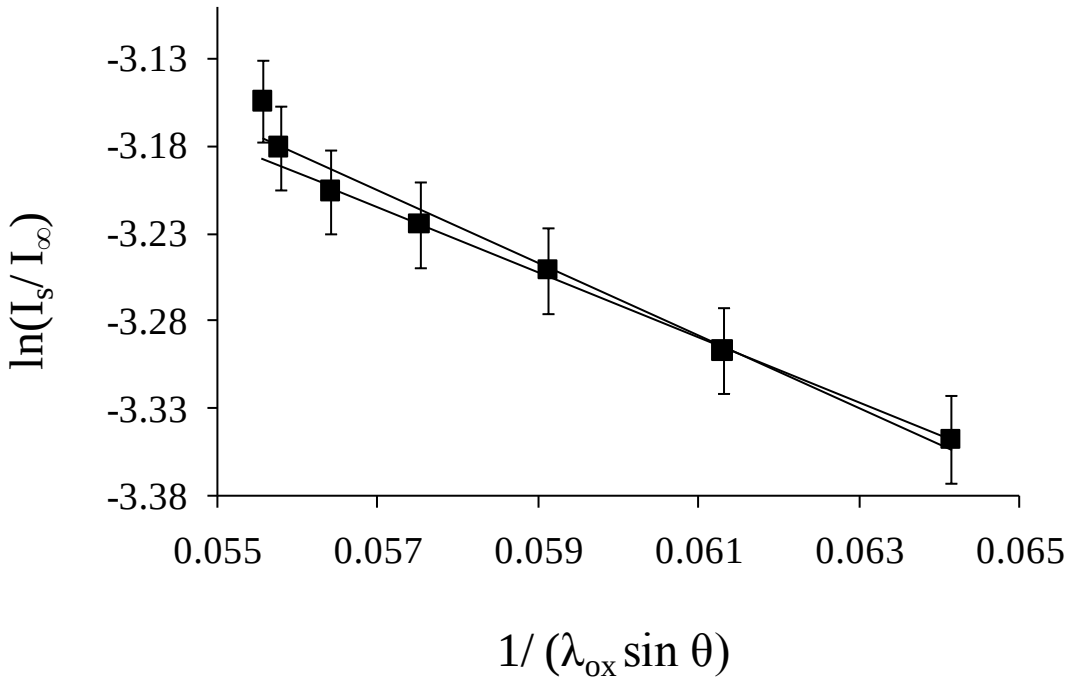

Figure 2.8. Linear fits of angle-dependent XPS Au $4f_{7/2}$ photoemission intensities plotted according to equation 2.1, with all points included and with the two points at highest take-off angle excluded. The error bars represent the propagated error of the measured photoemission intensities.

angles. Fitting only the linear regime of the data (points at the two highest angles omitted) gave an oxide thickness of 18 Å (Figure 2.8).

An alternative approach (equation 2.2), which treats the photoelectron intensity of

$$\ln (I_{ox}/I_s) = \ln (R) \cdot t_{ox}/(\lambda_{ox} \sin \theta) \qquad (2.2)$$

both the gold substrate and the oxide overlayer,[20] avoids the problem of differential attenuation due to contamination because both intensities are generated from the same spectrum and are thus attenuated to the same extent by the contamination. In this equation, I_{ox} is the intensity of theAu $4f_{7/2}$ peak of the oxide overlayer, and I_s is the intensity of the same peak from the underlying elemental gold. The constant, R, is a composite ratio of materials constants (equation 2.3), where A_s is the atomic weight

$$R = (A_s/A_{ox}) (\rho_{ox}/\rho_s) (\lambda_{ox}/\lambda_s) \qquad (2.3)$$

of gold, A_{ox} is the formula weight of gold oxide (Au_2O_3, 441.93 g/mol), ρ_s is the density of gold (19.3 g/cm^3), ρ_{ox} is the density of gold oxide (11.34 g/cm^3),[21] and λ_s is the attenuation length for gold (19 Å).[18] Using equation 2.2, the average value of t_{ox} calculated for angles between 60° to 90° (inclusive, 5° increments) gave an oxide thickness of 11 Å (Table 2.1). We believe that this value is the best estimate of oxide thickness, as it quantitatively accounts for both the substrate and oxide photoemission intensities. Averaging the values of thickness calculated at each angle avoids the effects of any forward focusing as a function of emission direction.[22-24]

Equation 2.1 can also be modified to include the contamination layer explicitly, by adding a second term to the right-hand side of the equation to account for the additional attenuation (equation 2.4), where λ_c is the attenuation length of a layer of

Takeoff Angle (°)	I_o (arb. units)	I_s (arb. units)	Oxide Thickness (Å)
60.00	52.5	202.5	11.4
65.00	51.2	214.8	11.2
70.00	50.1	226.9	11.0
75.00	47.3	236.2	10.5
80.00	45.2	245.2	10.1
85.00	46.3	255.8	10.0
90.00	47.1	266.4	9.9
		Average Thickness:	11 Å
		Error:	1 Å

Table 2.1. Oxide film thicknesses calculated using equation 2.2, and photoemission intensities for gold (I_s) and gold oxide (I_o) 4 $f_{7/2}$ peaks at take-off angles between 60 and 90°. The error is the standard deviation of the thickness values.

$$\ln (I_s/I_\infty) = (\lambda_c t_{ox} - \lambda_{ox} t_c)/(\lambda_{ox}\lambda_c \sin\theta) \quad (2.4)$$

organic contamination (assumed to be 30 Å)[24] and t_c is the thickness of the contamination layer. Using the value of t_{ox} obtained from equation 2.2, $\ln(I_s/I_\infty)$ could be plotted versus $1/\lambda_c\lambda_{ox}\sin\theta$ to obtain a value of t_c. As with the two-layer model, this plot was best fit with a line when the two highest angles were omitted, giving a t_c value of 13 Å (Figure 2.9). This value is higher than reported in the literature for contamination layers on gold (~6 Å),[25,26] which could be due to inconsistency inherent in comparisons of absolute intensities (I_s and I_∞) taken from separate sets of spectra, or to differences in the propensity for contamination of gold and gold oxide. It is very close, however, to the 12 Å we found by ellipsometery.

2.3.3 Wavelength-dependent Refractive Index

Values of the ellipsometric parameters, Ψ and Δ, were measured for a freshly deposited Au substrate before and after oxidation. Plots of Ψ and Δ, for gold and gold oxide —used to calculate film thickness— are shown in Figure 2.10. Data were collected using light with wavelengths between 350 and 800 nm. These data are close to those reported previously for Au_2O_3 films formed by UV/ozone treatment of gold.[27] The oxidized sample was then immediately transferred into the XPS instrument for the angle-resolved measurements described in the previous section. The film thickness derived by XPS was then input as a fixed parameter in the ellipsometric software to obtain the complex refractive index of the oxide over this range of wavelength (Figure 2.11). The value of n was relatively constant (~2.75) between 350 and 550 nm, but then abruptly fell to ~0.25 at and above 600 nm. The value of k increased sharply (from ~0.3 – 1.0 to

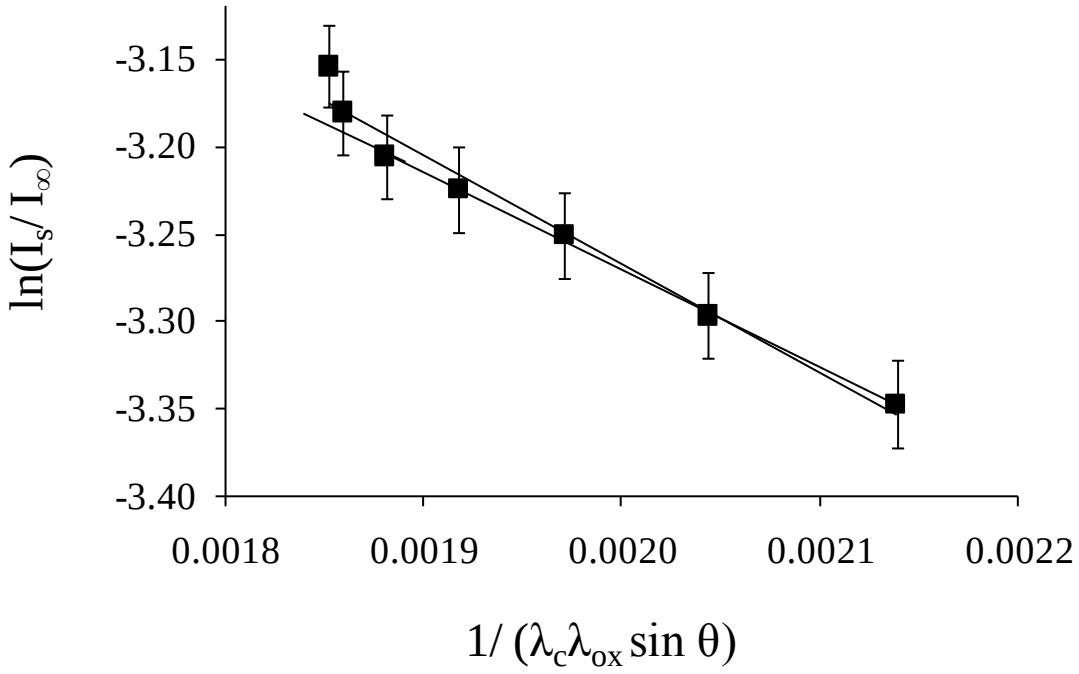

Figure 2.9. Linear fits of angle-dependent XPS Au $4f_{7/2}$ photoemission intensities plotted according to equation 2.4, with all points included and with the two points at highest take-off angle excluded. The error bars represent the propagated error of the measured photoemission intensities.

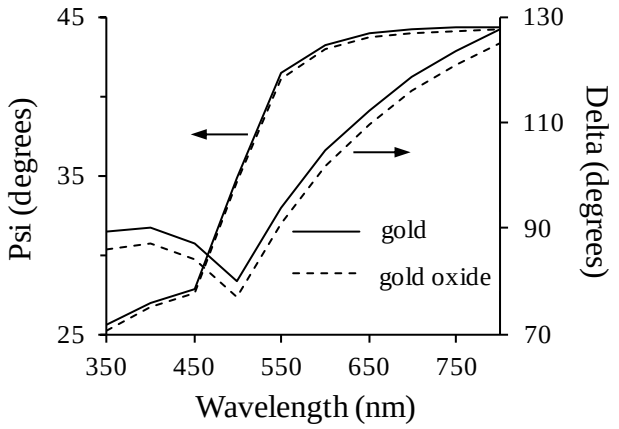

Figure 2.10. Measured ellipsometric parameters, Ψ and Δ, plotted as a function of wavelength for gold (solid line) and electrochemically formed gold oxide (dotted line) in air. These data were collected at an angle of incidence of 70°.

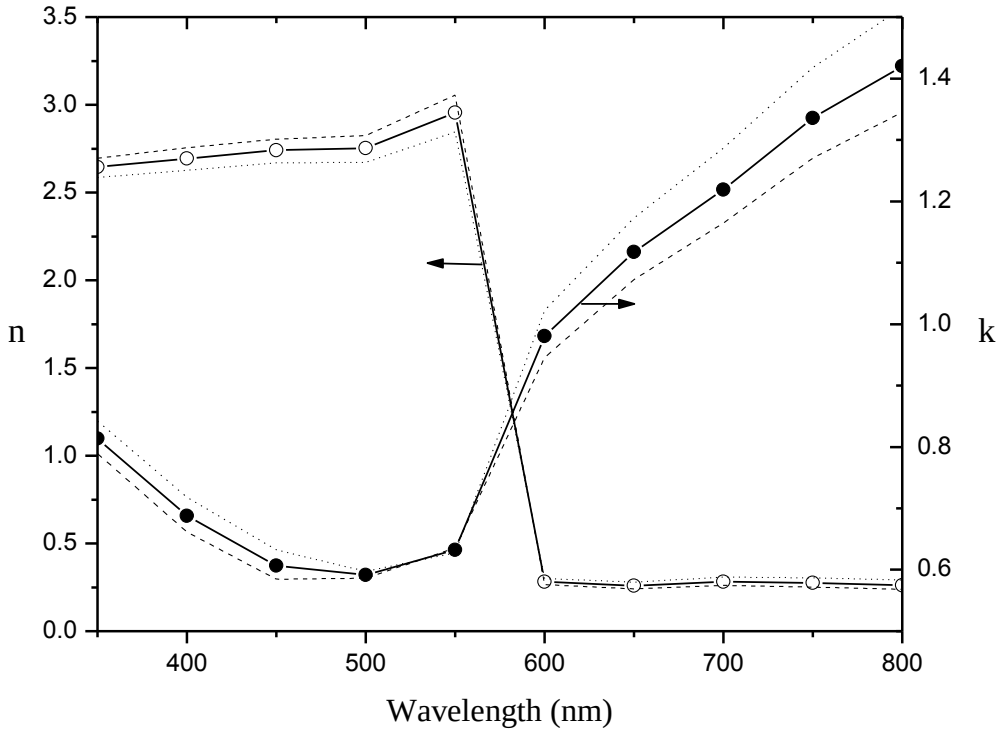

Figure 2.11. Complex refractive index of a thin film of gold oxide, formed electrochemically, as a function of wavelength. The primary source of uncertanty in these values is the thickness of the oxide film calculated from equation 2.2. To show the variation in this uncertanty as a function of wavelength, we have bracketed our data by values of n and k that result from thicknesses one standard deviation above (- - - - - -) and below (••••••••) the average value used.

~1.0 – 1.4) in the same region of the spectrum, consistent with an adsorption edge. Although the band-gap is calculated to be ~ 0.85 eV (~ 1459 nm),[28] ~ 1.36 eV (~ 912 nm),[29] or ~ 1.6 eV (~ 775 nm)[30] those authors note that the methods used in their calculations very likely gave underestimated values.

Previous studies of the refractive index of electrochemically formed gold oxides have generally taken one of two approaches: either the thickness of the oxide was estimated using coulometric measurements,[4-6] or it was measured simultaneously with the refractive index.[8,9] Kolb and McIntyre, for example, used coulometric measurements to estimate a thickness of 6 Å (based on an assumed density of 6 g/cm^3 for Au_2O_3) of an oxide film formed anodically on gold at 1.6 V.[7] They then used UV/Vis specular reflection spectroscopy to measure the differential reflectance (the difference in reflectance from the surface of two beams of light with different polarization) of the film and obtained ranges of n (~1 – 15) and k (~5 – 10), using a Kramers-Kronig analysis to relate the transmitted (real) to the absorbed (imaginary) components of the complex refractive index between wavelengths of 225 and 950 nm. They found a large increase in n (from ~ 2 to 15) around 565 nm, which is opposite to what is observed in our data, whereas their values of k remain relatively constant (between ~5 and 7). Kim and coworkers used a constant potential of 1.3 V (vs. saturated calomel electrode, SCE) to form an oxide film, and then coulometric stripping to estimate the thickness of the (assumed) Au_2O_3 layer to be 3.7 Å.[5] They reported values of n (~6.5 – 11) and k (~5.5 – 8) at wavelengths between 388 and 827 nm. Kim *et al*. also observed a sharp increase in n (from ~ 3 to 11) at ~ 500 nm, similar to the results of Kolb and McIntyre. Their reported increase in k (~ 5.5 to 7.5) at close to the same wavelength, however, is similar

to our data. Vela and coworkers studied "hydrous" gold-oxide layers formed by applying a square-wave periodic potential from 2.7 V to 0.45 V (*vs*. reversible hydrogen electrode, RHE).[6] Their samples were then held at 1.5 V and ellipsometric data collected in the range of 400–700 nm. Using thicknesses (1 – 400 nm) estimated by coulometric stripping measurements, values of n (1.76 – 1.93) and k (0 – 0.24) found were lower than most reported in the literature, which they attributed to the hydrous nature of the oxide.[6] These values of n are within the range of those we measured, but the values of k are lower, and no adsorption edge was found for these films.

Horkans and coworkers used ellipsometric and reflectance measurements to determine the film thickness and complex refractive index simultaneously.[8] They measured the optical intensity during cyclic voltammetry (0 – 1.6 V) and at a constant potential (1.35 V) *versus* normal hydrogen electrode, NHE. At the constant potential, they reported an oxide thickness of 5.4 ± 0.6 Å and a complex refractive index of 3.3 – 1.3i for wavelengths between 602 and 715 nm, with an estimated precision of 10%. These authors also noted that two-parameter (Ψ and Δ) solutions below 600 nm could not be found because the error in this region was larger than the measurement, likely due to the absorbance of light by the material starting at this wavelength. The value of n obtained in this manner (3.3) is close to our values found at shorter wavelength, but not to those in the same region of wavelength. Their value of k does not correspond to our value at the same wavelengths. Similarly, Ohtsuka used ellipsometric and reflectance measurements at 632.8 nm to determine the thickness and refractive index of an oxide film formed anodically during a linear potential sweep from -0.26 V to 1.64 V (vs. Ag/AgCl).[9] Optical data obtained at 1.64 V (once the film thickness stopped changing)

gave a thickness of 8.6 Å and complex refractive index of 3.1 –1.25i, which is in good agreement with the work of Horkans.

With the benefit of an independent measure of film thickness in our study, comparisons to these literature values indicate that direct optical measurements of thickness tend to give more consistently reliable results than indirect coulometric measurements. The discrepancies in the values of n and k found in different studies could have several sources, including differences not only in the accuracy with which thickness can be determined, but also in the nature of the films produced (e.g., "hydrous" or "compact") by the different methods. A systematic study of the various electrochemical protocols would be required, and may be warranted, to test this hypothesis.

2.4 Conclusion

In summary, we have obtained values for the complex refractive index of an electrochemically formed thin film of gold oxide for wavelengths between 350 and 800 nm. The thickness of the film was determined independently, using angle-resolved XPS, to be 11 Å. This thickness gave a real part of the refractive index (n) of 2.5–3.0 at wavelengths between 350 and 550 nm, and ~0.25 between 600 and 800 nm. The extinction coefficient also changed abruptly at the absorption edge, from ~0.6–0.8 between 350 and 550 nm, to ~1.0–1.4 between 600 and 800 nm. These results correspond more consistently to those from studies in which the oxide thickness was determined optically than to those in which it was determined coulometrically. In estimating the thickness of our oxide, an approach based on equation 2.2 proved to be the

most reliable, by avoiding anomalies due to surface contamination or to ratioing data from more than one set of spectra. This study demonstrates the value of combining XPS and VASE for determining the complex refractive index in a challenging system.

2.5 Experimental

General. Silver nitrate (Fisher, 99.8%), hydrogen peroxide (EMD, 30%), and sulfuric acid (EMD, 95%) were used as received. Gold (99.999%) was used as supplied by VEM Vacuum Engineering. Water was purified with a Millipore Simplicity® UV system (18.1 MΩ·cm).

Preparation of Samples. Gold electrodes were prepared on ~ 1 cm x 2 cm glass slides that had been cleaned using piranha solution. *Caution: Piranha solution, a 4:1 (v/v) mixture of concentrated H_2SO_4 and 30% H_2O_2, reacts violently with organic material and should be handled carefully.* Approximately 50 Å of Ti (as an adhesion promoter) and then 1000 Å of Au were deposited at a rate of ~ 3.4 Å/s onto the substrates by e-beam evaporation.

A thin film of gold oxide was produced electrochemically in aqueous 0.5-M sulfuric acid using a standard three-electrode cell comprising a gold working electrode, a platinum wire as the counter-electrode, and an aqueous $Ag/AgNO_3$ (10 mM) reference electrode. To oxidize each electrode, its potential was held at -0.2 V for 10 s, followed by 1.2 V for 10 s. The sample was then rinsed with deionized water (18.1 MΩ·cm) and dried under a stream of N_2.

X-ray Photoelectron Spectroscopy. Spectra were collected using a Scienta ESCA-300 spectrometer with monochromatic Al Kα X-rays generated using a rotating

anode and a 300-mm radius hemispherical analyzer. Samples were grounded by placing screws in contact with both electrode surface and the sample holder. The pressure in the sample chamber was $\sim 2\times10^{-9}$ Torr, and samples were analyzed at multiple take-off angles between the sample surface and the path to the analyzer.

High-resolution spectra of the oxide samples in the O 1s region were collected with a pass energy of 150 eV and a step energy of 0.05 eV (as for all high-resolution scans). The O 1s photoemission was best fit by four peaks in which the full-widths at half-maximum (fwhm) were allowd to vary. Gold 4f photoemission was collected at a pass energy of 300 eV for oxide-coated samples and at 150 eV for Ar-sputtered surfaces (to avoid detector saturation for the sputtered substrate). To normalize the Au 4f data, additional spectra were obtained for the sputtered (bare) Au at both pass energies using a sufficiently low x-ray power that the signals were not saturated at either pass energy. The ratio of these peak intensities was then used to normalize the two sets of data. For example, multiplication of the original 4f intensity from the sputtered sample (150 eV pass energy) by the ratio of intensities from the low-power spectra (300 eV/150 eV) allowed direct comparison of the original spectra (as in equation 2.1). To fit the Au $4f_{7/2}$ and $4f_{5/2}$ peaks, the fwhm were allowed to vary, but were constrained to be equal to each other, and the area of the $4f_{5/2}$ peak was constrained to be 75% that of the $4f_{7/2}$ peak.

Survey spectra were collected with a pass energy of 300 eV, and a step energy of 1 eV. Spectra were referenced to the elemental Au $4f_{7/2}$ peak, set at 84.0 eV. Samples were analyzed within 1 h of oxide formation, and the spectra were analyzed using CASAXPS® software (version 2.3.15dev77).

The attenuation length of gold oxide, used to determine oxide thickness, was estimated using the NIST electron effective-attenuation-length database.[18] The database calculates effective attenuation lengths (EALs) from expressions derived from the solution of a kinetic equation under the transport approximation.[31] The values of EAL are then plotted as a function of thickness, and an average value is given for a selected thickness range. Effects of elastic-electron scattering are neglected. Input parameters for the EAL estimation included the configuration of the XPS experiment (angles of x-ray incidence and of photoemission detection), the formula weight of gold oxide, and the density of gold oxide. The oxide composition of our films, indicated by the Au:O ratio measured at low take-off angle (15°), was approximately Au_2O_3. We therefore used a formula weight of 441.93 g/mol and a density of 11.34 g/cm^3.[21] The precision of the oxide thickness is determined by that of the calculated attenuation length and is reported to the nearest Å. All values from the work of others appear with the precision reported in the cited references.

Variable Angle Spectroscopic Ellipsometry. Ellipsometric parameters, Ψ and Δ, were measured using a J.A. Woollam W-VASE variable-angle spectroscopic-ellipsometer. Data were collected between 350 and 800 nm at 50-nm intervals with angles of incidence of 60° and 70°. Complex refractive indices were determined from these parameters using provided WVASE32® analysis software.

2.6 Acknowledgements

We gratefully acknowledge the National Science Foundation for support of this research (CHE-0749777) and for funding to purchase the spectroscopic ellipsometer (CHE-

0923370). We also thank Dr. Al Miller for assistance with acquisition and analysis of the XPS data.

2.7 References

1. Tremiliosi-Filho, G.; Dall'Antonia, L. H.; Jerkiewicz, G., Limit to Extent of Formation of the Quasi-two-dimensional Oxide State on Au Electrodes. *J. Electroanal. Chem.* **1997,** *422* (1-2), 149-159.
2. Xia, S. J.; Birss, V. I., A Multi-technique Study of Compact and Hydrous Au Oxide Growth in 0.1 M Sulfuric Acid Solutions. *J. Electroanal. Chem.* **2001,** *500* (1-2), 562-573.
3. Petrović, Ž.; Metikoš-Huković, M.; Babić, R.; Katić, J.; Milun, M., A Multi-technique Study of Gold Oxidation and Semiconducting Properties of the Compact Alpha-oxide Layer. *J. Electroanal. Chem.* **2009,** *629* (1-2), 43-49.
4. Sirohi, R. S.; Genshaw, M. A., Electrochemical Ellipsometric Study of Gold. *J. Electrochem. Soc.* **1969,** *116* (7), 910-914.
5. Kim, Y. T.; Collins, R. W.; Vedam, K., Fast Scanning Spectroelectrochemical Ellipsometry - Insitu Characterization of Gold Oxide. *Surf. Sci.* **1990,** *233* (3), 341-350.
6. Vela, M. E.; Zerbino, J. O.; Arvia, A. J., Ellipsometric Study of Hydrous Gold Oxide Layers and Gold Surfaces Resulting From their Electroreduction. *Thin Solid Films* **1993,** *233* (1-2), 82-85.
7. Kolb, D. M.; McIntyre, J. D., Spectrophotometric Determination of Optical Propereties of an Adsorbed Oxygen Layer on Gold. *Surf. Sci.* **1971,** *28* (1), 321-334.
8. Horkans, J.; Cahan, B. D.; Yeager, E., Electrode Potential Scanning Ellipsometric Spectroscopy - Study of Formation of Anodic Oxide Film on Noble-metals. *Surf. Sci.* **1974,** *46* (1), 1-23.
9. Ohtsuka, T., Precise Determination of Thickness and Optical-constant of Oxide Layer on Gold by 3-Parameter Ellipsometry. *Denki Kagaku* **1992,** *60* (12), 1123-1129.
10. Palik, E. D., *Handbook of Optical Constants of Solids*. Acedemic Press: San Diego, CA, 1998.
11. Juodkazis, K.; Juodkazytė, J.; Jasulaitienė, V.; Lukinskas, A.; Šebeka, B., XPS Studies on the Gold Oxide Surface Layer Formation. *Electrochem. Commun.* **2000,** *2* (7), 503-507.
12. Tremiliosi-Filho, G.; Dall'Antonia, L. H.; Jerkiewicz, G., Growth of Surface Oxides on Gold Electrodes Under Well-defined Potential, Time and Temperature Conditions. *J. Electroanal. Chem.* **2005,** *578* (1), 1-8.
13. Pireaux, J. J.; Liehr, M.; Thiry, P. A.; Delrue, J. P.; Caudano, R., Electron Spectroscopic Characterization of Oxygen-adsorption on Gold Surfaces. 2. Production of Gold Oxide in DC Reactive Sputtering. *Surf. Sci.* **1984,** *141* (1), 221-232.

14. Irissou, E.; Denis, M. C.; Chaker, M.; Guay, D., Gold Oxide Thin Film Grown by Pulsed Laser Deposition in an O_2 Atmosphere. *Thin Solid Films* **2005,** *472* (1-2), 49-57.
15. Krozer, A.; Rodahl, M., X-ray Photoemission Spectroscopy Study of UV/ozone Oxidation of Au Under Ultrahigh Vacuum Conditions. *J. Vac. Sci. Technol., A* **1997,** *15* (3), 1704-1709.
16. Saliba, N.; Parker, D. H.; Koel, B. E., Adsorption of Oxygen on Au(111) by Exposure to Ozone. *Surf. Sci.* **1998,** *410* (2-3), 270-282.
17. Koslowski, B.; Boyen, H. G.; Wilderotter, C.; Kastle, G.; Ziemann, P.; Wahrenberg, R.; Oelhafen, P., Oxidation of Preferentially (111)-oriented Au Films in an Oxygen Plasma Investigated by Scanning Tunneling Microscopy and Photoelectron Spectroscopy. *Surf. Sci.* **2001,** *475* (1-3), 1-10.
18. Powell, C. J. J., A, *NIST Electron Effective-Attenuation-Length Database - Version 1.2*. Gaithersburg, MD, **2009**.
19. Laibinis, P. E.; Whitesides, G. M.; Allara, D. L.; Tao, Y. T.; Parikh, A. N.; Nuzzo, R. G., Comparison of the Structures and Wetting Propeteries of Self-Assembled Monolayers on Normal-Alkanethiols on the Coinage Metal-Surfaces, Cu, Ag, Au. *J. Am. Chem. Soc.* **1991,** *113* (19), 7152-7167.
20. King, D. E., Oxidation of Gold by Ultraviolet-light and Ozone at 25-Degrees-C. *J. Vac. Sci. Technol., A* **1995,** *13* (3), 1247-1253.
21. Jones, P. G.; Rumpel, H.; Schwarzmann, E.; Sheldrick, G. M.; Paulus, H., Gold(III) Oxide. *Acta Crystallogr., B* **1979,** *35* (6), 1435-1437.
22. Seah, M. P.; Spencer, S. J., Ultrathin SiO_2 on Si II. Issues in Quantification of the Oxide Thickness. *Surf. Interface Anal.* **2002,** *33* (8), 640-652.
23. Seah, M. P.; White, R., Ultrathin SiO_2 on Si : III Mapping the Layer Thickness Efficiently by XPS. *Surf. Interface Anal.* **2002,** *33* (12), 960-963.
24. Seah, M. P.; Spencer, S. J.; Bensebaa, F.; Vickridge, I.; Danzebrink, H.; Krumrey, M.; Gross, T.; Oesterle, W.; Wendler, E.; Rheinlander, B.; Azuma, Y.; Kojima, I.; Suzuki, N.; Suzuki, M.; Tanuma, S.; Moon, D. W.; Lee, H. J.; Cho, H. M.; Chen, H. Y.; Wee, A. T. S.; Osipowicz, T.; Pan, J. S.; Jordaan, W. A.; Hauert, R.; Klotz, U.; van der Marel, C.; Verheijen, M.; Tarnminga, Y.; Jeynes, C.; Bailey, P.; Biswas, S.; Falke, U.; Nguyen, N. V.; Chandler-Horowitz, D.; Ehrstein, J. R.; Muller, D.; Dura, J. A., Critical Review of the Current Status of Thickness Measurements for Ultrathin SiO_2 on Si Part V. Results of a CCQM Pilot Study. *Surf. Interface Anal.* **2004,** *36* (9), 1269-1303.
25. Seah, M. P.; Spencer, S. J., Ultrathin SiO_2 on Si. I. Quantifying and Removing Carbonaceous Contamination. *J. Vac. Sci. & Technol., A* **2003,** *21* (2), 345-352.
26. Ron, H.; Matlis, S.; Rubinstein, I., Self-assembled Monolayers on Oxidized Metals. 2. Gold Surface Oxidative Pretreatment, Monolayer Properties, and Depression Formation. *Langmuir* **1998,** *14* (5), 1116-1121.
27. Tabor, R. F.; Morfa, A. J.; Grieser, F.; Chan, D. Y. C.; Dagastine, R. R., Effect of Gold Oxide in Measurements of Colloidal Force. *Langmuir* **2011,** *27* (10), 6026-6030.
28. Shi, H. Q.; Asahi, R.; Stampfl, C., Properties of the Gold Oxides Au_2O_3 and Au_2O: First-principles Investigation. *Phys. Rev.B* **2007,** *75* (20), 205125.

29. Burdett, J. K.; Sevov, S., Stability of the Oxidation States of Copper. *J. Am. Chem. Soc.* **1995,** *117* (51), 12788-12792.
30. Goldenblum, A.; Marian, A. B.; Teodorescu, V., Optical Properties of ZnO Nanocrystallites Embedded in a Gold-oxide Matrix. *J. Optoelectron. Adv. M.* **2006,** *8* (6), 2129-2132.
31. Tilinin, I. S.; Jablonski, A.; Zemek, J.; Hucek, S., Escape Probability of Signal Photoelectrons from Non-crystalline Solids: Influence of Anisotropy of Photoemission. *J. Electron Spectrosc. Relat. Phenom.* **1997,** *87* (2), 127-140.

Chapter 3

Relative Lability of Gold-Oxide Thin Films in Contact with Air, Solvents, or Electrolyte Solutions

This chapter includes material that has been reproduced in part with permission from: Cook, K. M.; Ferguson, G.S.; *Journal of Vacuum Science & Technology A*, **2013**, *31*, DOI: 10.1116/1.4791687

3.1 Abstract

The lability of gold-oxide thin films in contact with air, pure solvents, or electrolyte solutions was investigated by monitoring film thicknesses using spectroscopic ellipsometry. The compositions of selected surfaces were verified using low-energy ion scattering (LEIS). The oxide was inert in air over 24 h, but decomposed partially in tetrahydrofuran (THF) and water, and completely in ethanol, within the same period. The film thicknesses quickly decreased significantly in THF solutions of Bu_4NPF_6 and Bu_4NBF_4, but were more inert in solutions of Bu_4NClO_4 and $LiClO_4$ in the same solvent, making the latter more suitable choices as supporting electrolytes in electrochemical studies.

3.2 Introduction

Gold oxides are thermodynamically unstable,[1] with the exemplar Au_2O_3 having a significantly positive standard free energy of formation (78.70 kJ/mol).[2] As a result, gold oxides are powerful oxidizing agents, potentially important in the conversion of CO to CO_2 on gold/metal-oxide catalysts[3-5] and even capable of carbonizing organic polymers.[6] Nonetheless, oxide films on gold can be sufficiently inert under ordinary laboratory

conditions to allow spectroscopic characterization and use in certain applications. Thin oxide films can easily be produced on gold electrochemically,[7-10] *via* chemical oxidation,[11,12] and by photochemical oxidation with O_3.[13,14] In addition to their use as masking films on gold electrodes to allow selective surface chemistry,[15] oxide films have also proven useful as model systems for the study of interfacial phenomena such as corrosion and catalysis.[3-5,16]

The inherent instability of gold oxide has sometimes led to cautious approaches to its study and use in order to avoid uncertainty regarding the composition of samples due to spontaneous decomposition. For example, some studies on electrochemically formed oxides have been performed under an applied anodic potential.[17,18] Others, however, have estimated a substantial activation energy for thermal decomposition of the oxide. Temperature-programmed desorption (TPD) spectra, for example, indicated an activation energy for the desorption of O_2 from oxide monolayers on Au(111) of 30 kcal/mol (126 kJ/mol).[19] Measurements of surface resistance on thicker films (> 40 Å) gave a lower activation energy for the decomposition of Au_2O_3 (57 kJ/mol) and a half-life at 22 °C of 22 h.[20] This difference may reflect nonlinearity in the relationship between surface resistance and composition or reduction of the film by primary and secondary electrons generated by exposure to x-rays during analysis by XPS in the latter study.[21] In addition, recent examples of supported gold-oxide nanoparticles suggest that this inertness extends to the sub-micron size regime.[22-25]

In Chapter 2, we developed an analytical approach, combining x-ray photoelectron spectroscopy and spectroscopic ellipsometry, to determine the complex refractive index of gold-oxide thin films.[26] Using these data, the thickness of gold-oxide

thin films can be determined easily using ellipsometry, allowing kinetic studies of the decomposition of the films. In this chapter, we examine the relative lability of these films in contact with air and with various condensed phases, in order to determine under what conditions they would remain intact. The results allow the rational choice of solvents and electrolytes for the use of gold oxide, for example as passivation layers for selective formation of SAMs (Chapter 4). Although isolated pieces of data were available in the literature —e.g., its behavior in vacuum,[19] air,[20,27] and a few aqueous solutions,[27] and its fast decomposition (reduction) in ethanol[14]— this chapter provides kinetics data under a range of conditions and provides a practical guide for our use of gold oxide.

3.3 Results and Discussion

Gold electrodes were oxidized electrochemically at 1.2 V (*vs.* 10-mM $AgNO_3$/Ag) in 0.5-M aqueous sulfuric acid to produce thin oxide films having an average ellipsometric thickness of 9 ± 1 Å (calculated using the complex refractive index of gold oxide found in Chapter 2).[7-10,26] The presence of an oxide was confirmed by the appearance of a large cathodic wave in a linear sweep of potential from 0.5 V to -0.2 V in 0.5-M sulfuric acid, corresponding to reduction of the oxide to the metal (Figure 3.1). As also shown in Figure 3.1, this peak is absent from a scan of unoxidized gold. After the initial film thickness was measured, each sample was placed into a separate 20-mL scintillation vial containing air or a test liquid. The thickness of the oxide films was monitored as a function of the amount of time the film was in contact with the ambient

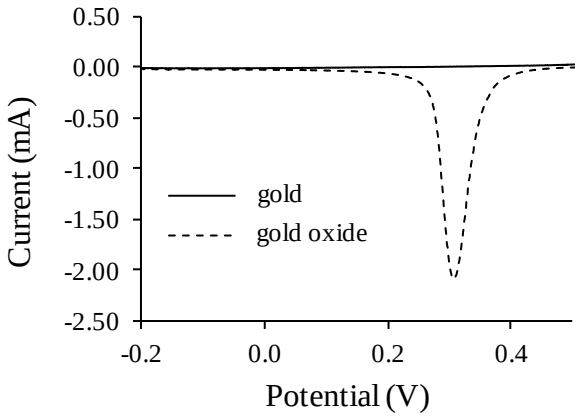

Figure 3.1. Cathodic linear potential sweep (0.1 V/s) in 0.5-M aqueous sulfuric acid of a clean gold electrode (solid line) and an electrochemically oxidized gold electrode (dotted line).

atmosphere, solvents, or electrolyte solutions (Figure 3.2). Initial measurements of the oxide thickness within 5 min of their formation are treated as occurring at t = 0 in our plots of the data. The film thicknesses were monitored by collecting ellipsometric data after removing the sample and rinsing with THF and deionized water (for THF solutions), or with just deionized water (for the water-soaked sample), and drying under a stream of N_2. After each measurement, the samples were placed back into their respective vials. Data were collected at 15-min intervals over the course of an hour, followed by a final measurement after 24 h. These choices reflect the timescale of typical electrochemical experiments. Each experiment was repeated in triplicate, and data are reported as the average of each set of measurements.

3.3.1 Lability in Air and Solvents

Figure 3.4 shows the thickness of oxide films on gold electrodes in contact with air, THF, deionized water, or ethanol. In air, the thickness remained unchanged over the entire 24-h period, which is more consistent with the large activation energy reported from TPD studies[19] than that based on measurements of surface resistance.[20] A low-energy ion scattering (LEIS) spectrum of a sample taken after 1 h of exposure to air confirmed the presence of the oxide layer, revealing peaks due to elastic, binary collisions with both gold and oxygen (Figure 3.5). The large reionization tail on the lower-energy side of the Au peak is consistent with the presence of a thin oxide overlayer at the surface of the sample.[28] A more detailed description of this tail is provided in the Experimental Section.

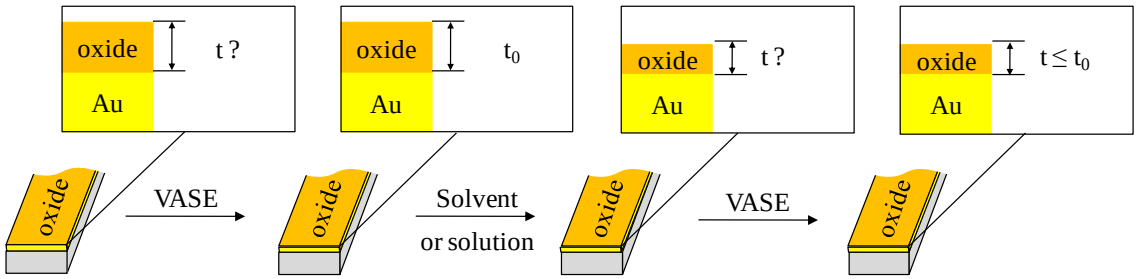

Figure 3.2. Summary of the process used to monitor the lability of gold-oxide thin films. In the first step, the thickness of a newly formed oxide film was measured ellipsometrically. The film was then exposed to air, solvent, or electrolyte solution. In the final step, the oxide film thickness was again measured ellipometrically to determine if any change had occurred as a result of the exposure.

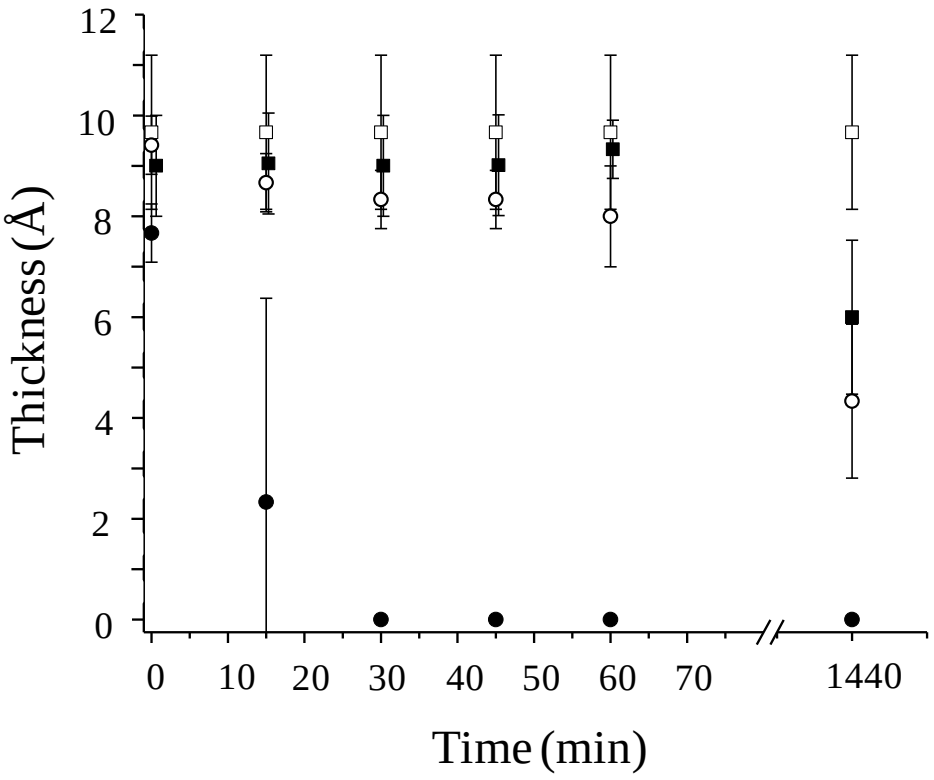

Figure 3.4. Ellipsometric thickness of gold-oxide thin films in air (open square), THF (filled square), water (open circle), and ethanol (filled circle) as a function of time. The values reported are the average of three measurements, and the error bars represent one standard deviation of these measurements. All data were taken at 15-min time intervals; overlapping points have been shifted slightly in the horizontal direction for clarity.

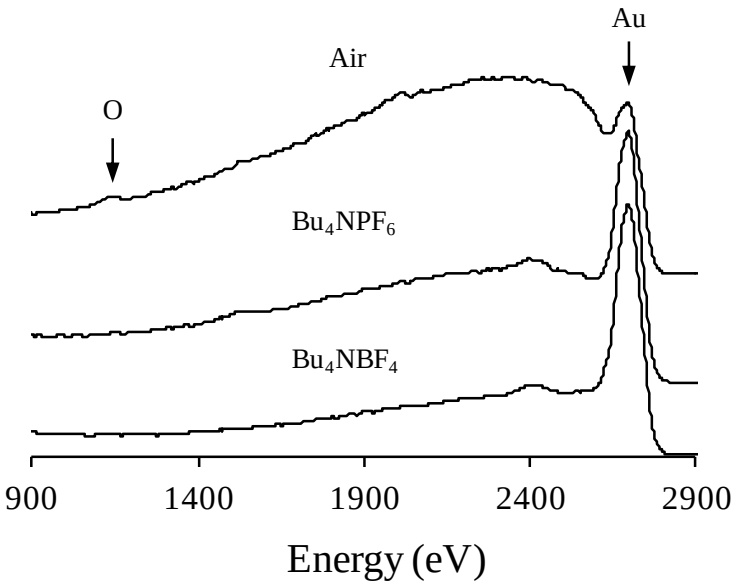

Figure 3.5. Low-energy ion scattering spectra from thin films of gold oxide that had been exposed to air, or solutions of Bu_4NPF_6 or Bu_4NBF_4 in THF for 1 h.

In THF, the film thickness was constant during the first hour of immersion, but decreased by about 33% over the next 23 h. Samples immersed in water behaved similarly, though decomposition occurred at a somewhat faster rate: their thickness decreased slightly during the first hour, but degraded by ~50% over the next 23 h. This behavior is consistent with, but does not demand, the presence of a mixed oxide (e.g., compact and hydrous oxide, α and β, respectively)[10,29,30] having components of differing solubility in water or in THF that contains water adsorbed from the ambient atmosphere. Gold (III) hydroxide, for example, is reported to be soluble in water by formation of complex ions.[31,32] The data in Figure 3.4 also show that ethanol is a sufficiently strong reducing agent to quickly reduce oxide films on gold, consistent with previous reports.[14,15] In this case, the oxide was completely removed within the first 30 min of immersion. Atomic force microscopy indicated little or no change in surface morphology between an electrode surface prior to oxidation and after oxidation and reduction in ethanol, however, an increase in root mean square roughness from 2.0 to 2.6 nm did occur (Figure 3.6).

3.3.2 Lability in Electrolyte Solutions

To examine the behavior of gold oxide under conditions relevant to electrochemical applications, the oxide thickness on gold electrodes was monitored in 0.1-M THF solutions of salts commonly used as supporting electrolytes in organic solvents, Bu_4NClO_4, $LiClO_4$, Bu_4NBF_4, and Bu_4NPF_6 (Figure 3.7). Consistent with the results for pure THF, films immersed in each of the electrolyte solutions decreased in

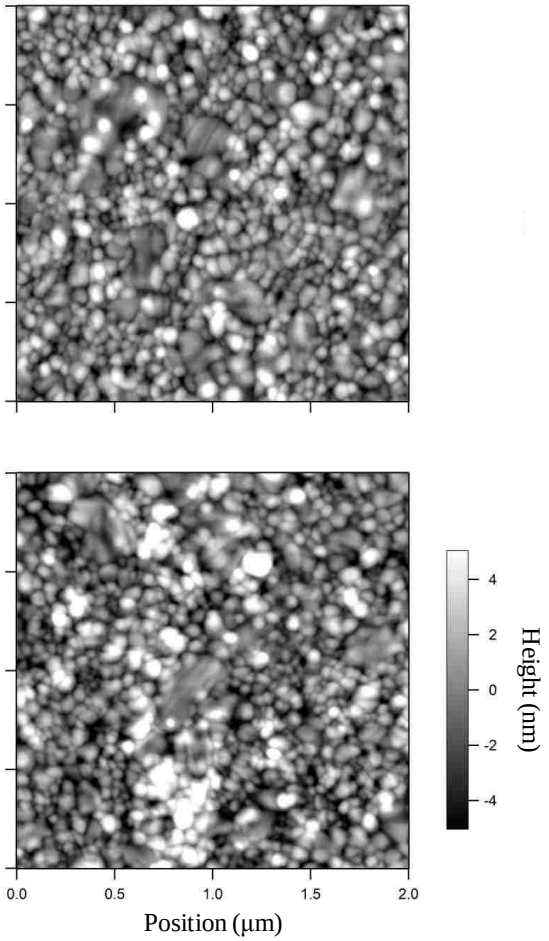

Figure 3.6. (Top) Atomic force micrograph of a gold electrode surface after cleaning by cycling its potential seven times from -0.9 V to 1.2 V in 0.5-M aqueous sulfuric acid. (Bottom) Atomic force micrograph image of the same gold electrode after oxidation at 1.2 V (10 s) in 0.5-M aqueous sulfuric acid, followed by reduction in ethanol (30 min).

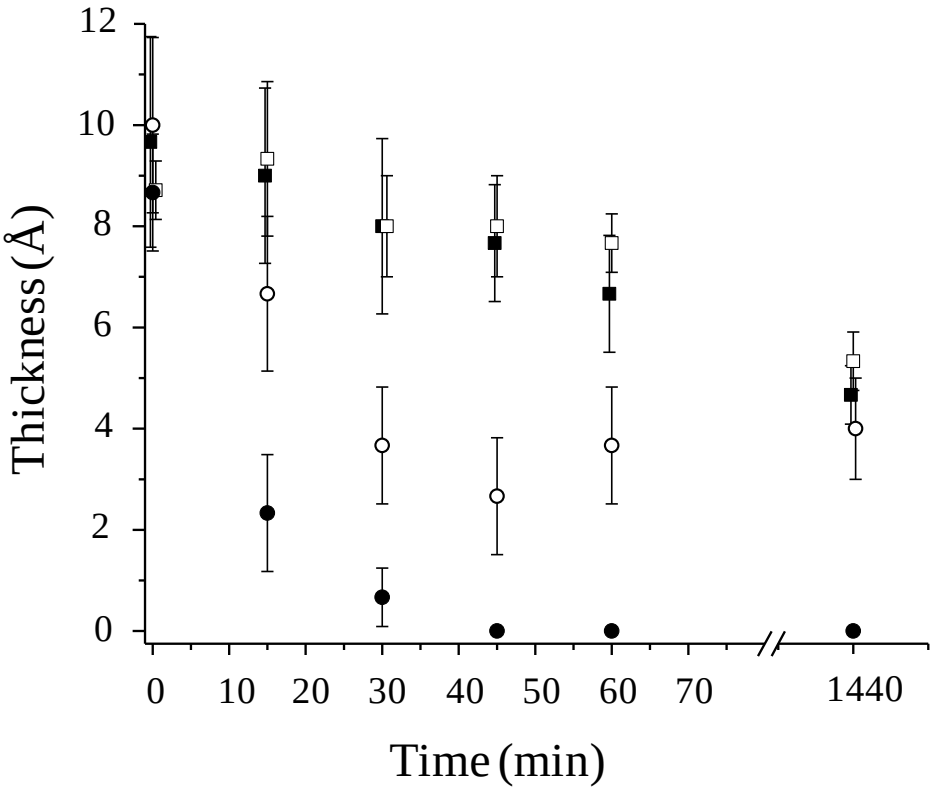

Figure 3.7. Ellipsometric thickness of gold-oxide thin films in THF solutions of Bu_4NClO_4 (open square), $LiClO_4$ (filled square), Bu_4NPF_6 (open circle), and Bu_4NBF_4 (filled circle) as a function of time. The values reported are the average of three measurements, and the error bars represent the standard deviation of these measurements. All data were taken at 15-min time intervals; overlapping points have been shifted slightly in the horizontal direction for clarity.

thickness significantly over 24 h, though there were large differences in both rate and extent of decomposition. The oxide was most inert in solutions of the perchlorate salts, for which the film thickness gradually degraded somewhat (by 10-30%) during the first hour and ultimately lost 40-50% of its thickness over the 24-h period.

In stark contrast to the perchlorate results, the solution containing tetrafluoroborate ion caused complete loss of the oxide film within 30-45 min. This behavior was confirmed with LEIS: the spectrum of a sample immersed in a solution of tetra-*n*-butyl ammonium tetrafluoroborate for 1 h showed a large peak due to gold, and no peak due to oxygen (Figure 3.5). These results, as well as the low intensity of the low-energy tail, suggest the lack of an oxide overlayer on this sample. The accelerated decomposition in this solution may reflect etching of the oxide by HF (equation 3.1),[33]

$$Au(OH)_x\ (s) + HF\ (soln) \rightleftharpoons Au^{3+}(soln) + F^-\ (soln) + x\ H_2O\ (l) \qquad (3.1)$$

which could be formed by hydrolysis of tetrafluoroborate ion.[34] Although the THF used in these experiments was initially dry, the solutions were handled in air and thus contained small amounts of water that could lead to hydrolysis.

For comparison, the behavior of samples in solutions containing hexafluorophosphate ion was intermediate between those in solutions of perchlorate and tetrafluoroborate salts. Their thickness fell by more than 50% during the first 30-45 min, but remained relatively constant thereafter. As shown in Figure 3.5, a sample immersed in a solution of tetra-*n*-butyl ammonium hexafluorophosphate ion solution for 1 h and analyzed by LEIS indicated a much-diminished oxide layer. The spectrum contained a prominent peak due to gold and only a hint of oxygen. The larger intensity of the low-energy tail, relative to that of the sample exposed to tetrafluoroborate ion, is consistent

with the presence of at least a partial oxide layer at the surface. The slower decomposition in the presence of PF_6^-, relative to BF_4^-, is consistent with the lower susceptibility of the former to hydrolysis. The equilibrium constant for hydrolysis of PF_6^- in water, for example, is 1.5×10^{-15} at 25 °C, whereas that of BF_4^- is 2.7×10^{-3} at 30 °C.[35,36] To the extent that this difference in reactivity may be reflected in wet THF, it could influence the concentration of HF available to etch the oxide.

3.4 Conclusions

In summary, the lability of gold-oxide thin films varies significantly in different environments. The thickness of these films remain unchanged in air for at least 24 hours, though significant decomposition occurred over the same period upon immersion in pure solvents, water or THF. In ethanol, a mild reducing agent, the oxide was quickly reduced to the metal. The behavior in electrolyte solutions depended strongly on the anion of the electrolyte. Fluorine-containing ions had the strongest effect on film thickness. Solutions of Bu_4NPF_6 in THF caused a significant decrease of the oxide film thickness in less than an hour, and solutions of Bu_4NBF_4 caused complete decomposition within 45 min. The action of these solutions, as well as the difference between them, may reflect the susceptibility of the anions to hydrolysis to produce HF. Oxide films were more inert in solutions of Bu_4NClO_4 or $LiClO_4$ in THF, making these electrolytes better candidates for short-term electrochemical experiments involving gold oxide. For this reason, we used $LiClO_4$ solutions in THF for our studies in this dissertation.

3.5 Experimental

General. Silver nitrate (99.8%) and tetrabutylammonium perchlorate (Bu_4NClO_4, 99.9995%) were used as received from Fisher Scientific. Ethanol (Anhydrous, J.T. Baker, 95%) was used as received. Tetrahydrofuran (THF, Mallinckrodt, 99%) was purified and dried using a Pure Solv system (Innovative Technology, Inc.). Hydrogen peroxide (30%), and sulfuric acid (95%) were used as received from EMD. Gold (99.999%) was used as supplied by VEM Vacuum Engineering. Lithium perchlorate ($LiClO_4$, anhydrous, Alfa-Aesar, 99%), tetrabutylammonium tetrafluoroborate (Bu_4NBF_4, TCI, 98%), and tetrabutylammonium hexafluorophosphate (Bu_4NPF_6, Adlrich, 98%) were used as received. Water was purified with a Millipore Simplicity® UV system (18.1 MΩ·cm).

Electrochemical Formation of Gold oxide. Gold electrodes were prepared on ~ 1-cm x 2-cm glass slides that had been cleaned using piranha solution. *Caution: Piranha solution, a 4:1 (v/v) mixture of concentrated H_2SO_4 and 30% H_2O_2, reacts violently with organic material and should be handled carefully.* Approximately 150 Å of Ti (as an adhesion promoter) and then 1500 Å of Au were deposited at a rate of ~ 3.4 Å/s onto the substrates by e-beam evaporation. Prior to use in experiments, gold electrodes were cleaned by cycling their potential seven times from -0.9 V to 1.2 V in 0.5-M aqueous sulfuric acid.

A thin film of gold oxide was produced electrochemically in 0.5-M aqueous sulfuric acid using a standard three-electrode cell comprising a gold working electrode, a platinum wire as the counter-electrode, and an aqueous $Ag/AgNO_3$ (10 mM) reference electrode. To oxidize each electrode, its potential was held at -0.2 V for 10 s, followed by

1.2 V for 10 s. The sample was then rinsed with deionized water (18.1 MΩ·cm) and dried under a stream of N_2.

Variable Angle Spectroscopic Ellipsometry (VASE). Ellipsometric parameters, Ψ and Δ, were measured using a J.A. Woollam V-VASE variable-angle spectroscopic ellipsometer. Data were collected at a single spot on each sample between 350 and 800 nm at 50-nm intervals with angles of incidence of 60° and 70°. Film thicknesses were determined by fitting these parameters to an optical model using WVASE32® analysis software. The model consisted of a gold substrate of optically infinite thickness coated in a thin film of gold oxide of undetermined thickness and having the values of n and k determined in Chapter 2.[26] The software solves for a consistent thickness of gold oxide corresponding to the measured values of Ψ and Δ for each sample. The optical constants of our bare gold electrodes were determined after electrochemical cleaning, and prior to their oxidation

Low Energy Ion Scattering (LEIS). Spectra of samples that had been exposed to air, solvent, or solutions of interest were generated using an ION-TOF Qtac 100 instrument. An iridium filament was used to produce a beam of He^+ ions with 3000 eV of kinetic energy. The ion beam struck the surface of the sample at normal incidence, and scattered ions were collected at an angle of 55°. The energies of the scattered ions were measured using an azimuthal detector operating with a pass energy of 3000 eV. Samples were analyzed under an ion current of 1.22×10^{-2} μA, with the beam rastered over a square region 2000 μm across, to give a total ion dose of 1.88×10^{14} cm^{-2} for a single scan.

Each scan sputters away a fraction of the atoms at the surface, so initially, contaminants adsorbed from the air are removed to reveal the underlying material of interest. Surface contamination or overlayers (e.g., oxides) can lead to more efficient reionization of scattered He atoms that were neutralized during inelastic collisions with the sample. These ions appear as a "tail" of intensity on the lower-energy side of peaks due to elastic, binary collisions. As such, the intensity of this tail can be used as a qualitative measure of the amount of contamination or oxide on the sample surface. We therefore monitored the intensity of the low-energy tail after successive scans until the change from scan to scan was (qualitatively) small and peaks due to elastic binary collisions with the ion beam were observed. At this point, we considered the last scan to best represent the composition of the uncontaminated surface. To minimize the removal of any oxide during this process, we also monitored the region of the spectrum (~ 1140 eV) where ions scattered elastically from single collisions with oxygen on the surface would be expected. The eighth scan is reported for the samples aged either in air or in a solution containing tetrafluoroborate ion, whereas the fifth scan is reported for the sample exposed to a solution containing hexafluorophosphate ion.

Atomic Force Microscopy. An Asylum Research MFP 3D-BIO atomic force microscope was used to generate lateral-force images of each surface. Data were collected over an area of 2 μm^2 in tapping mode using an AppNano ACTA probe operating at a scan rate of 2 Hz and at an angle of 90°, with respect to the surface.

3.6 Acknowledgements

We gratefully acknowledge the National Science Foundation for support of this research (CHE-0749777) and for funding to purchase the spectroscopic ellipsometer (CHE-0923370). We thank Lehigh University for support in the form of a Hornor Fellowship for KMC. We also thank Kyle Wagner for his assistance in obtaining AFM images.

3.7 References and Notes

1. Although the term "thermodynamically (un)stable" is redundant, we nonetheless use it, and related constructions, to provide as sharp a distinction as possible between the thermodynamic terms, stable and unstable, and the kinetic terms, inert and labile.
2. Gerke, R. H.; Rourke, M. D., The Potential of the Gold-auric Oxide Electrode. *J. Am. Chem. Soc.* **1927,** *49*, 1855-1858.
3. Alves, L.; Ballesteros, B.; Boronat, M.; Cabrero-Antonino, J. R.; Concepción, P.; Corma, A.; Correa-Duarte, M. A.; Mendoza, E., Synthesis and Stabilization of Subnanometric Gold Oxide Nanoparticles on Multiwalled Carbon Nanotubes and Their Catalytic Activity. *J. Am. Chem. Soc.* **2011,** *133* (26), 10251-10261.
4. Johnson, G. E.; Reilly, N. M.; Tyo, E. C.; Castleman, A. W., Gas-phase Reactivity of Gold Oxide Cluster Cations with CO. *J. Phys. Chem. C* **2008,** *112* (26), 9730-9736.
5. Bürgel, C.; Reilly, N. M.; Johnson, G. E.; Mitrić, R.; Kimble, M. L.; Castleman, A. W.; Bonačic-Koutecký, V., Influence of Charge State on the Mechanism of CO Oxidation on Gold Clusters. *J. Am. Chem. Soc.* **2008,** *130* (5), 1694-1698.
6. Hore, S.; Kaiser, G.; Hu, Y. S.; Schulz, A.; Konuma, M.; Götz, G.; Sigle, W.; Verhoeven, A.; Maier, J., Carbonization of Polyethylene on Gold Oxide. *J. Mater. Chem.* **2008,** *18* (46), 5589-5591.
7. Vela, M. E.; Zerbino, J. O.; Arvia, A. J., Ellipsometric Study of Hydrous Gold Oxide Layers and Gold Surfaces Resulting From their Electroreduction. *Thin Solid Films* **1993,** *233* (1-2), 82-85.
8. Kolb, D. M.; McIntyre, J. D., Spectrophotometric Determination of Optical Properties of an Adsorbed Oxygen Layer on Gold. *Surf. Sci.* **1971,** *28* (1), 321-334.
9. Juodkazis, K.; Juodkazytė, J.; Jasulaitienė, V.; Lukinskas, A.; Šebeka, B., XPS Studies on the Gold Oxide Surface Layer Formation. *Electrochem. Commun.* **2000,** *2* (7), 503-507.

10. Tremiliosi-Filho, G.; Dall'Antonia, L. H.; Jerkiewicz, G., Growth of Surface Oxides on Gold Electrodes Under Well-defined Potential, Time and Temperature Conditions. *J. Electroanal. Chem.* **2005,** *578* (1), 1-8.
11. Ron, H.; Rubinstein, I., Alkanethiol Monolayers on Preoxidized Gold - Encapsulation of Gold Oxide Under an Organic Layer. *Langmuir* **1994,** *10* (12), 4566-4573.
12. Pireaux, J. J.; Liehr, M.; Thiry, P. A.; Delrue, J. P.; Caudano, R., Electron Spectroscopic Characterization of Oxygen-adsorption on Gold Surfaces. 2. Production of Gold Oxide in DC Reactive Sputtering. *Surf. Sci.* **1984,** *141* (1), 221-232.
13. Sondag-Huethorst, J. A. M.; Fokkink, L. G. J., Potential-dependent Wetting of Octadecanethiol-modified Polycrystalline Gold Electrodes. *Langmuir* **1992,** *8* (10), 2560-2566.
14. Ron, H.; Matlis, S.; Rubinstein, I., Self-assembled Monolayers on Oxidized Metals. 2. Gold Surface Oxidative Pretreatment, Monolayer Properties, and Depression Formation. *Langmuir* **1998,** *14* (5), 1116-1121.
15. Cook, K. M.; Ferguson, G. S., Gold Oxide as a Protecting Group for Regioselective Surface Chemistry. *Chem. Commun.* **2011,** *47* (46), 12550-12552.
16. Tian, M.; Pell, W. G.; Conway, B. E., EQCN Study of Anodic Dissolution and Surface Oxide Film Formation at Au in the Presence of Cl^- or Br^- Ions: A Model Process for Corrosion Studies. *Corr. Sci.* **2008,** *50* (9), 2682-2690.
17. Sirohi, R. S.; Genshaw, M. A., Electrochemical Ellipsometric Study of Gold. *J. Electrochem. Soc.* **1969,** *116* (7), 910-914.
18. Ohtsuka, T., Precise Determination of Thickness and Optical-constant of Oxide Layer on Gold by 3-Parameter Ellipsometry. *Denki Kagaku* **1992,** *60* (12), 1123-1129.
19. Saliba, N.; Parker, D. H.; Koel, B. E., Adsorption of Oxygen on Au(111) by Exposure to Ozone. *Surf. Sci.* **1998,** *410* (2-3), 270-282.
20. Tsai, H. C.; Hu, E.; Perng, K.; Chen, M. K.; Wu, J. C.; Chang, Y. S., Instability of Gold Oxide Au_2O_3. *Surf. Sci.* **2003,** *537* (1-3), L447-L450.
21. Dickinson, T.; Povey, A. F.; Sherwood, P. M. A., X-ray Photoelectron Spectroscopic Studies of Oxide Films on Platinum and Gold Electrodes. *J. Chem. Soc., Faraday Trans. 1* **1975,** *71* (0), 298-311.
22. Ono, L. K.; Cuenya, B. R., Formation and Thermal Stability of Au_2O_3 on Gold Nanoparticles: Size and Support Effects. *J. Phys. Chem. C* **2008,** *112* (12), 4676-4686.
23. Goldys, E. M.; Sobhan, M. A., Fluorescence of Colloidal Gold Nanoparticles is Controlled by the Surface Adsorbate. *Adv. Funct. Mater.* **2012,** *22* (9), 1906-1913.
24. Riabinina, D.; Zhang, J. M.; Chaker, M.; Margot, J.; Ma, D. L.; Tijssen, P., Control of Plasmon Resonance of Gold Nanoparticles via Excimer Laser Irradiation. *Appl. Phys. A-Mater.* **2011,** *102* (1), 153-160.
25. Ono, L. K.; Cuenya, B. R., Size Effects on the Desorption of O(2) from Au(2)O(3)/Au(0) Nanoparticles Supported on SiO(2): A TPD Study. *J. Phys. Chem. C* **2008,** *112* (47), 18543-18550.

26. Cook, K. M.; Ferguson, G. S., Determination of the Wavelength-dependent Refractive Index of a Gold-Oxide Thin Film. *J. Phys. Chem. C* **2011,** *115* (46), 22976-22980.
27. Tabor, R. F.; Morfa, A. J.; Grieser, F.; Chan, D. Y. C.; Dagastine, R. R., Effect of Gold Oxide in Measurements of Colloidal Force. *Langmuir* **2011,** *27* (10), 6026-6030.
28. Brongersma, H. H.; Draxler, M.; de Ridder, M.; Bauer, P., Surface Composition Analysis by Low-energy Ion Scattering. *Surf. Sci. Rep.* **2007,** *62* (3), 63-109.
29. Petrović, Ž.; Metikoš-Huković, M.; Babić, R.; Katić, J.; Milun, M., A Multi-technique Study of Gold Oxidation and Semiconducting Properties of the Compact Alpha-oxide Layer. *J. Electroanal. Chem.* **2009,** *629* (1-2), 43-49.
30. Xia, S. J.; Birss, V. I., A Multi-technique Study of Compact and Hydrous Au Oxide Growth in 0.1 M Sulfuric Acid Solutions. *J. Electroanal. Chem.* **2001,** *500* (1-2), 562-573.
31. Johnston, H. L.; Leland, H. L., The Solubility of Gold Hydroxide in Alkali and Equilibria in the Saturated Solutions. *J. Am. Chem. Soc.* **1938,** *60* (6), 1439-1445.
32. Vlassopoulos, D.; Wood, S. A., Gold Speciation in Natural Waters: I. Solubility and Hydrolysis Reactions of Gold in Aqueous Solution. *Geochim. Cosmochim. Acta* **1990,** *54* (1), 3-12.
33. Fang, C.; Bandaru, N. M.; Ellis, A. V.; Voelcker, N. H., Electrochemical Fabrication of Nanoporous Gold. *J. Mater. Chem.* **2012,** *22*, 2952-2957.
34. Anbar, M.; Guttmann, S., The Isotopic Exchange of Fluoroboric Acid with Hydrofluoric Acid. *J. Phys. Chem.* **1960,** *64* (12), 1896-1899.
35. Plakhotnik, V. N.; Varekh, V. V., Hydrolysis of Nickel Tetrafluoroborate. *Zh. Fiz. Khim.* **1972,** *46* (12), 3126-9.
36. Shamakhova, N. N.; Plakhotnik, V. N.; Il'in, E. G., Stepwise Complexation in Aqueous Fluorophosphorus Systems. *Koord. Khim.* **1989,** *15* (11), 1504-9.

Chapter 4

Gold Oxide as a Protecting Group for Regioselective Surface Chemistry

This chapter includes material that has been reproduced in part with permission from The Royal Society of Chemistry: Cook, K. M.; Ferguson, G.S.; *Chemical Communications* **2011**, *47(46)*, 12550-12552

4.1 Abstract

Selective modification of electrode surfaces is a vital step in the development of practical applications of self-assembled monolayers (SAMs). In this chapter, a protection-deprotection approach similar to that commonly utilized in organic synthesis was used to direct self-assembly on one gold electrode in the presence of another. Gold oxide was used as the protecting layer, which prevented spontaneous adsorption of dialkyl disulfide on the protected electrode. A neighboring unprotected electrode could then be modified regioselectively by adsorption of a SAM. Analysis of electrodes at each step by x-ray photoelectron spectroscopy (XPS) was used to characterize the process and revealed the presence of monolayers only on electrodes where assembly was directed. The wetting behavior and ellipsometric thicknesses of these SAMs were also consistent with directed assembly of SAMs on individual electrodes.

4.2 Introduction

Spontaneous formation of self-assembled monolayers (SAMs) of organosulfur compounds is a convenient route to the uniform modification of gold surfaces.[1] Some applications (e.g. sensors, photovoltaics, microelectronics, and diagnostic chips), however, require selective modification only on specific regions of a substrate.[2] As

discussed in Chapter 1, methods have been developed to print patterns of SAMs on uniform substrates,[1-3] as well as to modify particular features selectively on pre-patterned substrates (e.g., electrode arrays).[1,4-10] This chapter describes our development of a facile electrochemical method using gold oxide as a protecting layer to allow the directed self-assembly of monolayers from dialkyl disulfides on selected gold electrodes. This approach integrates the well-established ‘‘protection–deprotection’’ strategy used successfully by synthetic organic chemists for decades into an electrochemical method with potentially broad applicability for the regiochemical control of surface structure. This approach complements our previous work on the site-selective formation of SAMs from alkyl thiosulfates and may provide a route to ω-functionality (e.g. hydroxyl, vinyl) not amenable to that method.[11-14]

The work described in this chapter builds on that in Chapters 2 and 3. In Chapter 2, a thin film of electrochemically formed gold oxide was characterized by a combination of XPS and spectroscopic ellipsometry to determine its composition and to find its complex refractive index over the visible range of wavelengths. Those data allowed us to monitor the lability of these thin films ellipsometrically when they were exposed to various solvents and supporting electrolytes, thereby establishing conditions under which the films are inert over a timeframe suitable for the experiments described in this chapter.

4.3 Results and Discussion

Previously, Rubinstein and coworkers demonstrated that although dialkyl disulfides spontaneously adsorb on gold to form SAMs, they do not adsorb on oxidized gold.[15-17] This behavior contrasts with that of alkanethiols, which form SAMs on both

gold and gold oxide, presumably by initial reduction of the latter to produce elemental gold followed by adsorption.[17-21] The inherent difference in the reactivity of disulfides with gold and gold oxide, coupled with the ease of formation and removal of oxide coatings on gold, offered a convenient strategy for differentiating electrodes in an array. The approach would be analogous to protection–deprotection sequences common in synthetic organic chemistry, for example in the use of silyl groups to temporarily block reactivity at a protected hydroxyl group.[22] The gold/gold oxide/disulfide system also served as an appropriate target because it would extend the types of precursors that can be used for the regioselective formation of SAMs and because dialkyl disulfides exchange much more slowly than alkanethiols with pre-formed monolayers.[23]

In preliminary studies, we examined whether reduction of a gold oxide thin film could be done concurrently with adsorption of a SAM on the same electrode. In these experiments, pulsed voltammetry was performed on an oxidized gold electrode in a solution containing dihexadecyl disulfide (1 mM, Figure 4.1, top) as an adsorbate and $LiClO_4$ (0.1 M) as a supporting electrolyte in tetrahydrofuran (THF). Trace H_2O in the solvent would need to serve as a source of protons in this system. The electrode potential was stepped from + 0.3 V to a reductive potential (*vs.* $Ag/AgNO_3$, 3 mM in acetonitrile), with 5 s at each potential. To optimize conditions for reduction/SAM formation, the reductive potential (-0.3 – -1.2 V) and number of pulses (10 – 60) were varied. In each case, however, the resulting surfaces were wet by hexadecane, indicating the lack of a SAM. Ellipsometric measurements indicated that the gold oxide was still present on the electrode after even sixty pulses from + 0.3 V to -0.9 V, as well as after forty such pulses

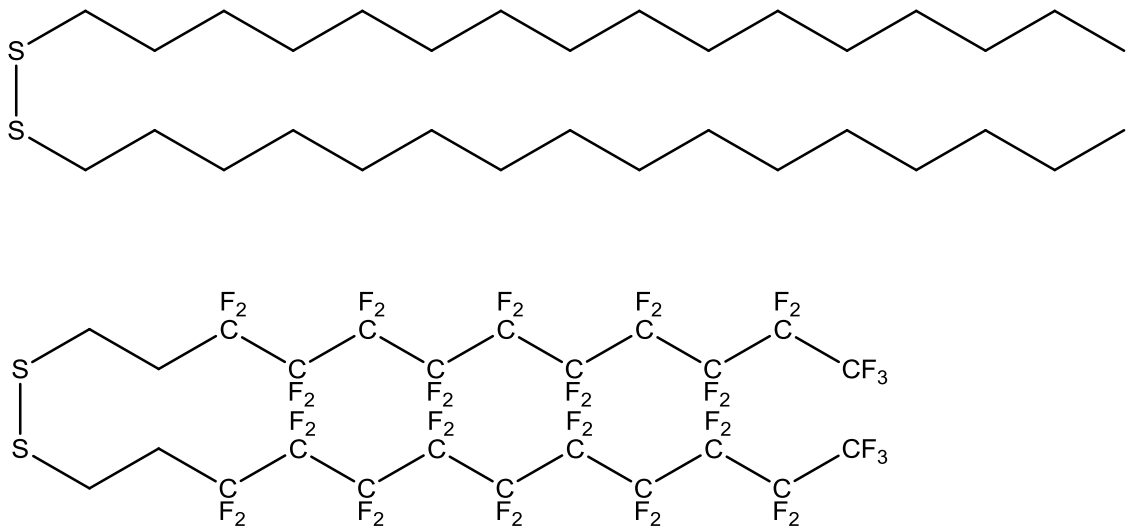

Figure 4.1. The molecules used in the regioselective surface modification of gold electrodes. At top, dihexadecyl disulfide, $[CH_3(CH_2)_{15}S]_2$. At bottom, $[CF_3(CF_2)_9(CH_2)_2S]_2$.

from + 0.3 V to -1.2 V. Therefore, we concluded that the oxide layer could not be reduced under these conditions, and that the protective oxide must be reduced prior to SAM formation.

To test this "protection-deprotection" approach, we used glass substrates bearing two independently addressable gold electrodes. As shown schematically in Figure 4.2, both electrodes initially represented viable sites for chemisorption of disulfide. Oxidation of one of these electrodes produced an oxide coating that rendered it inert to chemisorption, so a monolayer could be adsorbed on the other electrode selectively. After this adsorption step, the first electrode could be deprotected, regenerating a bare gold substrate, onto which a second, distinguishable monolayer could be adsorbed. As discussed in Chapter 1, gold oxide can be produced electrochemically, by application of an anodic potential in sulfuric acid, and the nature of the oxide can be controlled by the particular potential used.[24-26]

Although gold oxide is thermodynamically unstable, as discussed in Chapter 3, films formed in this way are (kinetically) inert over the timescale of the experiments described in this chapter.[18,27,28] In these studies, gold oxide was produced electrochemically in 0.5-M sulfuric acid using a standard three-electrode cell comprising a gold working electrode, a platinum wire as the counter-electrode, and an aqueous $Ag/AgNO_3$ (10 mM) reference electrode. To oxidize electrode 1 (Figure 4.2), its potential was held at -0.2 V for 10 s, followed by 1.2 V for 10 s. The sample was then rinsed with deionized water (18.1 $M\Omega \cdot cm$) and dried under a stream of N_2.

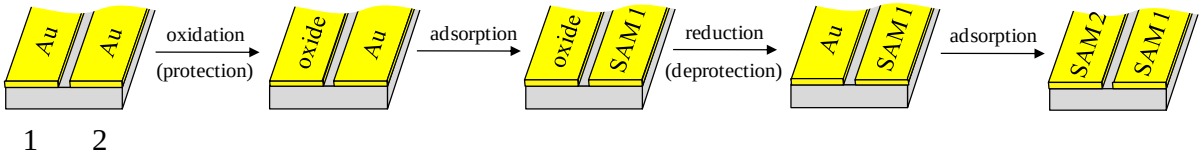

Figure 4.2. Schematic representation of a protection-deprotection approach to the selective, sequential modification of neighboring gold electrodes. In the first step, electrode 1 is oxidized electrochemically, which allows electrode 2 to be modified selectively. The oxide on electrode 1 is then reduced to regenerate the bare gold surface, and a second SAM is adsorbed on it. For clarity, the thicknesses of the gold electrodes and glass substrates are not drawn to scale.

A detailed discussion of gold oxide formed in this manner was given in Chapter 2, but a brief synopsis will be given here. Analysis by X-ray photoelectron spectroscopy (XPS) confirmed the addition of an oxide coating. A survey scan revealed the presence of gold, oxygen and a small amount of carbon (contamination). A high resolution spectrum in the Au 4f region contained both narrow peaks (fwhm, 0.7 eV) due to elemental gold (84.0 eV, $4f_{7/2}$; 87.7 eV, $4f_{5/2}$) and broad peaks (fwhm, 1.3 eV) consistent with a mixed oxide (~85.7 eV, $4f_{7/2}$; 89.4 eV, $4f_{5/2}$).[25,26,29-31,32] A high resolution spectrum in the oxygen 1s region contained a broad peak that could be fit with four components at 529.3, 530.1, 531.1, and 532.5 eV. These binding energies are similar to those reported for gold oxide grown by pulsed-laser deposition and are consistent with a mixed oxide containing both oxo and hydroxyl species.[28-30,33,34] The ratio of Au^{3+} to oxygen in this sample was 38 : 62, very close to that expected for Au_2O_3 (40 : 60).

To accelerate formation of a SAM on the *unmodified* electrode (**2**, Figure 4.2),[17] its potential was stepped from 0.3 V to -0.9 V, with 5 s at each potential, in the presence of dihexadecyl disulfide. This method reduced the time required to accomplish the synthetic sequence, and thus minimized decomposition of the protective gold oxide film on the adjacent electrode, **1**. Forty voltammetric pulses were applied to electrode **2** in a solution containing dihexadecyl disulfide (1 mM) and $LiClO_4$ (0.1 M) in THF. In optimization studies, we found that this combination of limiting potentials and number of pulses gave the highest quality monolayers. A schematic diagram of this electrochemical cell is provided in Figure 4.3, and typical plots of potential and current *versus* time are shown in Figure 4.4. As outlined in Chapter 3, $LiClO_4$ was found to be an ideal

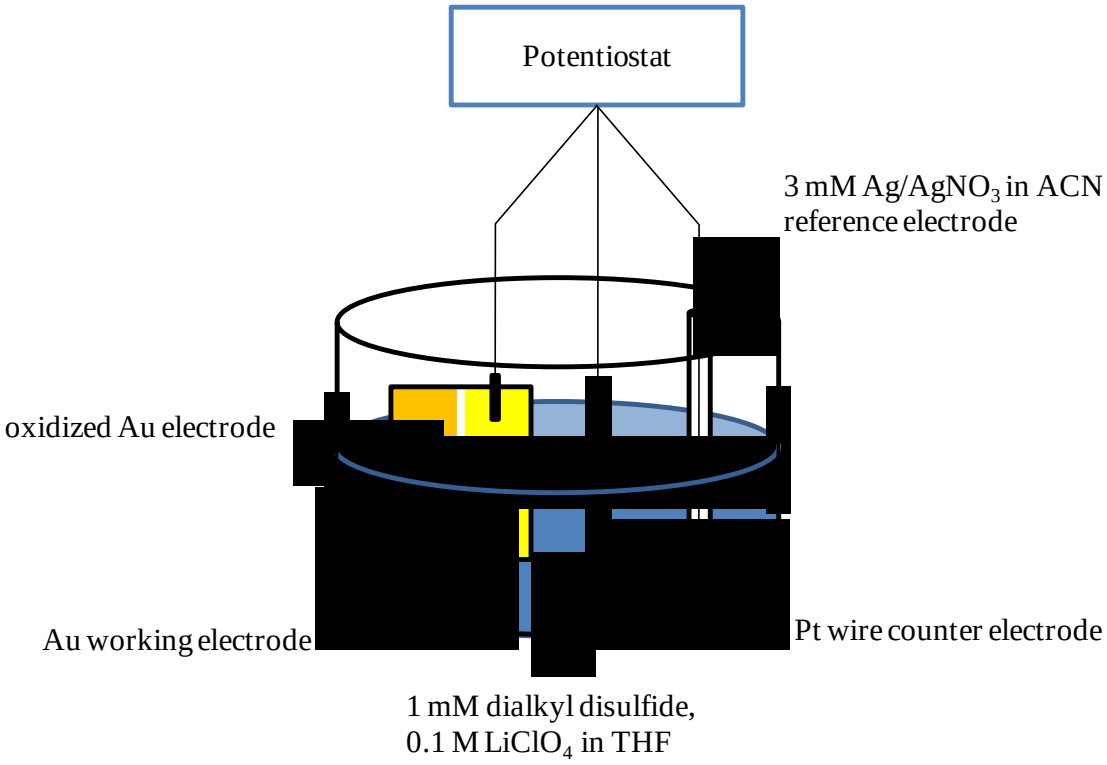

Figure 4.3. Schematic diagram of the electrochemical cell used to form SAMs on a gold electrode adjacent to an oxidized gold electrode.

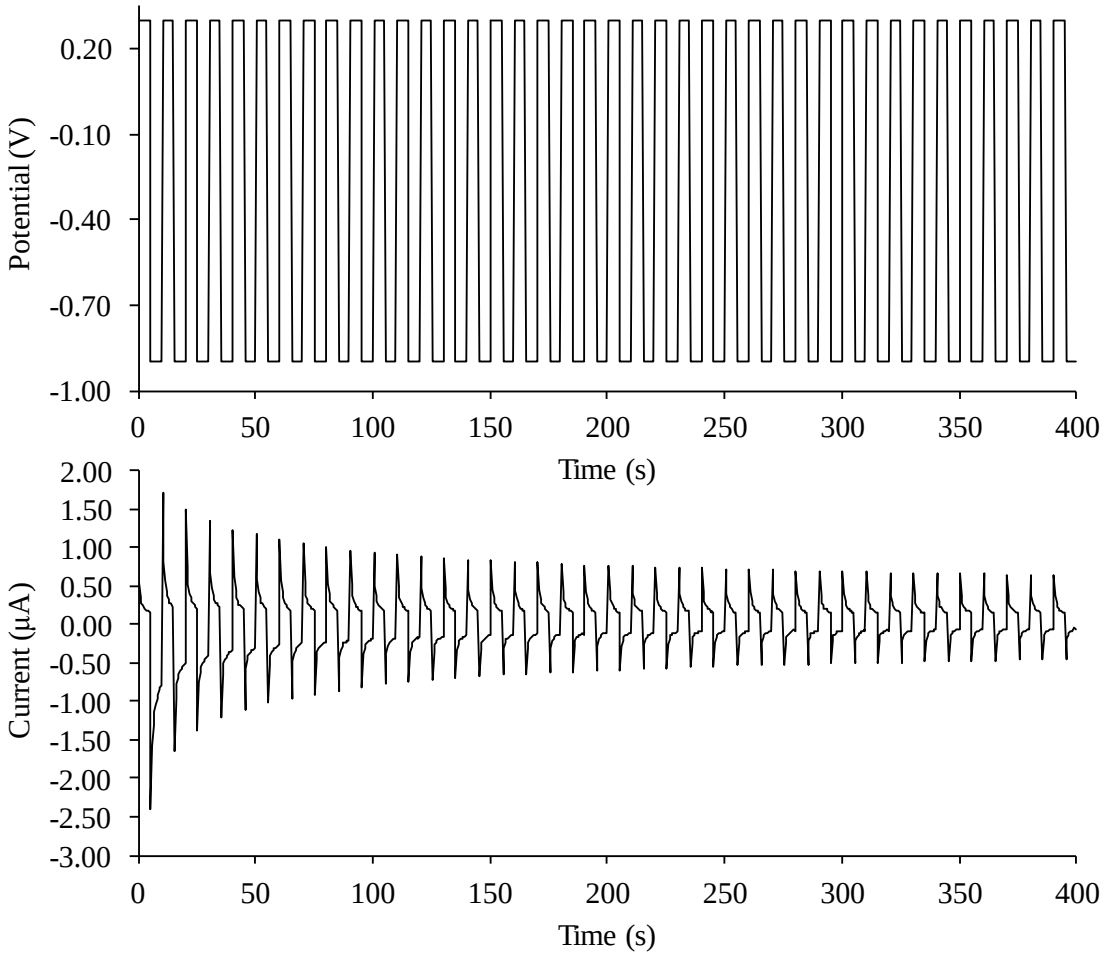

Figure 4.4. Typical plots of potential (top) and current (bottom) *versus* time for the accelerated formation of a SAM from dihexadecyl disulfide.

supporting electrolyte for these studies, as gold-oxide films were stable in THF solutions of this salt within the timeframe of our experiments.

The sample was then removed from solution, rinsed with THF, and water, and dried under a stream of N_2. The contact angles of hexadecane (θ_a, 48°; θ_r 43°) and of water (θ_a, 112°; θ_r 97°), as well as the ellipsometric thickness (16 Å), were consistent with formation of an ordered monolayer film on the surface.[13,35,36] The contact angles of hexadecane (wetting) and water (55°) on the oxidized electrode **1** indicated that a SAM had not adsorbed on this surface. Ellipsometry also indicated the continued presence of the oxide coating.[33]

High-resolution XPS spectra in the Au 4f region confirmed that electrode **2** remained in a reduced state after this step (Figure 4.5 c). A slight reduction of the oxide film on electrically isolated electrode **1** occurred, consistent with our studies of this system presented in Chapter 3. To determine the selectivity of SAM formation, high-resolution spectra were also collected in the sulfur 2p region (Figure 4.6 a), and these data revealed the presence of thiolate only on electrode **2** (162.1 eV, S $2p_{3/2}$; 163.3 eV, S $2p_{1/2}$), consistent with SAM formation only on that electrode.[37] Weak photoemission intensity centered at ~167.5 eV for electrode **1** is consistent with a small amount of sulfate at the surface of the electrode, presumably from the solution in which that electrode was oxidized.[38] Subsequent treatment of electrode **1** in ethanol (Figures 4.5 d and 4.6 b) reduced the oxide on that electrode (84.0 eV, Au $4f_{7/2}$; 87.6, Au $4f_{5/2}$), while the SAM on electrode **2** remained intact (84.0 eV, Au $4f_{7/2}$; 87.6, Au $4f_{5/2}$; 162.0 eV, S $2p_{3/2}$; 163.3 eV, S $2p_{1/2}$). A SAM was then adsorbed on electrode **1** by stepping its

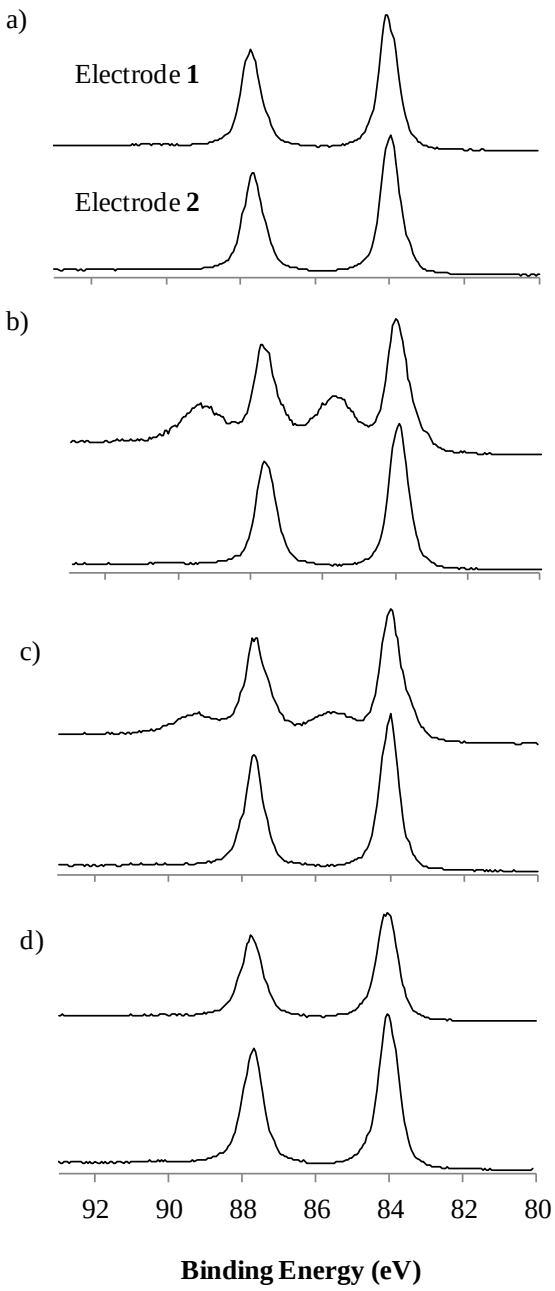

Figure 4.5. High resolution x-ray photoelectron spectra of electrodes **1** and **2** in the Au 4f region: a) both electrodes unmodified; b) after electrochemical oxidation of electrode **1**; c) after adsorption of a SAM on electrode **2** from $(C_{16}H_{33}S)_2$; and d) after reduction of the oxide coating on electrode **1**. Spectra were referenced to the Au $4f_{7/2}$ peak, set at 84.0 eV, and intensities normalized to the largest Au $4f_{7/2}$ peak.

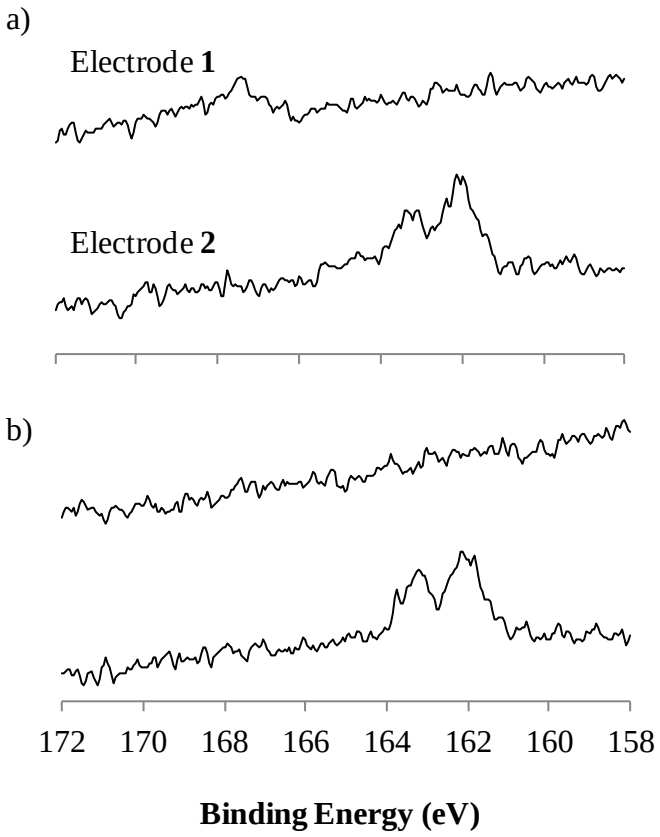

Figure 4.6. High resolution x-ray photoelectron spectra of electrodes **1** and **2** in the sulfur 2p region: a) after adsorption of a SAM on electrode **2** from $(C_{16}H_{33}S)_2$; and b) after reduction of the oxide on electrode **1**. Intensities were normalized to the largest sulfur $2p_{3/2}$ peak.

potential from 0.3 V to -0.9 V, with 5 s at each potential, in the presence of $[CF_3(CF_2)_9(CH_2)_2S]_2$ (Figure 4.1, bottom). The contact angles of hexadecane (80°) and water (121°), as well as the ellipsometric thickness (9 Å), on this electrode indicated the presence of a fluorinated SAM.[13,39] The contact angles and ellipsometric thickness of the dihexadecyl disulfide SAM on electrode **2** remained the same as before the adsorption of a SAM on electrode **1**.

High resolution XPS spectra in the S 2p region verified the presence of a SAM on both electrodes (electrode **1**, 161.9 eV, S $2p_{3/2}$; 163.1 eV, S $2p_{1/2}$; electrode **2** 162.0 eV, S $2p_{3/2}$; 163.2 eV, S $2p_{1/2}$). Furthermore, a high resolution spectrum in the F 1s region showed the presence of fluorinated SAM only on electrode **1** (688.3 eV, fwhm 1.6 eV), verifying that no cross-contamination of electrode **2** occurred during monolayer formation (Figure 4.7, left).[13] As expected, a high resolution spectrum of electrode **1** in the C 1s region showed three major peaks corresponding to the CF_3, CF_2 and CH_2 carbons (293.3 eV, fwhm 1.0 eV; 290.9 eV, fwhm 1.1 eV; and 284.3 eV, fwhm 1.5 eV, respectively; Figure 4.7, right).[13] A high resolution spectrum of electrode **2** in the C 1s region showed only one peak corresponding to the carbon atoms in the dihexadecyl disulfide (284.8 eV, fwhm 1.1 eV; Figure 4.7, right). These results unambiguously demonstrate that this protection–reaction–deprotection sequence allows the regioselective modification of independently addressable electrodes on a single substrate.

4.4 Conclusions

In summary, we have developed a method that successfully uses gold oxide as a temporary protecting layer for the directed self-assembly of monolayers from

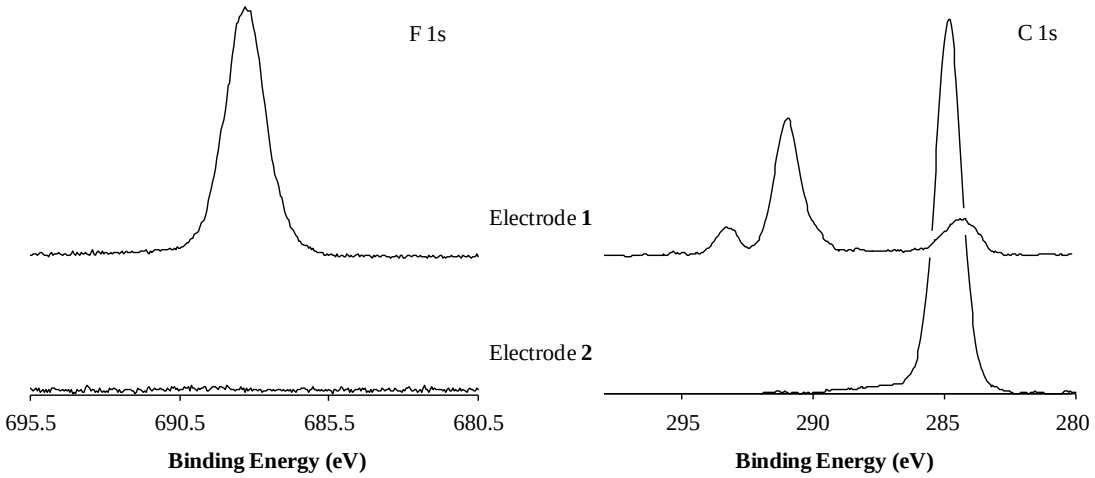

Figure 4.7. High resolution x-ray photoelectron spectrum of electrodes **1** and **2** in the F 1s and C 1s regions after the selective adsorption of a hydrocarbon SAM on electrode **2** and a fluorocarbon SAM on electrode **1**.

dihexadecyl disulfide on gold. This approach is similar to the protection–deprotection scheme used for analogous reasons in synthetic organic chemistry. The analogy is not strict, of course, because the electrodes are independently addressable, and therefore can be selectively protected or deprotected without relying on inherent differences in chemical kinetics. Although there are alternative strategies for reaching a similar target—e.g., reductive desorption,[4] cathodic blocking,[8] or directed electrochemisorption[11-14]—the approach described here may have important advantages in certain applications. For example, this method does not involve thiols or thiolates that could exchange with components in previously adsorbed SAMs, nor does it produce reactive by-products (such as SO_3) that could complicate incorporation of nucleophilic functionality into the SAM. This procedure holds promise for microelectronic applications, including sensors, biosensors, and photovoltaics, and the work in Chapter 5 focuses on its applicability to microelectrodes and its use with ω-functionalized disulfide precursors.

4.5 Experimental

General. Hexadecanethiol (92.0%) and iodine (99.8%) was purchased from Aldrich and used as received. Lithium perchlorate ($LiClO_4$, 99.0%), 1-iodo-1*H*,1*H*,2*H*,2*H*-perfluorododecane (97%), and sodium thiosulfate pentahydrate (99%) were used as received from Alfa Aesar. Reagent grade methanol (99.9%) and hexanes (95.8%) were used as purchased from Pharmco-AAPER. Ethanol (Anhydrous, J.T. Baker, 95%) was used as received. Acetonitrile (ACN, Acros, 99.8%) and tetrahydrofuran (THF, Mallinckrodt, 99%) were purified and dried using a PureSolv system (Innovative Technology, Inc.). Silver nitrate (Fisher, 99.8%) was used as

received. Hydrogen peroxide (30%) and sulfuric acid (95%) were used as received from EMD. Hexadecane (99%, Aldrich) was passed through activated alumina twice before use in contact-angle measurements. Gold (99.999%) was used as supplied by VEM Vacuum Engineering.

Preparation of Gold Electrodes. Two gold electrodes were prepared on a single substrate by the application of 5-mm-wide polyimide tape along the center of a piranha-cleaned glass slide prior to metal deposition. *Caution: Piranha solution, a 4:1 (v/v) mixture of concentrated H_2SO_4 and 30% H_2O_2, reacts violently with organic material and should be handled carefully.* Approximately 50 Å of Ti (as an adhesion promoter) and then 1000 Å of Au were evaporated onto the substrates by e-beam vapor deposition. After metal deposition, the tape was removed to produce two electrically isolated electrodes, ~1 cm wide and separated by a ~5-mm space. Electrodes were used within a week after deposition, or cleaned prior to use by adsorption of a SAM from hexadecanethiol in ethanol (1 mM, 24 h) and subsequently cycling its potential (-1.2 V to 1.5 V, 100 mV/s) ten times in 0.5 M aqueous sulfuric acid to remove the SAM and any contaminants.

Synthesis of C_{16} Disulfide. Dihexadecyl disulfide, $[CH_3(CH_2)_{15}S]_2$, was synthesized using a procedure adapted from the literature.[17] Briefly, hexadecanethiol (2.0 g, 7.7 mmol) was dissolved in 150 mL of hexanes, and I_2 (0.50 g, 2.0 mmol) was dissolved in 5 mL of methanol. The I_2 solution was slowly added to the thiol solution with stirring, and the reaction was allowed to proceed for 24 h. The yellow/brown color of the I_2 in the methanol phase persisted. The clear hexanes phase was separated and washed with methanol to remove the remaining thiol, and the crude product was

crystallized by adding ethanol. The product was then recrystallized from hexanes/ethanol and analyzed by NMR (isolated yield based on I_2, 62%).

Synthesis of $[CF_3(CF_2)_9(CH_2)_2S]_2$. The starting material, $CF_3(CF_2)_9(CH2)_2S_2O_3Na$, was synthesized using a previously published procedure.[13] This compound (0.50 g, 0.73 mmol) was dissolved in 200 mL of ethanol, and I_2 (0.185 g, 0.730 mmol) was dissolved in 50 mL of methanol. The I_2 solution was slowly added to the alkyl-thiosulfate solution with stirring, and the reaction mixture was allowed to stir at room temperature for 48 h. A few drops of 3 M aqueous $NaHSO_3$ were added to reduce the excess I_2. A 50/50 (v/v%) mixture of water and ether was then added to the reaction mixture, and the ether phase was separated. The solvent was removed from this phase by rotary evaporation. The product was then washed with water and analyzed by NMR (isolated yield, 67%; CAS # 118552-82-2).

Contact-Angle and Ellispometry Measurements. Advancing contact angles of water and of hexadecane were measured with a Rame-Hart NRL model 100 goniometer. A minimum of six measurements on three independent drops were made for each sample. Ellispometric parameters (psi and delta) were collected using a J. A. Woollam variable-angle spectroscopic ellipsometer (VASE). Data were collected at angles of 60.00° and 70.00° in the range of 300-800 nm, and thicknesses were calculated with the WVASE32® software using the refractive index of hexadecane over this range of wavelength (measured independently) as a model for both monolayers. This approach allowed very good fits of the experimental values of psi and delta, despite the difference in composition of the fluorinated SAM.

Electrochemistry. Gold oxide was produced electrochemically in 0.5-M sulfuric acid using a standard three-electrode cell comprising a gold working electrode, a platinum wire as the counter-electrode, and an aqueous $Ag/AgNO_3$ (10 mM) reference electrode. To oxidize each gold electrode, its potential was held at -0.2 V for 10 s, followed by 1.2 V for 10 s. The sample was then rinsed with deionized water (18.1 MΩ·cm) and dried under a stream of N_2.

To form a monolayer, a three-electrode cell comprising an oxidized gold working electrode, a platinum wire counter-electrode and a $Ag/AgNO_3$ (3 mM in ACN) reference electrode was used, and the potential was stepped from 0.3 V to -0.9 V, with 5 s at each potential, in the presence of a disulfide. Forty of these voltammetric pulses were applied to the electrode in a solution containing $[CH_3(CH_2)_{15}S]_2$ or $[CF_3(CF_2)_9(CH_2)_2S]_2$ (1 mM) and $LiClO_4$ (0.1 M) in tetrahydrofuran (THF). The sample was then removed from solution, rinsed with THF, and water, and dried under a stream of N_2.

X-ray Photoelectron Spectroscopy. Spectra were collected using a Scienta ESCA-300 spectrometer with monochromatized Al Kα X-rays generated using a rotating anode. Photoemission was measured with a 300-mm-diameter hemispherical analyzer. Samples were grounded by placing screws in contact with both electrode surfaces and the sample holder. The pressure in the sample chamber was $\sim 2\times10^{-9}$ Torr, and samples were analyzed at a 20° take-off angle between the sample surface and the path to the analyzer. The pass energy for high-resolution spectra in the Au, O and S regions were 75 eV, 150 eV, and 300 eV, respectively, and the step energy for all high-resolution scans was 0.05 eV. Survey spectra were taken at a 300-eV pass energy and a step energy of 1 eV. High resolution Au spectra were referenced to the Au $4f_{7/2}$ peak, set at 84.0 eV, and intensities

normalized to the largest Au $4f_{7/2}$ peak. High resolution S photoemission intensities were normalized to the largest sulfur $2p_{3/2}$ peak. Samples were analyzed by XPS within 1 h of monolayer formation, and the spectra were analyzed using CASAXPS® software.

4.6 Acknowledgements

We gratefully acknowledge the National Science Foundation for support of this research (CHE-0749777) and for funding to purchase the spectroscopic ellipsometer (CHE-0923370). We also thank Dr. Al Miller for assistance with acquisition of the XPS data and Dr. Joseph Labukas for assistance with their analysis.

4.7 References

1. Love, J. C.; Estroff, L. A.; Kriebel, J. K.; Nuzzo, R. G.; Whitesides, G. M., Self-assembled Monolayers of Thiolates on Metals as a Form of Nanotechnology. *Chem. Rev.* **2005,** *105* (4), 1103-1169.
2. Kumar, A.; Biebuyck, H. A.; Whitesides, G. M., Patterning Self-assembled Monolayers - Applications in Materials Science. *Langmuir* **1994,** *10* (5), 1498-1511.
3. Smith, R. K.; Lewis, P. A.; Weiss, P. S., Patterning Self-assembled Monolayers. *Prog. Surf. Sci.* **2004,** *75* (1-2), 1-68.
4. Widrig, C. A.; Chung, C.; Porter, M. D., The Electrochemical Desorption of n-Alkanethiol Monolayers From Polycrystalline Au and Ag Electrodes. *J. Electroanal. Chem.* **1991,** *310* (1-2), 335-359.
5. Imabayashi, S.-I.; Hobara, D.; Kakiuchi, T.; Knoll, W., Selective Replacement of Adsorbed Alkanethiols in Phase-Separated Binary Self-Assembled Monolayers by Electrochemical Partial Desorption. *Langmuir* **1997,** *13* (17), 4502-4504.
6. Diao, P.; Guo, M.; Hou, Q. C.; Xiang, M.; Zhang, Q., Electrochemically Partitioned Assembly of Organosulfur Monolayers and Nanoparticles. *J. Phys. Chem. B* **2006,** *110* (41), 20386-20391.
7. Diao, P.; Hou, Q. C.; Guo, M.; Xiang, M.; Zhang, Q., Effect of Substrate Potentials on the Structural Disorders of Alkanethiol Monolayers Prepared by Electrochemically Directed Assembly. *J. Electroanal. Chem.* **2006,** *597* (2), 103-110.
8. Riepl, M.; Mirsky, V. M.; Wolfbeis, O. S., Electrical Control of Alkanethiols Self-Assembly on a Gold Surface as an Approach for Preparation of Microelectrode Arrays. *Microchim. Acta* **1999,** *131* (1), 29-34.

9. Mullen, T. J.; Dameron, A. A.; Weiss, P. S., Directed Assembly and Separation of Self-Assembled Monolayers via Electrochemical Processing. *J. Phys. Chem. B* **2006,** *110* (29), 14410-14417.
10. Niu, L.; Knoll, W., Electrochemically Addressable Functionalization and Parallel Readout of a DNA Biosensor Array. *Anal. Chem.* **2007,** *79* (7), 2695-2702.
11. Hsueh, C.-C.; Lee, M.-T.; Freund, M. S.; Ferguson, G. S., Electrochemically Directed Self-assembly on Gold. *Angew. Chem., Int. Ed.* **2000,** *39* (7), 1228-1230.
12. Lee, M.-T.; Hsueh, C.-C.; Freund, M. S.; Ferguson, G. S., Electrochemical Self-assembly of Monolayers from Alkylthiosulfates on Gold. *Langmuir* **2003,** *19* (13), 5246-5253.
13. Labukas, J. P.; Drake, T. J. H.; Ferguson, G. S., Compatibility of ω-Functionality in the Electrochemically Directed Self-Assembly of Monolayers on Gold from Alkyl Thiosulfates. *Langmuir* **2010,** *26* (12), 9497-9505.
14. Labukas, J. P.; Ferguson, G. S., Direct Route to Well-Defined, Chemically Diverse Electrode Arrays. *Langmuir* **2011,** *27* (7), 3219-3223.
15. Nuzzo, R. G.; Allara, D. L., Adsorption of Bifunctional Organic Disulfides on Gold Surfaces. *J. Am. Chem. Soc.* **1983,** *105* (13), 4481-4483.
16. Ron, H.; Matlis, S.; Rubinstein, I., Self-assembled Monolayers on Oxidized Metals. 2. Gold Surface Oxidative Pretreatment, Monolayer Properties, and Depression Formation. *Langmuir* **1998,** *14* (5), 1116-1121.
17. Ron, H.; Rubinstein, I., Self-assembled Monolayers on Oxidized Metals. 3. Alkylthiol and Dialkyl Disulfide Assembly on Gold Under Electrochemical Conditions. *J. Am. Chem. Soc.* **1998,** *120* (51), 13444-13452.
18. Ron, H.; Rubinstein, I., Alkanethiol Monolayers on Preoxidized Gold - Encapsulation of Gold Oxide Under an Organic Layer. *Langmuir* **1994,** *10* (12), 4566-4573.
19. Woodward, J. T.; Walker, M. L.; Meuse, C. W.; Vanderah, D. J.; Poirier, G. E.; Plant, A. L., Effect of an Oxidized Gold Substrate on Alkanethiol Self-assembly. *Langmuir* **2000,** *16* (12), 5347-5353.
20. Sharpe, R. B. A.; Burdinski, D.; Huskens, J.; Zandvliet, H. J. W.; Reinhoudt, D. N.; Poelsema, B., Oxidized Gold as an Ultrathin Etch Resist Applied in Microcontact Printing. *J. Am. Chem. Soc.* **2006,** *128* (49), 15560-15561.
21. Zheng, Z.; Yang, M.; Zhang, B., Reversible Nanopatterning on Self-assembled Monolayers on Gold. *J. Phys. Chem. C* **2008,** *112* (17), 6597-6604.
22. Wuts, P. G. M.; Greene, T. W., *Greene's Protective Groups in Organic Synthesis*. 4th ed.; Wiley-Interscience: Hoboken, 2007.
23. Bain, C. D.; Troughton, E. B.; Tao, Y.-T.; Evall, J.; Whitesides, G. M.; Nuzzo, R. G., Formation of Monolayer Films by the Spontaneous Assembly of Organic Thiols from Solution onto Gold. *J. Am. Chem. Soc.* **1989,** *111* (1), 321-335.
24. Juodkazis, K.; Juodkazytė, J.; Šebeka, B.; Lukinskas, A., Cyclic Voltammetric Studies on the Reduction of a Gold Oxide Surface Layer. *Electrochem. Commun.* **1999,** *1* (8), 315-318.
25. Juodkazis, K.; Juodkazytė, J.; Jasulaitienė, V.; Lukinskas, A.; Šebeka, B., XPS Studies on the Gold Oxide Surface Layer Formation. *Electrochem. Commun.* **2000,** *2* (7), 503-507.

26. Tremiliosi-Filho, G.; Dall'Antonia, L. H.; Jerkiewicz, G., Growth of Surface Oxides on Gold Electrodes Under Well-defined Potential, Time and Temperature Conditions. *J. Electroanal. Chem.* **2005,** *578* (1), 1-8.
27. Tsai, H. C.; Hu, E.; Perng, K.; Chen, M. K.; Wu, J. C.; Chang, Y. S., Instability of Gold Oxide Au_2O_3. *Surf. Sci.* **2003,** *537* (1-3), L447-L450.
28. Saliba, N.; Parker, D. H.; Koel, B. E., Adsorption of Oxygen on Au(111) by Exposure to Ozone. *Surf. Sci.* **1998,** *410* (2-3), 270-282.
29. Pireaux, J. J.; Liehr, M.; Thiry, P. A.; Delrue, J. P.; Caudano, R., Electron Spectroscopic Characterization of Oxygen-adsorption on Gold Surfaces. 2. Production of Gold Oxide in DC Reactive Sputtering. *Surf. Sci.* **1984,** *141* (1), 221-232.
30. Irissou, E.; Denis, M. C.; Chaker, M.; Guay, D., Gold Oxide Thin Film Grown by Pulsed Laser Deposition in an O_2 Atmosphere. *Thin Solid Films* **2005,** *472* (1-2), 49-57.
31. Krozer, A.; Rodahl, M., X-ray Photoemission Spectroscopy Study of UV/ozone Oxidation of Au Under Ultrahigh Vacuum Conditions. *J. Vac. Sci. Technol., A* **1997,** *15* (3), 1704-1709.
32. To fit the Au 4f7/2 and 4f5/2 peaks, values of fwhm were allowed to float, but were constrained to be equal to each other.
33. Cook, K. M.; Ferguson, G. S., Determination of the Wavelength-dependent Refractive Index of a Gold-Oxide Thin Film. *J. Phys. Chem. C* **2011,** *115* (46), 22976-22980.
34. The component peaks at 531.1 and 532.5 eV are also consistent with adsorbed contaminants: See ref. 29–31.
35. Biebuyck, H. A.; Bain, C. D.; Whitesides, G. M., Comparison of Organic Monolayers on Polycrystalline Gold Spontaneously Assembled from Solutions Containing Dialkyl Disulfides or Alkanethiols. *Langmuir* **1994,** *10* (6), 1825-1831.
36. Bain, C. D.; Whitesides, G. M., Correlations Between Wettability and Structure in Monolayers of Alkanethiols Adsorbed on Gold. *J. Am. Chem. Soc.* **1988,** *110* (11), 3665-3666.
37. Bourg, M. C.; Badia, A.; Lennox, R. B., Gold-sulfur Bonding in 2D and 3D Self-assembled Monolayers: XPS Characterization. *J. Phys. Chem. B* **2000,** *104* (28), 6562-6567.
38. Nieto, F. J. R.; Fachini, E.; Cabrera, C. R.; Arvia, A. J., X-ray Photoelectron Spectroscopy of Oxygen-containing Layers Formed by a Linear Potential Scan on Stepped Gold (111) Films in Aqueous 1-M Sulphuric Acid. *Thin Solid Films* **2009,** *517* (5), 1534-1540.
39. Fukushima, H.; Seki, S.; Nishikawa, T.; Takiguchi, H.; Tamada, K.; Abe, K.; Colorado, R.; Graupe, M.; Shmakova, O. E.; Lee, T. R., Microstructure, Wettability, and Thermal Stability of Semifluorinated Self-assembled Monolayers (SAMs) on Gold. *J. Phys. Chem. B* **2000,** *104* (31), 7417-7423.

Chapter 5

Spatially Selective Formation of Hydrocarbon, Fluorocarbon, and Hydroxyl-terminated Monolayers on a Microelectrode Array

This chapter includes material that has been reproduced in part with permission: Cook, K. M.; Nissley, D. A.; Ferguson, G. S., Spatially Selective Formation of Hydrocarbon, Fluorocarbon, and Hydroxyl-Terminated Monolayers on a Microelectrode Array. *Langmuir* **2013**, DOI: 10.1021/la401250d.

5.1 Abstract

The protection–deprotection strategy, using gold oxide as a passivating layer developed in Chapter 4, was used to direct the self-assembly of monolayers (SAMs) selectively at individual gold microelectrodes in an array. This approach allowed the formation of hydroxyl-terminated monolayers, without side-reactions, in addition to hydrocarbon and fluorocarbon SAMs. Fluorescence microscopy was used to visualize selective de-wetting of hydrophobic monolayers by an aqueous dye solution, and spatially-resolved x-ray photoelectron spectroscopy was used to demonstrate a lack of cross-contamination on neighboring microelectrodes in the array.

5.2 Introduction

The study of self-assembled monolayers (SAMs) has focused on scientific questions regarding their formation, structure, and properties,[1,2] as well as on technological applications such as their use to control wetting properties,[3,4] create biocompatible surfaces,[5,6] impart chemical resistance,[7] and fabricate sensors.[8-10] In Chapter 1, we discussed the fact that many of these applications require the formation of SAMs in specific patterns, and although the application of patterned SAMs on uniform

substrates is relatively straightforward, the regioselective formation of SAMs on specific features on a complex substrate remains challenging.[11-14] Even more challenging is the production of a chemically diverse set of SAMs on such a substrate while maintaining the purity of each monolayer.

Our group has previously studied the anodic activation of alkyl thiosulfates at selected electrodes in an array, which provides one solution to the regioselective placement of SAMs of varying functionality,[15-19] though the SO_3 by-product of oxidation can lead to side-reactions at the surface of the SAM. Monolayers formed from hydroxyl-terminated alkyl thiosulfates, for example, contained large amounts of sulfate, resulting presumably from the reaction of SO_3 with the terminal hydroxyl groups.[17] To address such problems with monolayer precursors bearing nucleophilic functional groups, we developed a protection-deprotection approach that uses gold oxide as a masking layer on particular electrodes to allow selective formation of SAMs from dialkyl disulfide on others.[20] As discussed in Chapter 4, this method relies on the inability of dialkyl disulfides to reduce gold oxide,[21-23] and we used it successfully to form hydrocarbon and fluorocarbon SAMs on neighboring macroscopic (~ 1-mm widths and 5-mm spacings) electrodes without cross-contamination. This chapter describes the extension of this approach both to the functionalization of *micro*electrodes and to the inclusion of hydroxyl-terminated monolayers.

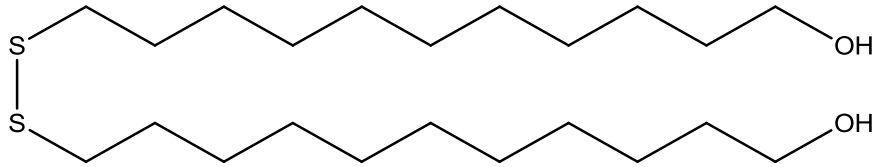

Figure 5.1. Adsorbate used in the formation of hydroxyl-terminated SAMs on gold, $[HO(CH_2)_{11}S]_2$.

5.3 Results and Discussion

To demonstrate that the protection-deprotection approach can be used to form hydroxyl-terminated SAMs regioselectively on gold, we investigated the use of $[HO(CH_2)_{12}S]_2$ as an adsorbate (Figure 5.1). For ease of analysis, macroscopic (1-cm x 2-cm) gold electrodes were used as substrates in our initial studies. Monolayers were formed by the application of forty stepped-potential pulses from 0.3 V to -0.9 V, for 5 s each, to the working electrode in a THF solution containing $[HO(CH_2)_{12}S]_2$ (1.13 mM) and $LiClO_4$ (0.105 M) as a supporting electrolyte. The electrode was then rinsed with THF, water, and dried under a stream of N_2. The advancing contact angle of water (31°) was consistent with the formation of a hydroxyl-terminated monolayer from disulfide, and the surface was wet by hexadecane, as expected.[24,25] The ellipsometric thickness (11 Å) was also consistent with the particular disulfide used.[24,25]

High resolution x-ray photoelectron spectra of this surface confirmed the presence of a hydroxyl-terminated monolayer (Figure 5.2). A spectrum in the C 1s region contained an asymmetric peak with additional photoemission intensity on its high-binding-energy side, indicating the presence of more than one component. This spectrum could be adequately fit by two peaks, located at 284.5 eV (fwhm, 1.2 eV) and assigned to the aliphatic chain, and at 285.9 eV (fwhm, 2.0 eV) and assigned to the carbon bound directly to the hydroxyl group.[26] A spectrum in the O 1s region could be fit with a single peak at 532.4 eV (fwhm, 1.4 eV) corresponding to the hydroxyl oxygen.[27] A spectrum in the S 2s region revealed the expected spin-orbit doublet due to thiolate bound to the gold electrode (161.8 eV, S $2p_{3/2}$, fwhm, 1.1 eV; 163.2 eV, S $2p_{1/2}$, fwhm, 1.1 eV),[28] and indicated that no contamination by other sulfur species was present on the surface.

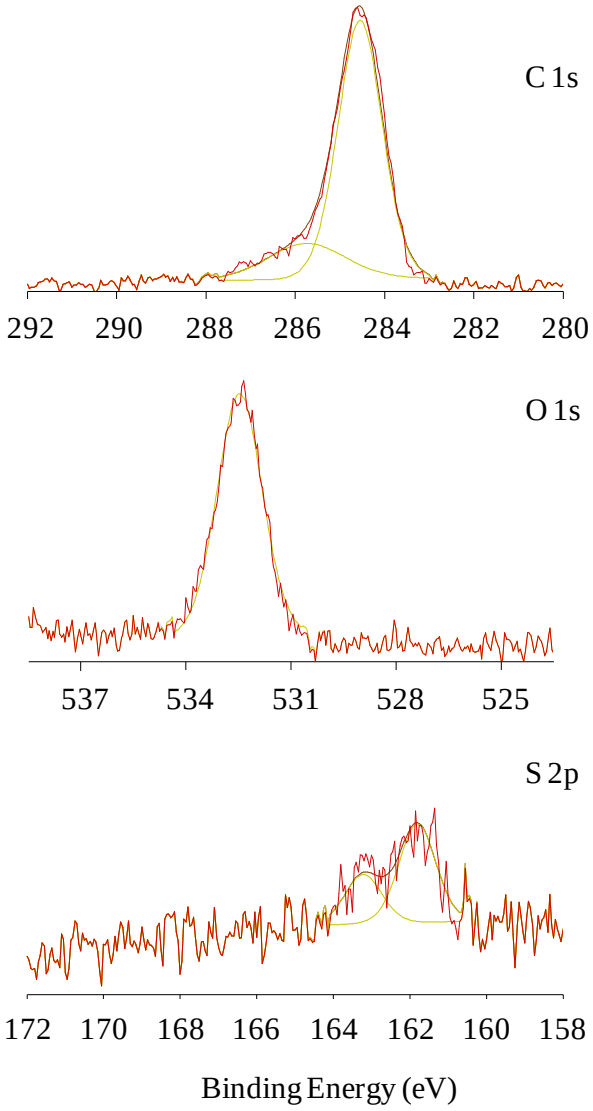

Figure 5.2. High resolution x-ray photoelectron spectra, in the C 1s, O 1s, and S 2p regions, of a gold electrode modified with $[HO(CH_2)_{12}S]_2$.

To demonstrate that this method could be extended to the regioselective placement of SAMs on *micro*electrodes, each of the three microelectrodes on a triple-track tester (TTT) was functionalized with a different SAM. Prior to monolayer formation, the TTT was cleaned by UV/O_3 oxidation. Like electrochemical oxidation,[20] this process produces a thin oxide film on the gold, which can serve as a masking layer until removed. To reduce the oxide present on an individual track and make that track active to monolayer formation, a potential of -0.9 V (*vs.* Ag/$AgNO_3$) was applied in a solution of 0.500-M H_2SO_4.[29-31] A monolayer was then formed on the reduced track of interest by the application of forty stepped-potential pulses from 0.3 V to -0.9 V, for 5 s at each potential, in a THF solution containing 1 mM of the dialkyl disulfide of interest and 0.1 M $LiClO_4$ as a supporting electrolyte.[20] After rinsing and drying, the next oxidized track to be used was reduced electrochemically, and the next SAM formed. Monolayers were formed on the three microelectrodes in the following order and with the following disulfides: track **A**, $[CH_3(CH_2)_{15}S]_2$; track **C**, $[CF_3(CF_2)_9(CH_2)_2S]_2$; and track **B**, $[HO(CH_2)_{12}S]_2$ (Figure 5.3).

As two of these tracks (**A** and **C**) should be hydrophobic and one (**B**) hydrophilic, we used dewetting by an aqueous solution of fluorescent dye (rhodamine 6G) to differentiate the two types of surface by fluorescence microscopy (Figure 5.4, top). The layer of dye solution on the wetted electrode was sufficiently thick that quenching of the fluorescence by the Au was not a problem. This approach had been used successfully in our group previously for similar analyses. [15,19] The solution spontaneously de-wet the hydrophobic tracks, bearing hydrocarbon or fluorocarbon chains, which therefore appear dark in the image; whereas, the solution formed a wetting film on the hydrophilic track,

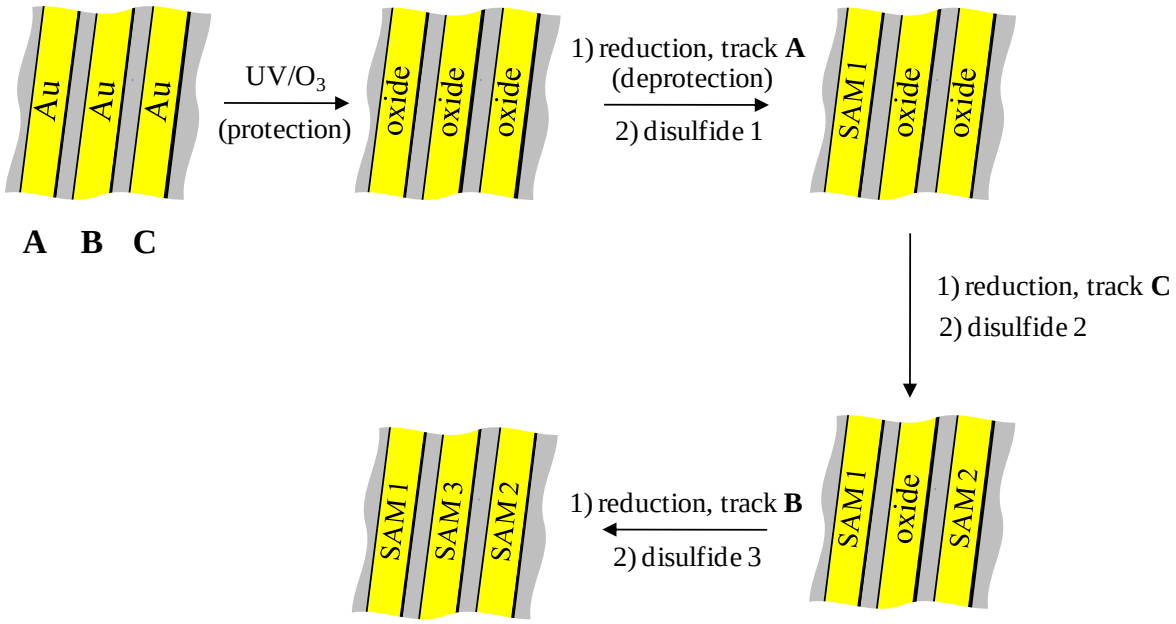

Figure 5.3. Summary of the sequential protection–deprotection approach used to modify neighboring gold microelectrodes in an array selectively. In the first step, all of the microelectrodes were protected via oxidization by UV/O_3. Electrode **A** was then reduced electrochemically and modified selectively with $[CH_3(CH_2)_{15}S]_2$. In the next step, track **C** was reduced and then modified selectively with $[CF_3(CF_2)_9(CH_2)_2S]_2$. In the final step, track **B** was reduced and then modified with $[HO(CH_2)_{12}S]_2$. The size and spacing of the gold electrodes on the alumina substrate are not drawn to scale.

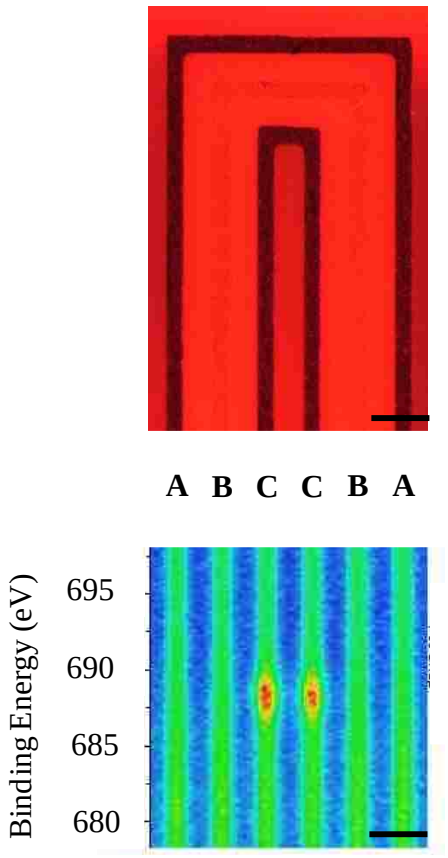

Figure 5.4. (Top) Fluorescence micrograph of a chemically modified TTT, covered with a thin film of a 1-mM aqueous solution of the dye rhodamine 6G. Electrodes **A** and **C** bore hydrophobic hydrocarbon and fluorocarbon monolayers, respectively, and were de-wet by the solution. Electrode **B** bore a hydrophilic hydroxyl-terminated SAM and remained wet by the solution. (Bottom) Spatially-resolved XPS data collected in the F 1s region. The horizontal axis defines spatial position across the TTT, whereas the vertical axis defines binding energy of the detected photoelectrons. The color scale from blue to red indicates increasing intensity of photoemission, thus the red intensity on electrode **C** indicates strong F 1s photoemission. The scale bar in each figure corresponds to 200

μm.bearing a SAM terminated by hydroxyl groups, and obscured it by fluorescence in the image.

To distinguish between the two hydrophobic tracks, we used spatially resolved XPS to map the location of F 1s photoemission across the sample. Spatially resolved measurements were made by moving the x-ray beam in linear increments across the gold electrodes of the TTT and collecting data at each location. The false-color image in Figure 5.4 (bottom) is a composite of these spectra, with the horizontal axis indicating the relative spatial position of the beam on the sample and the vertical axis indicating binding energy in the F 1s region. The Au tracks appear uniformly green in the figure, indicating an elevated baseline intensity due to the higher yield of inelastically scattered photoelectrons from gold relative to the alumina substrate (uniformly blue). The presence of strong F 1s photoemission only on track **C** confirmed the selective placement of the fluorocarbon SAM on that microelectrode. No fluorine was detected on tracks **A** or **B**, indicating that these microelectrodes were not contaminated by the fluorocarbon adsorbate when a SAM was added to track **C**.

5.4 Conclusions

Unlike the oxidative adsorption of SAMs from alkly thiosulfates, which liberates the potent Lewis acid SO_3, a protection-deprotection approach can be used to form hydroxyl-terminated SAMs regioselectively on gold without complicating side-reactions. Extension of this method to allow the stepwise formation of a chemically diverse array of microelectrodes bearing hydrocarbon, fluorocarbon, and hydroxyl-terminated SAMs demonstrates its potential usefulness in applications involving such complex substrates.

The combination of fluorescence microscopy and spatially resolved XPS showed not only that each SAM formed selectively on the individual track to which it was directed, but that it occurred without cross-contamination of neighboring SAMs. We anticipate that this approach may be general enough to accommodate other nucleophilic functional groups, thus providing a viable synthetic route to a broad range of technologically and biologically relevant surfaces.

5.5 Experimental

General. Hexadecanethiol (92.0%) and iodine (99.8%) were purchased from Aldrich and used as received. Lithium perchlorate ($LiClO_4$, 99.0%), 1-iodo-1*H*,1*H*,2*H*,2*H*-perfluorododecane (97%), and sodium thiosulfate pentahydrate (99%) were used as received from Alfa Aesar. 12-Bromo-1-dodecanol (98.0%) was used as received by TCI America. Reagent-grade methanol (99.9%) and hexanes (95.8%) were used as purchased from Pharmco-AAPER. Ethanol (Anhydrous, J.T. Baker, 95%), silver nitrate (Fisher, 99.8%), and rhodamine 6G dye (Acros, 99%) were used as received. Acetonitrile (ACN, Acros, 99.8%) and tetrahydrofuran (THF, Mallinckrodt, 99%) were purified and dried using a PureSolv system (Innovative Technology, Inc.). Hydrogen peroxide (30%) and sulfuric acid (95%) were used as received from EMD. Hexadecane (99%, Aldrich) was passed through activated alumina twice before use in contact-angle measurements. Gold (99.999%) was used as supplied by VEM Vacuum Engineering. Dihexadecyl disulfide, $[CH_3(CH_2)_{15}S]_2$, was synthesized by the oxidation of hexadecanethiol with iodine.[23] The fluorinated disulfide, $[CF_3(CF_2)_9(CH_2)_2S]_2$, was synthesized using a previously published procedure.[20]

Preparation of Gold Electrodes. Macroscopic (1 cm x 2 cm) gold electrodes were formed on glass substrates by e-beam vapor deposition. Approximately 150 Å of Ti (as an adhesion promoter) and then 1500 Å of Au were evaporated onto the piranha-cleaned glass slides. *Caution: Piranha solution, a 4:1 (v/v) mixture of concentrated H_2SO_4 and 30% H_2O_2, reacts violently with organic material and should be handled carefully.* The microelectrodes on a triple-track tester (TTT) –a gift from AT&T Bell Laboratories (previous company name)– were used to demonstrate the selective formation of SAMs on closely spaced microelectrodes. This substrate comprised a serpentine pattern of three gold microelectrodes (~ 50-μm wide) separated by ~ 100-μm spacings on an alumina substrate.

Synthesis of $[HO(CH_2)_{12}S]_2$. The alkyl thiosulfate, $HO(CH_2)_{12}S_2O_3Na$ (0.200 g, 0.62 mmol), was dissolved in a mixture of 50 mL of water and 25 mL of ethanol and stirred. Iodine (0.087 g, 0.34 mmol) was dissolved in 25 mL of ethanol, added to the other solution, and this mixture was stirred for 20 h at room temperature. The excess iodine was then reduced by addition of 3 drops of 3-M aqueous $NaHSO_3$. The total volume was then reduced to ~25 mL by rotary evaporation, and the remaining mixture was refrigerated overnight. A white precipitate was collected by vacuum filtration, rinsed with deionized water, and dried under vacuum. The isolated yield was 83%. ^{1}H NMR (in $CDCl_3$): $[HOCH_2\ CH_2(CH_2)_8CH_2\ CH_2S]_2$, 3.62 (t, 4H); $[HOCH_2\ CH_2(CH_2)_8CH_2\ CH_2S]_2$, 1.64 (m, 4H); $[HOCH_2\ CH_2(CH_2)_8CH_2\ CH_2S]_2$, 1.21-1.37 (m, 32H); $[HOCH_2CH_2(CH_2)_8CH_2\ CH_2S]_2$, 1.54 (m, 5H, obscured by water); $[HOCH_2\ CH_2(CH_2)_8CH_2\ CH_2S]_2$, 2.66 (t, 4H).

Contact-Angle and Ellipsometry Measurements. Advancing contact angles of water and of hexadecane were measured with a Rame-Hart NRL model 100 goniometer. A minimum of six measurements were made on three independent drops at various locations on each sample. Ellipsometric parameters (psi and delta) were collected using a J. A. Woollam variable-angle spectroscopic ellipsometer (VASE). Data were collected at angles of 60.00° and 70.00° in the wavelength range of 350-800 nm, and thicknesses were calculated with the WVASE32® software using the complex refractive index of hexadecane over this range of wavelength (measured independently) as a model for all three monolayers. This approach allowed very good fits of the experimental values of psi and delta, despite the significant differences in composition.

Electrochemistry. To form a monolayer, a three-electrode cell comprising a gold working electrode, a platinum wire counter-electrode, and a $Ag/AgNO_3$ (2.94 mM in ACN) reference electrode was used. The potential at the working electrode was stepped from 0.3 V to -0.9 V, for 5 s at each potential, in a solution containing the dialkyl disulfide of interest (~ 1 mM) and $LiClO_4$ (~ 0.1 M) in tetrahydrofuran (THF). Forty of these voltammetric pulses were applied, and the sample was then removed from solution, rinsed with THF and water, and dried under a stream of N_2.

For the selective formation of SAMs on the TTT, all of the gold tracks were oxidized by irradiation with ultraviolet light in the presence of ozone, followed by reduction of the resulting oxide only from the track of interest by applying a potential of -0.9 V for 30 s in 0.500-M aqueous H_2SO_4. The TTT was then rinsed with water and dried under a stream of N_2 before SAM formation on the reduced surface.

X-ray Photoelectron Spectroscopy (XPS). Spectra of SAMs on macroscopic electrodes were collected using a Scienta ESCA-300 spectrometer with monochromatized Al Kα X-rays generated using a rotating anode. Photoemission was measured with a 300-mm-diameter hemispherical analyzer. Samples were grounded by placing screws in contact with both the electrode surface and the sample holder. The pressure in the sample chamber was $\sim 2\times10^{-9}$ Torr, and samples were analyzed at a 20° take-off angle between the sample surface and the path to the analyzer. Spectra were collected within 1 h of monolayer formation and analyzed using CASAXPS® software (version 2.3.15dev77). A survey spectrum was taken at a 300-eV pass energy and with a step energy of 1 eV. The pass energy for high-resolution spectra in the C, O, and S regions was 150 eV, and the step energy was 0.05 eV. The C 1s photoemission was fit with two peaks whose full-widths at half-maximum (fwhm) were allowed to vary. The sulfur 2p photoemission was fit with peaks due to the $2p_{3/2}$ and $2p_{1/2}$ spin-orbit components, with the fwhm allowed to vary but constrained to be equal to one another, and areas in a 2:1 ratio, respectively. The O 1s peak could be fit by a single component with a fwhm of 1.5 eV.

Spatially resolved spectra were collected using a Thermo Scientific K-Alpha spectrometer with monochromatized Al Kα X-rays. Photoemission was measured with a 180° micro-focused hemispherical analyzer. The sample was grounded by placing screws in contact with the electrode contacts and the sample holder. The pressure in the sample chamber was $\sim 2\times10^{-8}$ Torr, and samples were analyzed at a 45° take-off angle between the sample surface and the path to the analyzer. A survey spectrum was taken using a 400-μm spot size (long axis) and at a 300-eV pass energy with a step energy of 1 eV. This spectrum indicated small amounts of iodine (0.59 at. %) and silver (1.56 at. %)

contamination on the surface of the TTT. The likely source of iodine is I_2, which has a high affinity for gold, from the ambient atmosphere of our laboratory. The silver may have leached from our reference electrode and been reduced during the electrochemical treatment of the TTT. These minor contaminants did not, however, interfere with the selective formation of SAMs on the substrate.

High resolution, spatially resolved data were collected in the F 1s region by sequentially moving the x-ray spot linearly across the microelectrodes. A spot size of 30-μm (long axis) was used, and the spot was moved in increments of 15 μm. The pass energy for high-resolution spectra was 150 eV with a step energy of 0.169 eV. The sample was stored under N_2, and spectra were collected within 12 h of monolayer formation and analyzed using Avantage® software.

Fluorescence Microscopy. Fluorescence images of the TTT were collected using a Nikon Eclipse E800 fluorescence microscope, through a Nikon G-2E/C filter at 4x magnification, and with a 10-mM aqueous solution of rhodamine 6G fluorescent dye as the probe liquid. No alterations to the color of the images were performed.

5.6 Acknowledgements

We gratefully acknowledge the National Science Foundation for support of this research (CHE-0749777) and for funding to purchase the spectroscopic ellipsometer (CHE-0923370). We thank Daniel A. Nissley for synthesizing the hydroxyl-terminated disulfide. We thank Lehigh University for a Hornor Fellowship for KMC and an Environmental Initiative Summer Research Grant for DAN. We also thank Drs. Al Miller (Lehigh), Rob Pafchek (Lehigh), and James Lallo (Laboratory for Surface

Modification, Rutgers University) for their assistance with acquisition of the XPS data, and Lee Graham (Lehigh) for his assistance in obtaining the fluorescence microscopy images.

5.7 References

1. Love, J. C.; Estroff, L. A.; Kriebel, J. K.; Nuzzo, R. G.; Whitesides, G. M., Self-assembled Monolayers of Thiolates on Metals as a Form of Nanotechnology. *Chem. Rev.* **2005,** *105* (4), 1103-1169.
2. Ulman, A., Formation and Structure of Self-assembled Monolayers. *Chem. Rev.* **1996,** *96* (4), 1533-1554.
3. Ulman, A., Wetting Studies of Molecularly Engineered Surfaces. *Thin Solid Films* **1996,** *273*, 48-53.
4. Chaudhury, M. K.; Whitesides, G. M., How To Make Water Run Uphill. *Science* **1992,** *256* (5063), 1539-1541.
5. Whitesides, G. M.; Ostuni, E.; Takayama, S.; Jiang, X.; Ingber, D. E., Soft Lithography in Biology and Biochemistry. *Annu. Rev. Biomed. Eng.* **2001,** *3* (1), 335-373.
6. Gonçalves, I. C.; Martins, M. C. L.; Barbosa, M. A.; Ratner, B. D., Protein Adsorption on 18-Alkyl Chains Immobilized on Hydroxyl-terminated Self-assembled Monolayers. *Biomaterials* **2005,** *26* (18), 3891-3899.
7. Srisombat, L.; Jamison, A. C.; Lee, T. R., Stability: A Key Issue for Self-assembled Monolayers on Gold as Thin-film Coatings and Nanoparticle Protectants. *Colloids Surf., A* **2011,** *390* (1-3), 1-19.
8. Chaki, N. K.; Vijayamohanan, K., Self-assembled Monolayers as a Tunable Platform for Biosensor Applications. *Biosens. Bioelectron.* **2002,** *17*, 1-12.
9. Tencer, M.; Nie, H.-Y.; Berini, P., Electrochemical Differentiation and TOF-SIMS Characterization of Thiol-coated Gold Features for (Bio)chemical Sensor Applications. *J. Electrochem. Soc.* **2009,** *156* (12), J386-J392.
10. Tencer, M.; Olivieri, A.; Tezel, B.; Nie, H. Y.; Berini, P., Chip-scale Electrochemical Differentiation of SAM-coated Gold Features Using a Probe Array. *J. Electrochem. Soc.* **2012,** *159* (3), J77-J82.
11. Smith, R. K.; Lewis, P. A.; Weiss, P. S., Patterning Self-assembled Monolayers. *Prog. in Surf. Sci.* **2004,** *75* (1-2), 1-68.
12. Xia, Y.; Whitesides, G. M., Soft Lithography. *Angew. Chem. Int. Ed.* **1998,** *37* (5), 550-575.
13. Widrig, C. A.; Chung, C.; Porter, M. D., The Electrochemical Desorption of n-Alkanethiol Monolayers From Polycrystalline Au and Ag Electrodes. *J. Electroanal. Chem.* **1991,** *310* (1-2), 335-359.
14. Diao, P.; Guo, M.; Hou, Q. C.; Xiang, M.; Zhang, Q., Electrochemically Partitioned Assembly of Organosulfur Monolayers and Nanoparticles. *J. Phys. Chem. B* **2006,** *110* (41), 20386-20391.

15. Hsueh, C.-C.; Lee, M.-T.; Freund, M. S.; Ferguson, G. S., Electrochemically Directed Self-assembly on Gold. *Angew. Chem., Int. Ed.* **2000,** *39* (7), 1228-1230.
16. Lee, M.-T.; Hsueh, C.-C.; Freund, M. S.; Ferguson, G. S., Electrochemical Self-assembly of Monolayers from Alkylthiosulfates on Gold. *Langmuir* **2003,** *19* (13), 5246-5253.
17. Labukas, J. P.; Drake, T. J. H.; Ferguson, G. S., Compatibility of ω-Functionality in the Electrochemically Directed Self-Assembly of Monolayers on Gold from Alkyl Thiosulfates. *Langmuir* **2010,** *26* (12), 9497-9505.
18. Labukas, J. P.; Ferguson, G. S., Electrochemically Directed Two-component Monolayers on Gold. *J. Mater. Res.* **2011,** *26* (2), 262-267.
19. Labukas, J. P.; Ferguson, G. S., Direct Route to Well-Defined, Chemically Diverse Electrode Arrays. *Langmuir* **2011,** *27* (7), 3219-3223.
20. Cook, K. M.; Ferguson, G. S., Gold Oxide as a Protecting Group for Regioselective Surface Chemistry. *Chem. Commun.* **2011,** *47* (46), 12550-12552.
21. Nuzzo, R. G.; Allara, D. L., Adsorption of Bifunctional Organic Disulfides on Gold Surfaces. *J. Am. Chem. Soc.* **1983,** *105* (13), 4481-4483.
22. Ron, H.; Matlis, S.; Rubinstein, I., Self-assembled Monolayers on Oxidized Metals. 2. Gold Surface Oxidative Pretreatment, Monolayer Properties, and Depression Formation. *Langmuir* **1998,** *14* (5), 1116-1121.
23. Ron, H.; Rubinstein, I., Self-assembled Monolayers on Oxidized Metals. 3. Alkylthiol and Dialkyl Disulfide Assembly on Gold Under Electrochemical Conditions. *J. Am. Chem. Soc.* **1998,** *120* (51), 13444-13452.
24. Mittler-Neher, S.; Spinke, J.; Liley, M.; Nelles, G.; Weisser, M.; Back, R.; Wenz, G.; Knoll, W., Spectroscopic and Surface-analytical Characterization of Self-assembled Layers on Au. *Biosens. Bioelectron.* **1995,** *10* (9-10), 903-916.
25. Gupta, P.; Ulman, A.; Fanfan, S.; Korniakov, A.; Loos, K., Mixed Self-assembled Monolayers of Alkanethiolates on Ultrasmooth Gold Do Not Exhibit Contact-angle Hysteresis. *J. Am. Chem. Soc.* **2005,** *127* (1), 4-5.
26. Bain, C. D.; Troughton, E. B.; Tao, Y.-T.; Evall, J.; Whitesides, G. M.; Nuzzo, R. G., Formation of Monolayer Films by the Spontaneous Assembly of Organic Thiols from Solution onto Gold. *J. Am. Chem. Soc.* **1989,** *111* (1), 321-335.
27. Bain, C. D.; Evall, J.; Whitesides, G. M., Formation of Monolayers by the Coadsorption of Thiols on Gold: Variation in the Head Group, Tail Group, and Solvent. *J. Am. Chem. Soc.* **1989,** *111* (18), 7155-7164.
28. Bain, C. D.; Biebuyck, H. A.; Whitesides, G. M., Comparison of Self-assembled Monolayers on Gold: Coadsorption of Thiols and Disulfides. *Langmuir* **1989,** *5* (3), 723-727.
29. Juodkazis, K.; Juodkazytė, J.; Šebeka, B.; Lukinskas, A., Cyclic Voltammetric Studies on the Reduction of a Gold Oxide Surface Layer. *Electrochem. Commun.* **1999,** *1* (8), 315-318.
30. Tremiliosi-Filho, G.; Dall'Antonia, L. H.; Jerkiewicz, G., Limit to Extent of Formation of the Quasi-two-dimensional Oxide State on Au Electrodes. *J. Electroanal. Chem.* **1997,** *422* (1-2), 149-159.
31. Tremiliosi-Filho, G.; Dall'Antonia, L. H.; Jerkiewicz, G., Growth of Surface Oxides on Gold Electrodes Under Well-defined Potential, Time and Temperature Conditions. *J. Electroanal. Chem.* **2005,** *578* (1), 1-8.

Chapter 6

Exploratory Studies of Silver (I)-thiolate Polymers: Their Use as Potential Precursors to Monolayers and Nanoparticles

6.1 Abstract

Exploratory studies involving silver (I)-thiolate polymers were conducted to explore their possible use as precursors to monolayer films and nanoparticles. Low-energy ion scattering (LEIS) and x-ray photoelectron spectroscopy (XPS) measurements suggested the adsorption of these polymers onto gold surfaces from solution, but the surfaces produced were not the same as those formed by self-assembly of alkanethiols on gold bearing a submonolayer of underpotential-deposited silver. In separate studies, the silver(I)-thiolate polymers could be decomposed into silver nanoparticles by thermolysis or photolysis as confirmed by transmission electron microscopy (TEM) and UV/vis spectrophotometry.

6.2 Introduction

Polymeric silver (I)-thiolate complexes, with the general formula $(AgSR)_n$ were first characterized in 1964.[1] Polymers derived from *n*-alkanethiols (with chain lengths of 3, 4, 6, 8, 9, 10, 11, 12, 15, 16, 17, and 18 carbons) are insoluble in benzene, chloroform, acetone, alcohols, and dimethyl sulfoxide,[2-4] and only appear to be soluble in hot toluene.[5] Crystallographic data indicate that these polymers form layered assemblies of linear structures with pendant alkyl groups (Figure 6.1 d) at room temperature.[3-5] Results from differential scanning calorimetry (DSC) are consistent with transitions to lamellar,

micellar, and amorphous states, whose characteristic temperatures depend on the length of the alkyl chain.[4,5]

Silver(I)-thiolate polymers with secondary or tertiary α-carbon atoms are soluble and capable of crystallization in non-polar solvents such as chloroform, benzene, and toluene.[1-3,6,7] The structure of these materials has been studied in pure form and in solution. For example, Åkerström et al., and Dance et al. described the dependence of both solution-phase species and crystal structure on the degree of branching at the α-carbon atom.[1-3,6] Polymers having a secondary α-carbon, i.e., those derived from 4-methyl-2-pentanethiol, 2-hexanethiol, 3-hexanethiol, and 3-methyl-2-pentanethiol, tend to exist as dodecamers (n = 12) in benzene solution.[2] The authors suggested that the structures of the solution species are twelve-membered rings (Figure 6.1 a). Crystallographic data indicate that the dodecameric compounds crystallize as solids with the same cyclic arrangements. An exception is the polymer derived from 2,2-dimethyl-3-butanethiol, which exists as an octomer (n = 8) in benzene solution.

Polymers having a tertiary α-carbon, i.e., those derived from 3-methyl-3-pentanethiol, 2-methyl-2-pentanethiol, 2,3-dimethyl-2-butanethiol, 2-methyl-2-butanethiol, and 2-methyl-2-propanethiol are also octomers in benzene.[2,6] The octameric compounds may have 8-membered-ring structures in solution (Figure 6.1 b), but they crystallize as two intertwined and unconnected $(AgSR)_\infty$ chains (Figure 6.1 c).[2,6] The solution-phase and crystallographic behavior of a polymer derived from cyclohexanethiol mirrored that of $(AgSR)_{12}$ compounds.[7]

Silver(I)-thiolate polymers have previously been used in antibacterial applications[8] and as precursors for nanoparticles of silver and silver sulfide (both free in

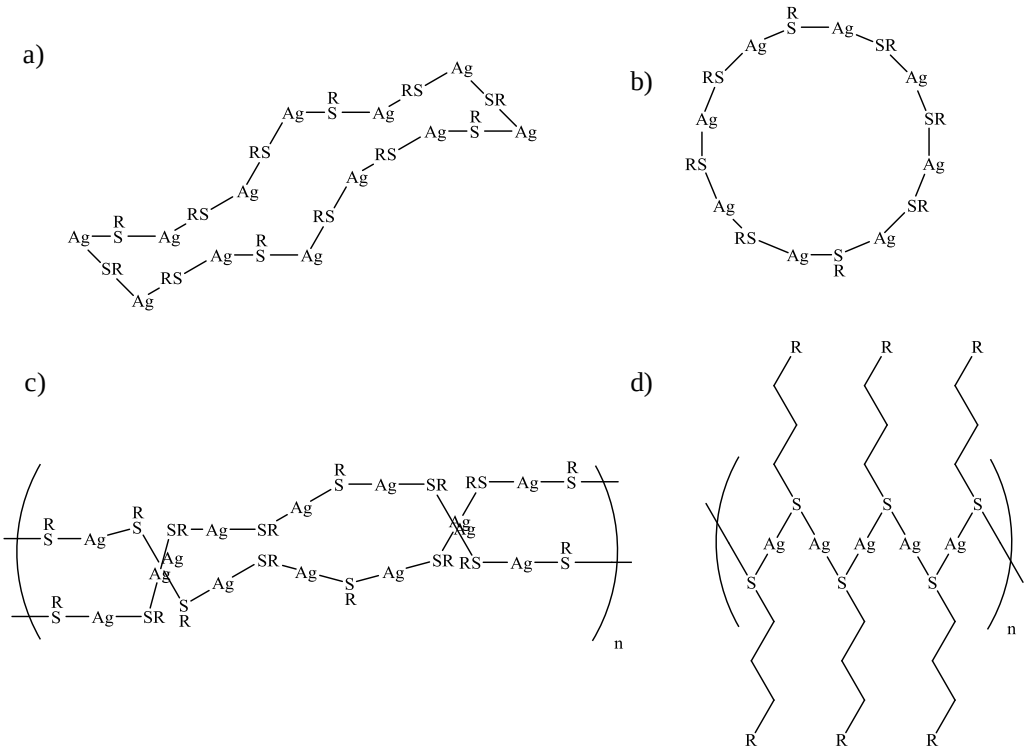

Figure 6.1. Proposed structures for silver(I)-thiolate polymers: a) twelve-membered rings, b) eight-membered rings, c) intertwined chains, and d) linear chains

solution, and embedded in a polymer matrix).[9-12] For example, silver(I)-dodecylmercaptide embedded in amorphous polystyrene was thermally decomposed at 200 °C to form silver clusters capped with mixed thiol monolayers.[12] Schaaff and Rodinone generated semi-conducting silver sulfide nanocrystals by the reaction of a silver(I)-thiolate polymer derived from dodecanethiol with sodium sulfide.[10] This synthesis, however, did not have a high yield, nor did it provide great control over the size of the nanocrystals. Morsali and coworkers reported a synthesis of silver nanoparticles by the thermolysis of a silver(I)-polymer.[9,11] For example, a silver(I)-malic acid polymer was synthesized by the reaction of silver nitrate and malic acid.[9] This polymer formed a two-dimensional network that could be thermolyzed neat (673 K) to form Ag clusters, or dispersed in oleic acid solution (523 K), resulting in aggregates of oleic acid-capped silver nanoparticles (Figure 6.2). It is unclear, however, if these particles aggregated permanently, or if they are soluble in common solvents. Analogous gold(I)-thiolate polymers have been converted to small (2 – 4 nm) Au nanoparticles by treatment with various reducing agents.[13]

We initiated the work described in this chapter as an attempt to utilize the silver-sulfur bond already present in silver(I)-thiolate polymers as a convenient starting material for the formation of monolayer films and silver nanoparticles. If successful, the latter process would provide a potentially attractive alternative to reduction as a route to nanoparticles. Of particular interest were: thermolysis in free solution at lower temperatures, not constrained in a polymer matrix or coordination network; and photolysis to induce decomposition in a controlled way.

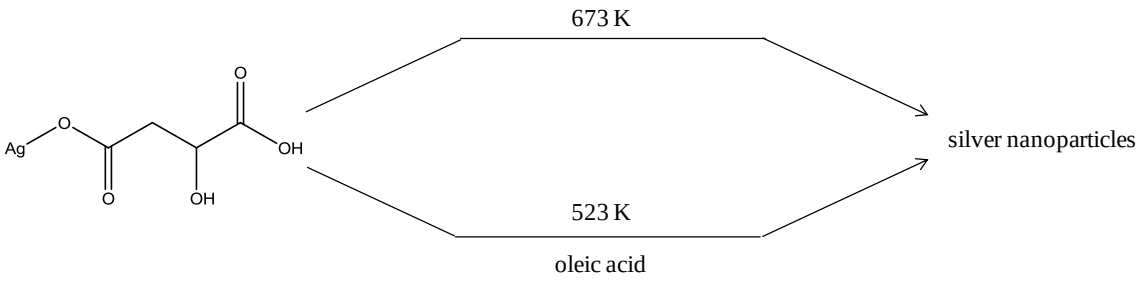

Figure 6.2. Pathways to the formation of silver nanoparticles from a silver(I)-malic acid polymer.

6.3 Results and Discussion

Our studies focused on the synthesis of soluble silver (I)-thiolate polymers, solubility studies of these polymers, adsorption of monolayer films on gold from the polymers, and thermolytic or photolytic decomposition of the polymers to form silver nanoparticles.

6.3.1 The Synthesis of Silver (I)-thiolate Polymers

Initially, the synthesis of $(AgSR)_n$ polymers was carried out in acetonitrile by the reaction of $AgNO_3$ and a thiol in the presence of triethylamine (TEA) (equation 6.1).[2]

$$n\ RSH + n\ AgNO_3 \xrightarrow{TEA} (AgSR)_n + n\ HNO_3 \qquad (6.1)$$

The presumed role of the triethylamine was to consume the HNO_3 byproduct (0.05 M) of the reaction. This approach allowed the synthesis of $[AgS(CH_2)_{11}CH_3]_n$, $[AgSCH_2CHOHCH_2OH]_n$, $[AgSCH_2CH_2COOH]_n$, and $[AgSC(CH_3)_2(CH_2)_5CH_3]_n$. The commercially available starting material for the $[AgSC(CH_3)_2(CH_2)_5CH_3]_n$ polymer was a mixture of isomers, nonetheless, we will follow the manufacturers' nomenclature and refer to it as the *tert*-nonyl polymer for the sake of simplicity. The *n*-alkyl and diol polymers were brittle, pale yellow solids. The carboxylic-acid polymer was a brittle, white solid, and the *tert*-nonyl polymer was separated as a pale yellow oil. These colors are consistent with previous literature accounts of similar silver (I)-thiolate polymers.[1-5] This synthesis, however, did not result in a consistent physical appearance or color for the diol and acid polymers. In these cases, reproducible results were obtained after the omission of triethylamine from the procedure.

6.3.2 Solubility of Silver (I)-thiolate Polymers

The *n*-dodecyl polymer, $[AgS(CH_2)_{11}CH_3]_n$, was only soluble in refluxing toluene (~ 111 °C), forming a yellow solution. It was not soluble in chloroform, dichloromethane, hexanes, tetrahydrofuran, acetonitrile, ethanol, acetone, or toluene at room temperature. This lack of solubility severely limited the study of its solution-phase properties. Upon cooling, this solution formed an orange solid, which could be isolated by filtration, and then re-suspended in toluene upon heating. Removal of solvent from the filtrate solution left a white solid with a ^{1}H NMR spectrum consistent with didodecyl disulfide, indicating some thermal decomposition of the polymer at this temperature.

The diol polymer, $[AgSCH_2CHOHCH_2OH]_n$, was insoluble in ethanol, methanol, acetone, THF, as well as the non-polar solvents, hexanes and toluene. Prolonged (~ 24 h) periods in ethanol or methanol caused the surface of the solid to blacken, consistent with reduction of the Ag^+ to Ag^0 by the solvent. The polymer was soluble, however, in water after gentle heating (to 30 °C), resulting in a pale yellow solution.

As expected, the *tert*-nonyl polymer, $[AgSC(CH_3)_2(CH_2)_5CH_3]_n$, was by-far the most soluble polymer of those synthesized. This oil was soluble in hexanes, hexadecane, toluene, THF, chloroform, dichloromethane, and ethanol.

The carboxylic-acid polymer, $[AgSCH_2CH_2COOH]_n$, was insoluble in all solvents examined, except for aqueous NaOH. A minimum molar ratio of hydroxide to repeat unit of 1:1 was required for solubility.

We expected that the chemistry of these polymers would depend on the particular species present in solution (e.g., polymer, cyclic oligomer, monomer), so we attempted to determine the molecular weight of the diol polymer in water and *tert*-nonyl polymer in

hexanes, by freezing point depression and vapor-phase osmometry, respectively. Unfortunately, these studies did not yield consistent or conclusive results.

6.3.3 Adsorption of Silver (I)-thiolate Polymers on Gold

Under-potential deposition (UPD) of a sub-monolayer of silver onto gold has been shown to impart added stability to SAMs formed from alkanethiols.[14-16] The ratio of Ag to S in these stabilized SAMs is 1:1, so we hypothesized that adsorption of silver (I)-thiolate polymers on gold might provide a direct route to these materials (Figure 6.3).

In an attempt to form a SAM on gold from $[AgSCH_2CHOHCH_2OH]_n$ in water, a gold film was immersed in a 1-mM solution (based on repeat units) of the polymer for 24 h. The sample was then rinsed with warm water and dried under a stream of N_2. The advancing contact angle of water was 49°, and a receding drop wet the surface. For comparison, a SAM formed from the corresponding thiol ($HSCH_2CHOHCH_2OH$, 1 mM in water, 24 h) on a UPD-Ag/Au surface had an advancing contact angle of water of 35°, and a receding drop wet the surface. The difference in these contact-angles may indicate either that the adsorption of $[AgSCH_2CHOHCH_2OH]_n$ on gold did not form the same structure as results from adsorption of the thiol on UPD-Ag/Au, or that the surface derived from the polymer was contaminated.

An XPS survey spectrum of this sample revealed the presence of silver, carbon, oxygen, and sulfur (Figure 6.4). A high-resolution spectrum in the Ag 3d region (Figure 6.5) revealed a spin-orbit doublet that could be fit by peaks at 368.3 eV (Ag $3d_{5/2}$, fwhm, 0.63 eV) and 374.4.6 eV (Ag $3d_{3/2}$, fwhm, 0.63 eV). Although the data were truncated at the high-binding energy side of the $3d_{5/2}$ peak, the peak locations and quantitative data

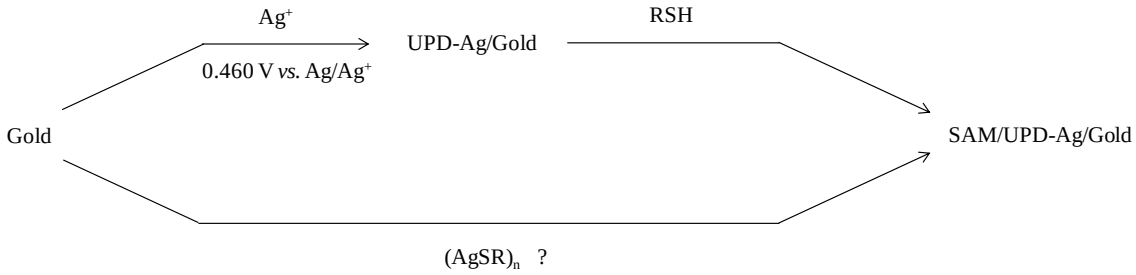

Figure 6.3. Established (top) and proposed (bottom) pathways to the formation of SAMs on UPD-Ag/gold.

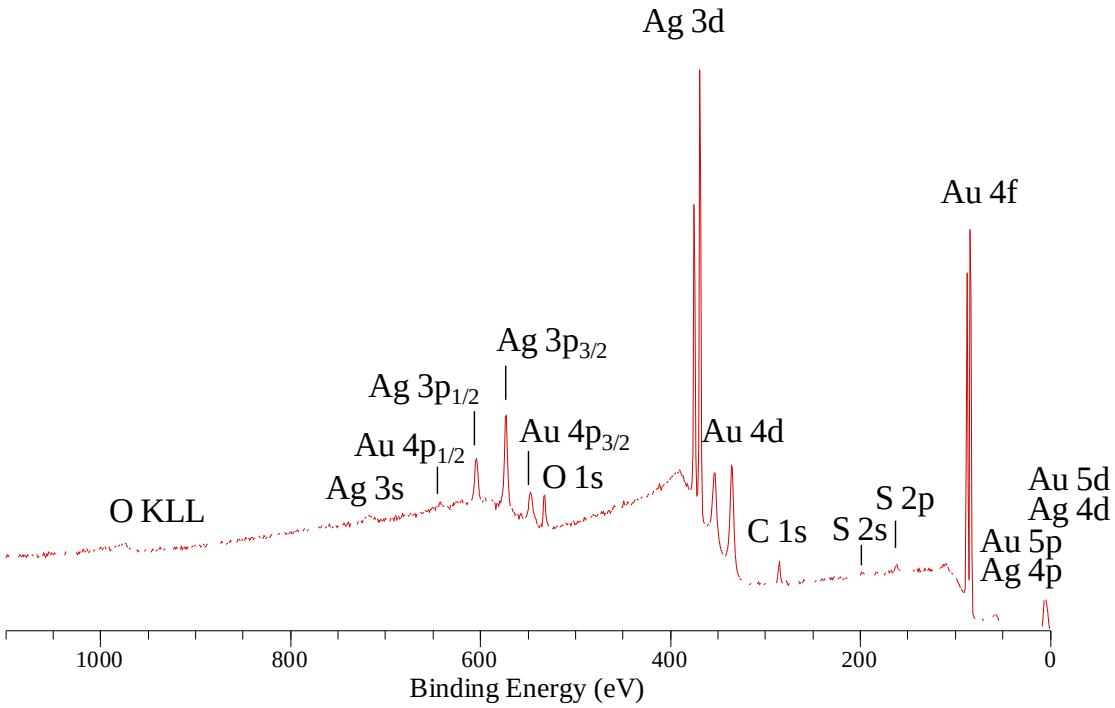

Figure 6.4. An XPS survey spectrum of a gold film immersed in a 5-mM aqueous solution of $[AgSCH_2CHOHCH_2OH]_n$ for 24 h.

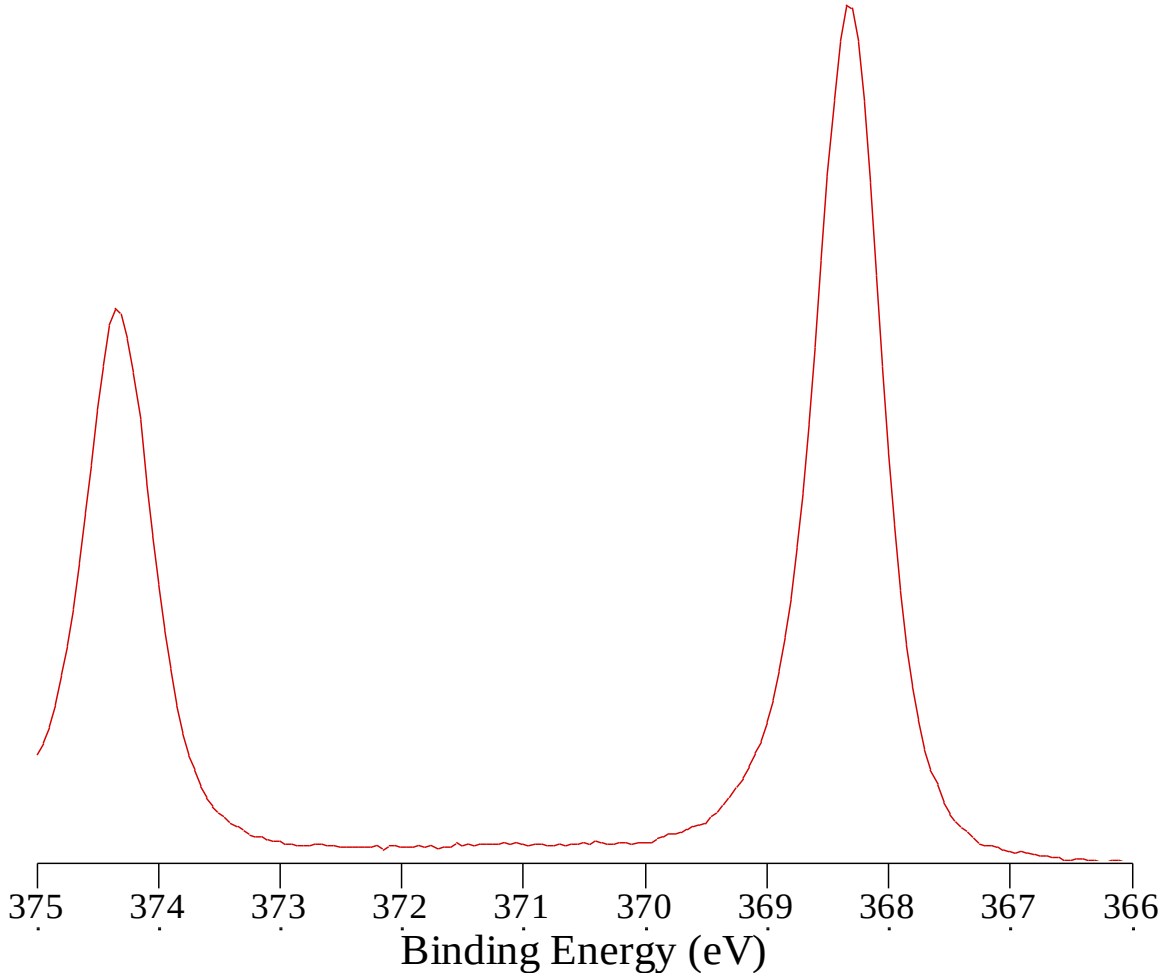

Figure 6.5. A high-resolution XPS spectrum in the Ag 3d region of a gold film immersed in a 5-mM aqueous solution of $[AgSCH_2CHOHCH_2OH]_n$ for 24 h.

could still be obtained. These binding energies are 0.5-eV higher than those reported for UPD-Ag on gold bearing a SAM derived from octadecanethiol (Ag $3d_{5/2}$, 367.8 eV),[15] and correspond instead to metallic silver or Ag_2S, suggesting some decomposition to form those species.[17] A high-resolution spectrum in the C 1s region (Figure 6.6) contained photoemission that could be adequately fit by two peaks, at 286.1 eV (fwhm, 1.4 eV) consistent with carbon atoms bound to the hydroxyl groups, and at 284.7 eV (fwhm, 1.1eV) arising from the methylene carbon.[18] The ratio of the peak areas for these peaks, however, is ~ 4:5 which is different from the expected ratio of 2:1, and indicates the loss of some of the hydroxyl groups. A spectrum in the O 1s region (Figure 6.7) could be fit by two peaks, located at 532.5 eV (fwhm, 1.7 eV) assigned to the hydroxyl groups, and at 530.8 eV (fwhm, 1.4 eV) perhaps due to contamination.[19-21] The ratio of these components was 14:1, respectively, indicating only a small amount of the second component. A high-resolution spectrum in the S 2p region (Figure 6.8) revealed photoemission that could be fit by two spin-orbit doublets, at 162.3 eV (S $2p_{3/2}$, fwhm, 1.0 eV) and 163.6 eV (S $2p_{1/2}$, fwhm, 1.0 eV), and at 161.2 eV (S $2p_{3/2}$, fwhm, 0.84 eV)and 162.9 eV (S $2p_{1/2}$, fwhm, 0.84 eV). The higher-binding energy doublet (72.4% of the S 2p photoemission) is consistent with a thiolate SAM on a silver surface and a UPD-Ag/Au surface.[15,22] Although the chemical state of sulfur in the lower-binding energy doublet (26.6% of the S 2p photoemission) is unclear, it is consistent with Ag_2S, suggesting the presence of this species.[17] The overall ratio of Ag:S was 2.0:3.6, not 1:1 as in the precursor polymer. A possible explanation for the high sulfur content could be partial decomposition to Ag_2S or silver metal and disulfide, which could then assemble on the gold surface, resulting in a lower Ag:S ratio than expected.

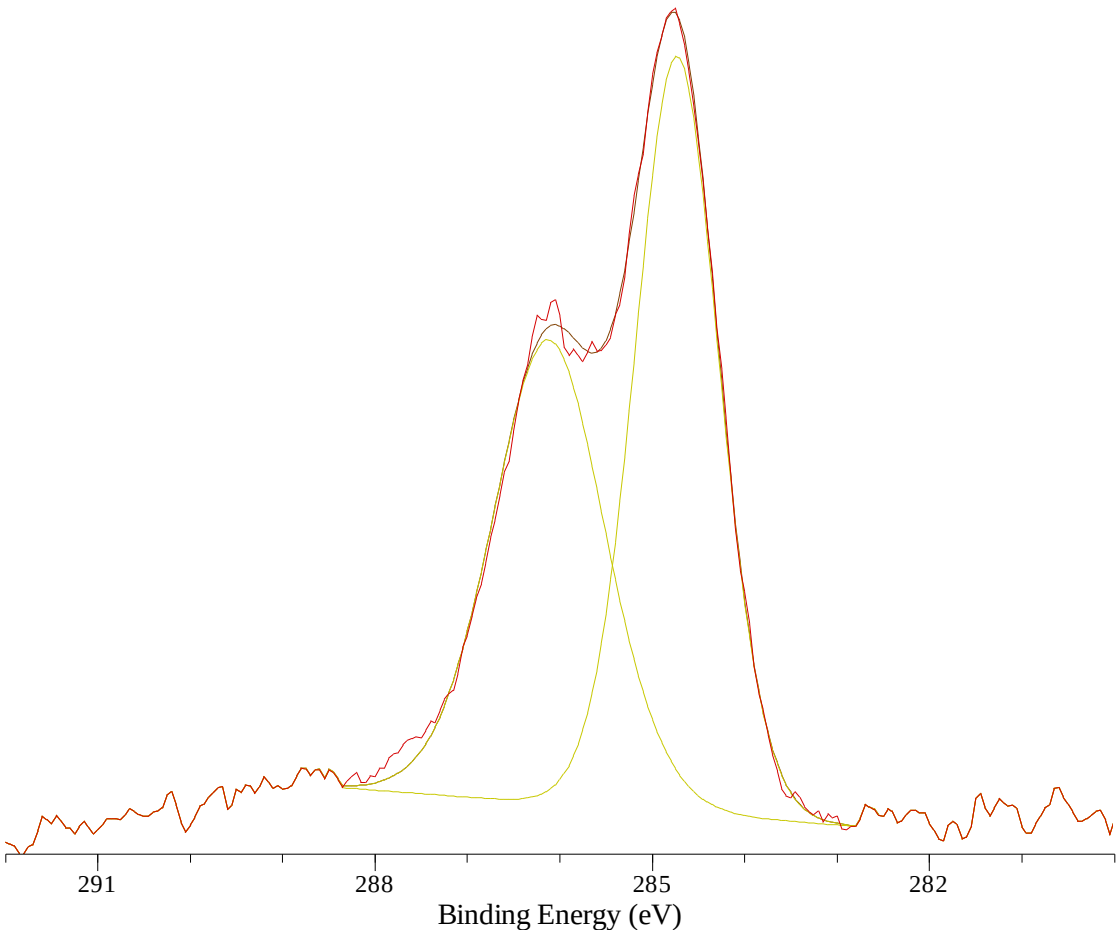

Figure 6.6. A high-resolution XPS spectrum in the C 1s region of a gold film immersed in a 5-mM aqueous solution of $[AgSCH_2CHOHCH_2OH]_n$ for 24 h.

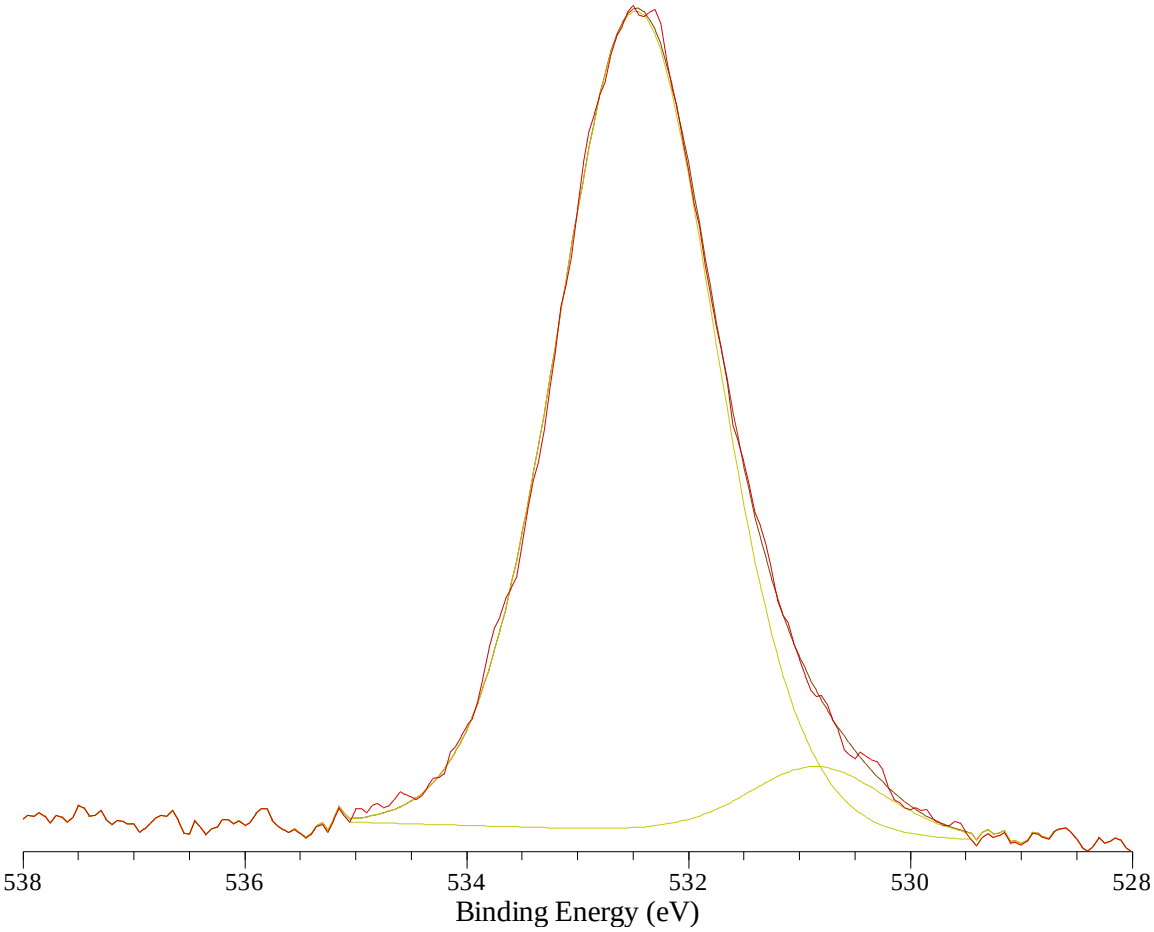

Figure 6.7. A high-resolution XPS spectrum in the O 1s region of a gold film immersed in a 5-mM aqueous solution of $[AgSCH_2CHOHCH_2OH]_n$ for 24 h.

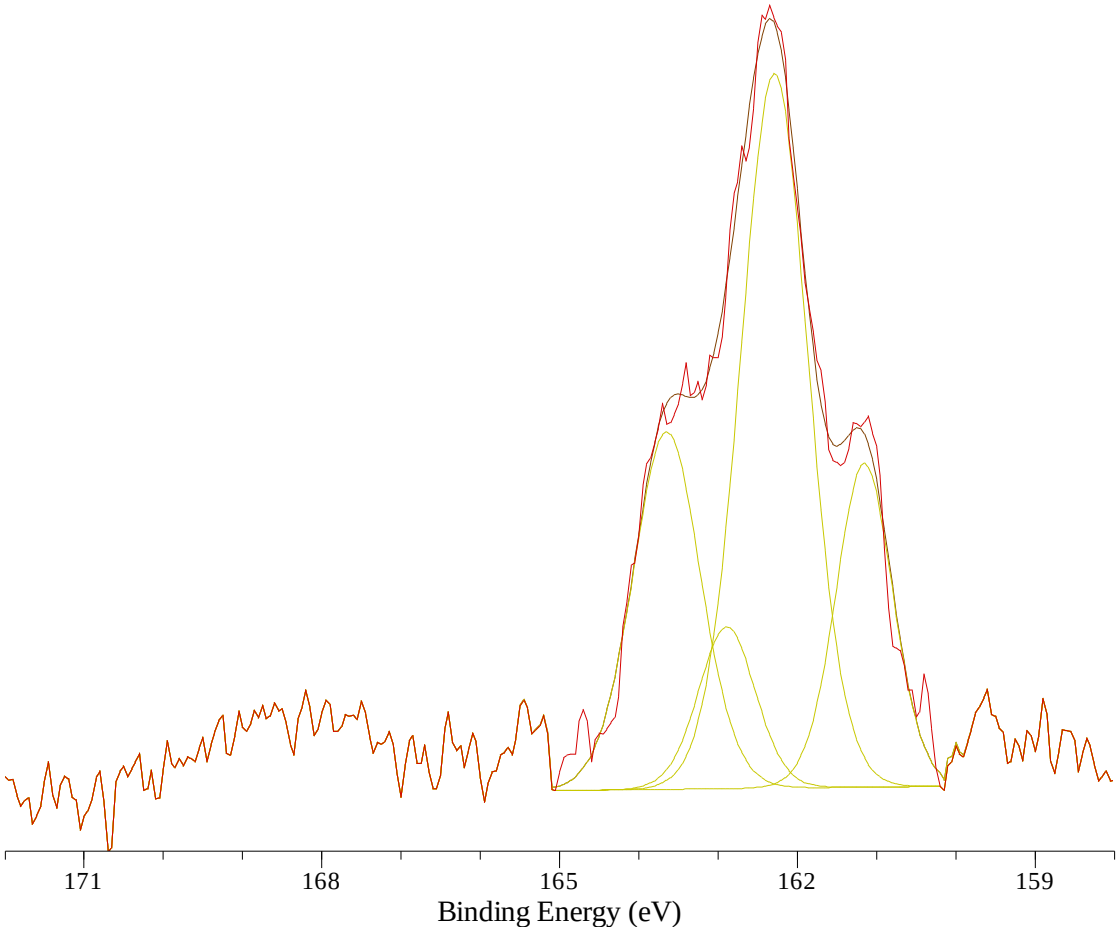

Figure 6.8. A high-resolution XPS spectrum in the S 2p region of a gold film immersed in a 5-mM aqueous solution of $[AgSCH_2CHOHCH_2OH]_n$ for 24 h.

We used low-energy ion scattering (LEIS) to provide information about atomic composition with respect to depth. As probe ions strike the surface in this experiment, atoms are removed by sputtering so that over successive scans a depth profile of composition can be obtained. The initial spectrum indicated the presence of Au, Ag, C, O, and S. As the scans progressed, the silver and gold signals became more prevalent (Figure 6.9), consistent with the Ag atoms on top of the Au surface and with sulfur and carbon on top of silver.

An attempt to replace any adsorbed thiolate with a different thiol, while leaving the Ag in place was not successful. When films were immersed in a 1-mM solution of hexadecanethiol for 24 h., there was little change in the advancing contact angle of water on the surface (42°), indicating that replacement of the original thiolate groups was not achieved.

We also attempted to form SAMs from the *tert*-nonyl polymer, $[AgSC(CH_3)_2(CH_2)_5CH_3]_n$. A gold film was treated with a 5-mM solution (based on repeat units) of the polymer in ethanol for 24 h. Samples were then removed and rinsed with ethanol, water, and dried under a stream of N_2. The advancing contact angle of water was 95°, and the receding angle was 68°. An XPS survey spectrum revealed the presence of gold, silver, carbon, and sulfur (Figure 6.10). A high-resolution spectrum in the Ag 3d region (Figure 6.11) could be fit with two spin-orbit doublets, in a ratio of 5.8:1.0. The larger doublet appeared at 367.8 eV (Ag $3d_{5/2}$, fwhm, 0.78 eV) and 373.8 eV (Ag $3d_{3/2}$, fwhm, 0.78 eV), and the smaller at 368.3 eV (Ag $3d_{5/2}$, fwhm, 0.80 eV) and 374.8 eV (Ag $3d_{3/2}$, fwhm, 0.80 eV). In contrast to the SAM formed from the diol

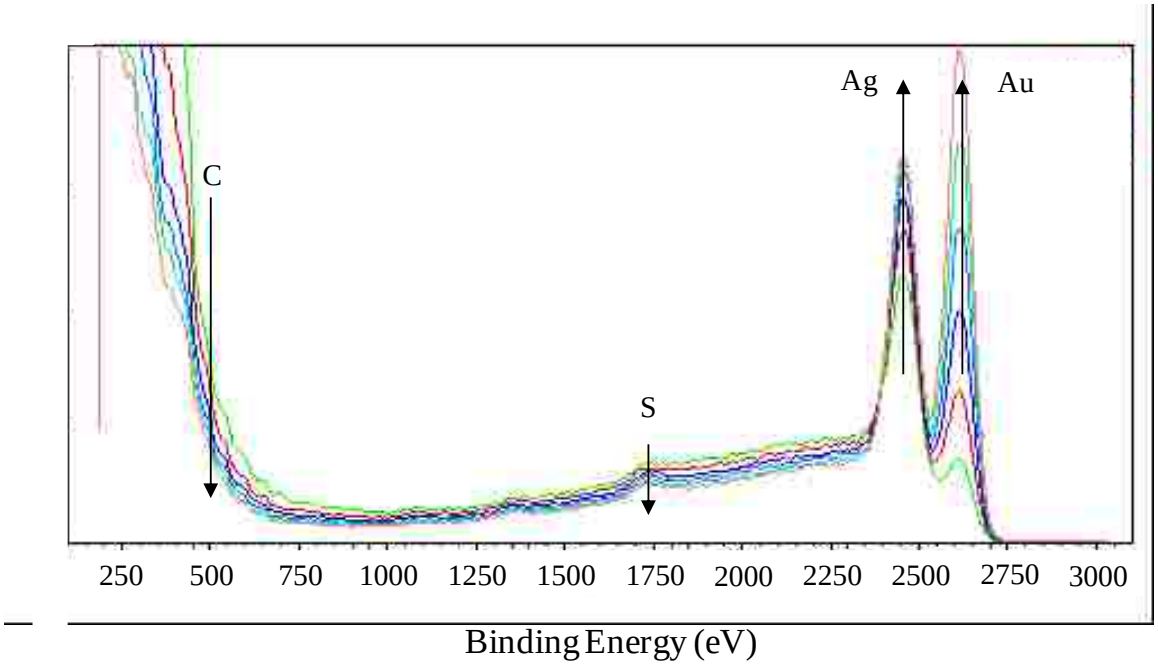

Figure 6.9. Low-energy ion scattering spectra of a gold film immersed in a 5-mM aqueous solution of $[AgSCH_2CHOHCH_2OH]_n$ for 24 h. The change in the spectra during the progression of scans is indicated by arrows. As the number scans increases, the peaks associated with silver (~ 2420 eV) and gold (~ 2625 eV) became more pronounced, while the peak associated with sulfur (~ 1750 eV) and the scattering that results from carbon (below ~ 700 eV) decreased.

polymer,the predominant Ag 3d doublet appears at the same binding energy as reported for a SAM formed on UPD-Ag (Ag $3d_{5/2}$, 367.8 eV).[15] The smaller component appears at the same binding energy found for the diol polymer, possibly indicative of the presence of a small amount of Ag_2S or silver metal, as speculated for that system. A spectrum in the S 2p region (Figure 6.12) revealed a spin-orbit doublet (161.8 eV, S $2p_{3/2}$, fwhm, 0.94 eV; 163.0 eV, S $2p_{1/2}$, fwhm, 0.94 eV) consistent with thiolate sulfur. The ratio of Ag:S was 2.0:3.6, however, rather than the expected 1:1. As with adsorption of the diol polymer, this ratio may indicate some decomposition of the polymer to Ag_2S or silver metal and disulfide, which could then assemble on the gold surface.

We also attempted to form SAMs from the carboxylic-acid polymer, $[AgSCH_2CH_2COOH]_n$. A gold film was immersed in an aqueous solution containing 5-mM polymer (based on repeat units) and 0.397-M NaOH for 24 h, then removed from solution and rinsed with deionized water, 0.20-M HCl, and dionized water again. To determine if the surface of these films contained any carboxylic-acid groups, a contact-angle titration was performed:[23-25] Aqueous solutions of various pH values were used as probe liquids for contact-angle measurements. The variation in contact angle as a function of pH can give an indication of the acidic or basic nature of a surface. As shown in Figure 6.13, the contact angle was relatively constant from pH 1 to 4, decreased between 4 and 6, and was again relatively constant at high pH. This behavior is consistent with the presence of carboxylic-acid groups at the surface, with the charged carboxylate ion being more hydrophilic than the uncharged acid form.

A XPS survey spectrum revealed the presence of gold, silver, carbon, and sulfur,

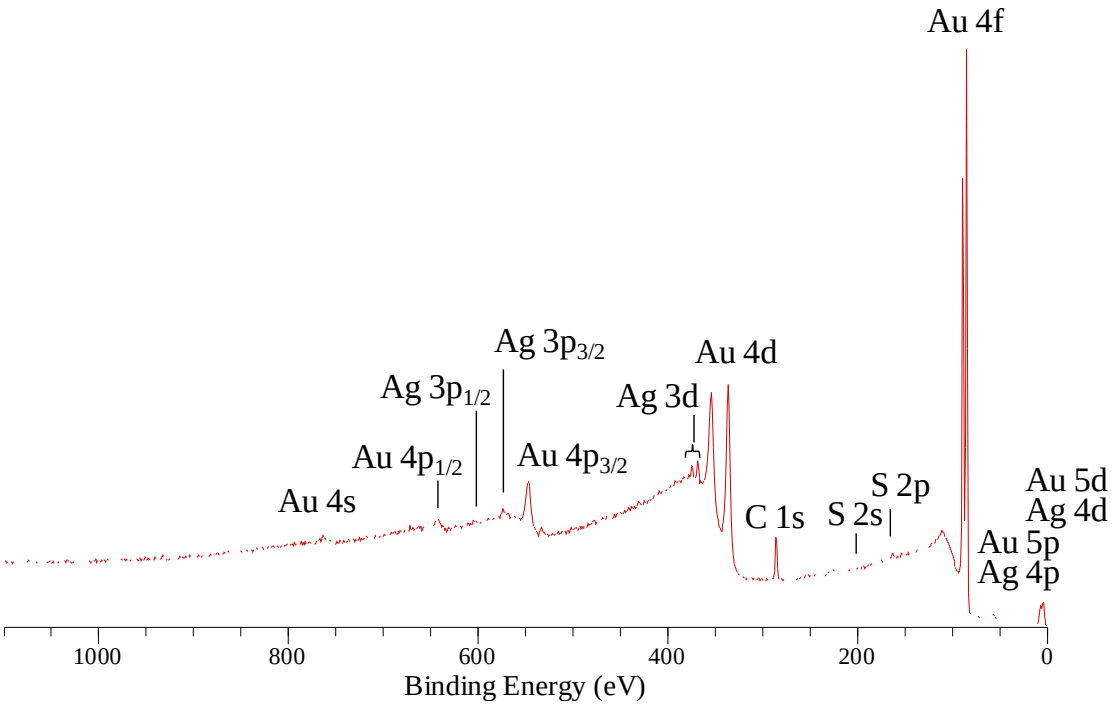

Figure 6.10. An XPS survey spectrum of a gold film immersed in a 5-mM solution of $[AgSC(CH_3)_2(CH_2)_5CH_3]_n$ in ethanol for 24 h.

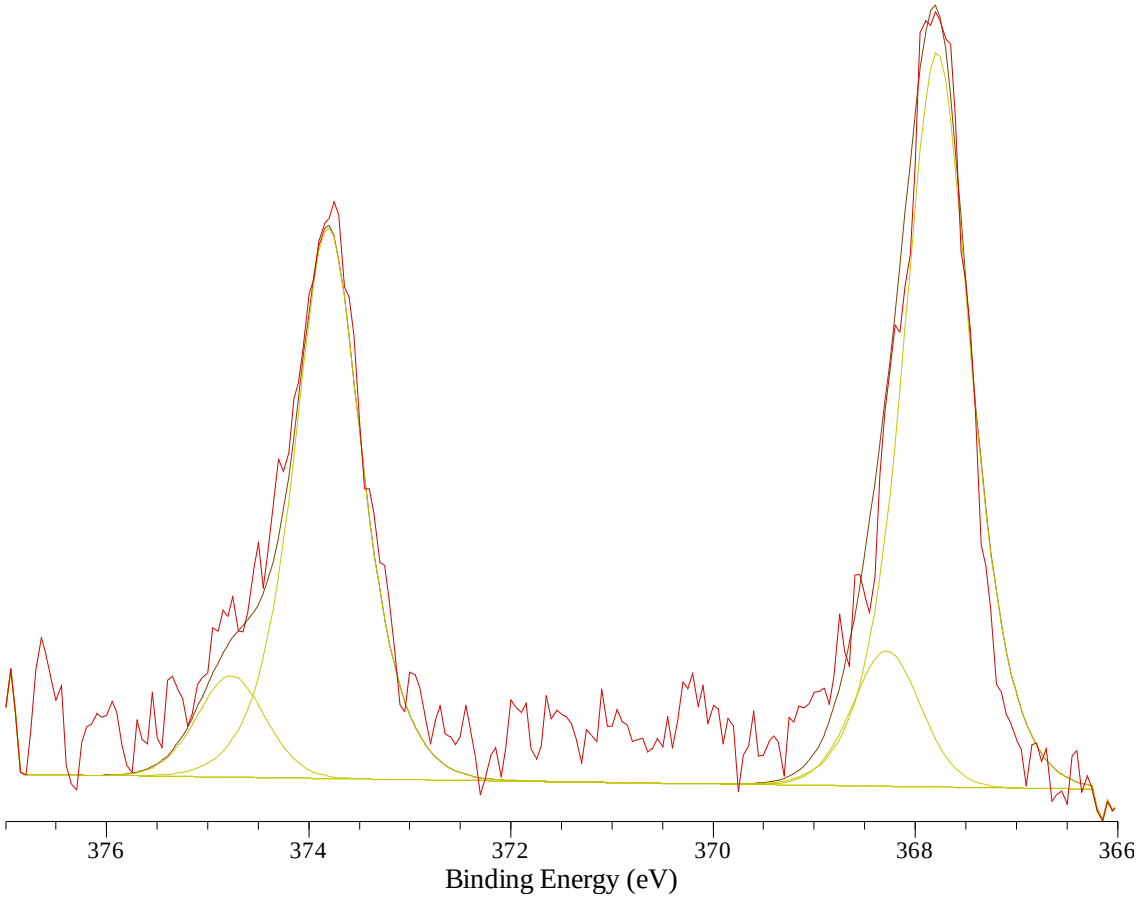

Figure 6.11. A high-resolution XPS spectrum in the Ag 3d region of a gold film immersed in a 5-mM solution of $[AgSC(CH_3)_2(CH_2)_5CH_3]_n$ in ethanol for 24 h.

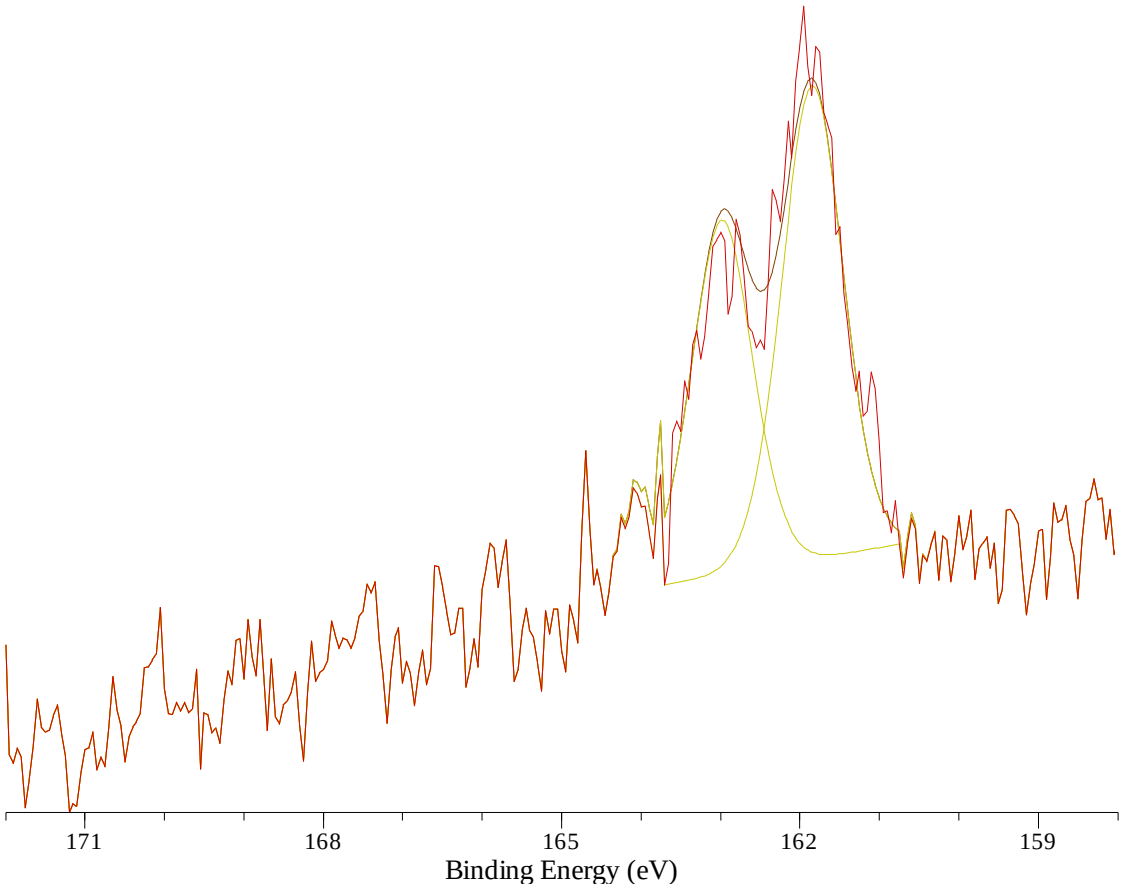

Figure 6.12. A high-resolution XPS spectrum in the S 2p region of a gold film immersed in a 5-mM solution of $[AgSC(CH_3)_2(CH_2)_5CH_3]_n$ in ethanol for 24 h.

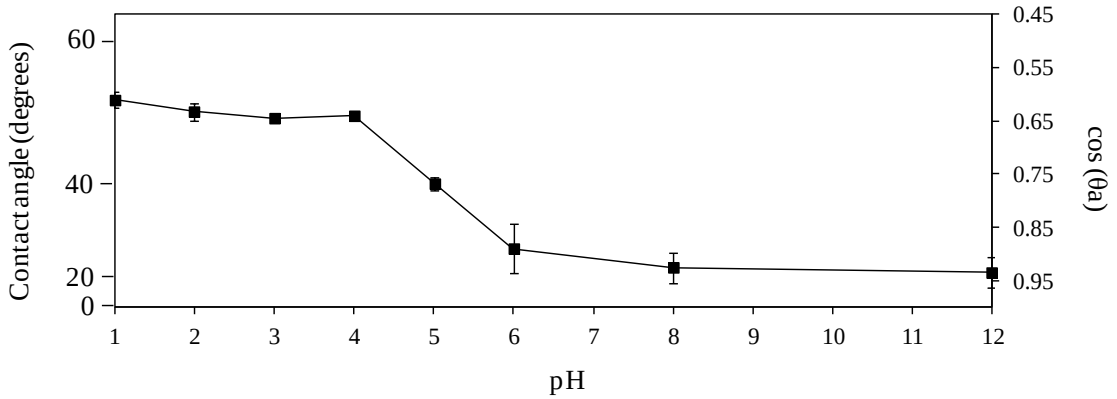

Figure 6.13. Contact-angle titration of a gold film immersed in a 5-mM solution of $[AgSCH_2CH_2COOH]_n$ in aqueous 0.397-M NaOH for 24 h. The error bars represent the standard deviation of six measurements on the sample.

but no oxygen (Figure 6.14). The lack of photoemission from oxygen in this spectrum is not consistent with a surface terminated by carboxylic-acid groups. A high-resolution spectrum in the Ag 3d region (Figure 6.15) revealed a spin-orbit doublet at 367.8 eV (Ag $3d_{5/2}$, fwhm, 0.78 eV) and 373.8 eV (Ag $3d_{3/2}$, fwhm, 0.78 eV) which corresponded well to that of UPD-silver coated with a SAM from octadecane thiol,[15] as well as that of the *tert*-nonyl polymer. A high-resolution spectrum in the C 1s region (Figure 6.16) contained photoemission that could be adequately fit by a single peak at 284.6 eV (fwhm, 1.1 eV), with no peak at higher binding energy (~ 289.3 eV) characteristic of a carboxyl carbon.[18] The absence of this peak is consistent with the absence of oxygen in the survey scan, but not the contact-angle titration on an analogous sample. These spectra may suggest some decarboxylation, possibly catalyzed by the presence of Ag^+ (Figure 6.17),[26] though this seems unlikely given the affinity of sulfur for silver. A high-resolution spectrum in the S 2p region (Figure 6.18) revealed a spin-orbit doublet (161.8 eV, S $2p_{3/2}$, fwhm, 0.94 eV; 163.0 eV, S $2p_{1/2}$, fwhm, 0.94 eV) consistent with thiolate sulfur, close to that found for the *tert*-nonyl polymer on gold. The ratio of Ag:S was 7:3, in contrast to the other polymers. Although this ratio is indicative of some decomposition to deposit Ag metal or Ag_2S, the spectrum in the silver region indicated only thiolate-bound silver.

From the XPS data for these polymers, we conclude that the diol polymer appears to significantly decompose, resulting in a mixture of species being adsorbed on gold. High-resolution XPS spectra in the silver and sulfur regions suggest the presence of silver metal and/or Ag_2S, rather than thiolate species, and the Ag:S ratio inconsistent with the formation of a SAM on UPD-Ag/Au. The contact-angle data for this surface are slightly

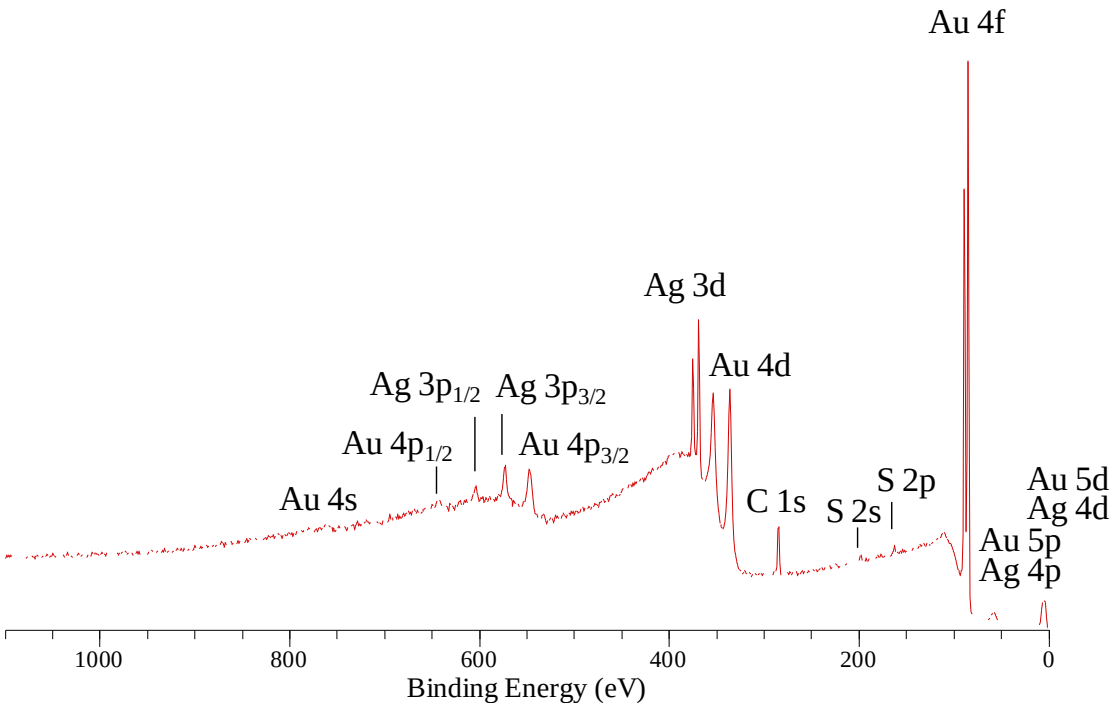

Figure 6.14. An XPS survey spectrum of a gold film immersed in a 5-mM solution of $[AgSCH_2CH_2COOH]_n$ in aqueous 0.397-M NaOH for 24 h.

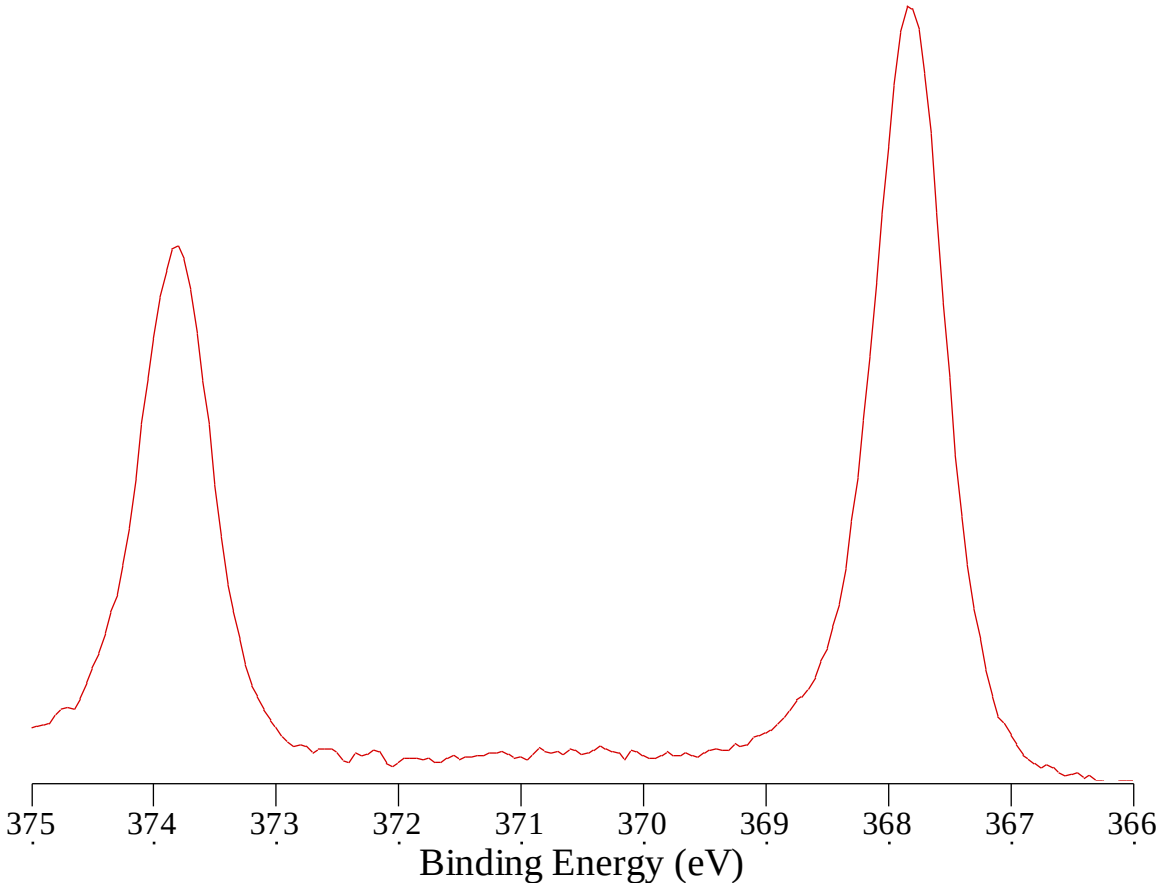

Figure 6.15. A high-resolution XPS spectrum in the Ag 3d region of a gold film immersed in a 5-mM solution of $[AgSCH_2CH_2COOH]_n$ in aqueous 0.397-M NaOH for 24 h.

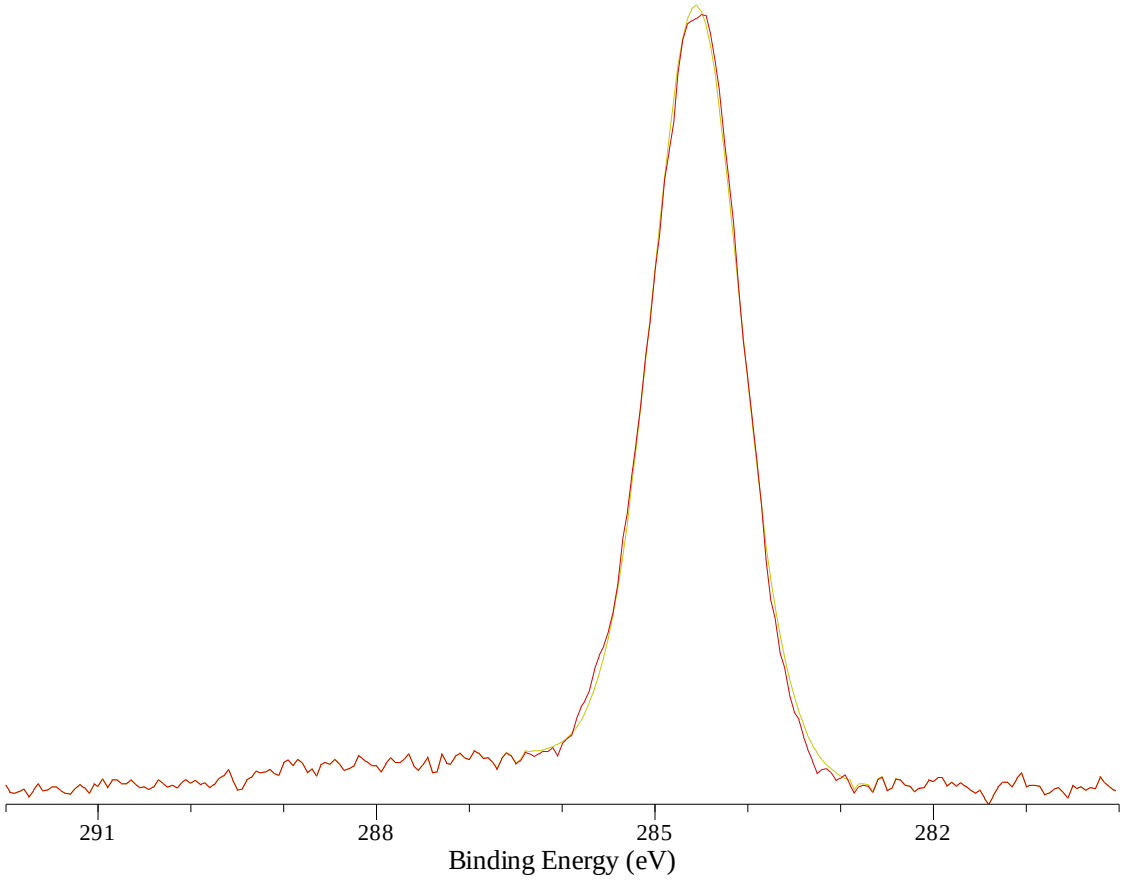

Figure 6.16. A high-resolution XPS spectrum in the C 1s region of a gold film immersed in a 5-mM solution of $[AgSCH_2CH_2COOH]_n$ in aqueous 0.397-M NaOH for 24 h.

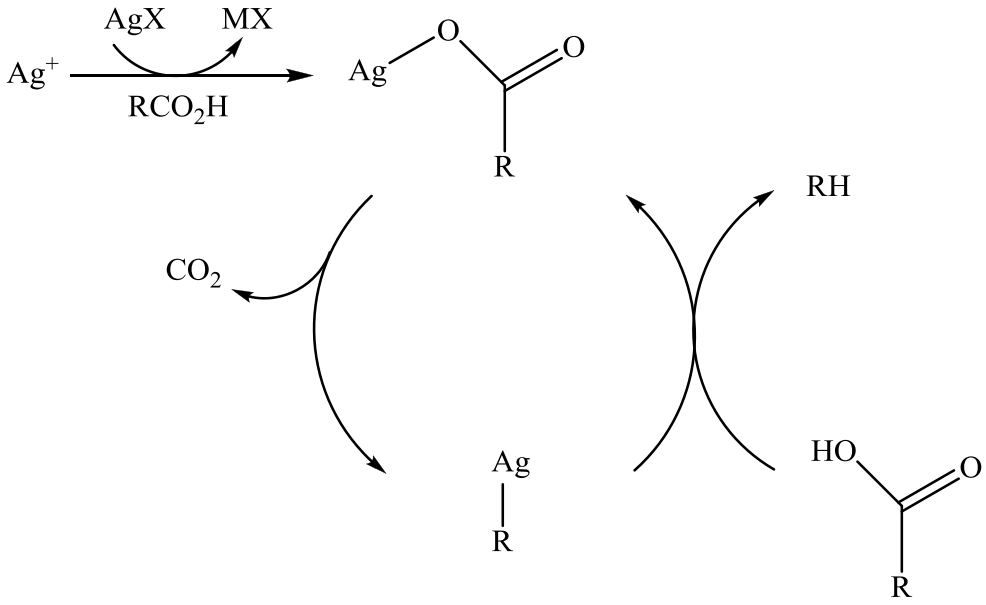

Figure 6.17. Mechanism proposed for silver-catalysed decarboxylation in reference 25.

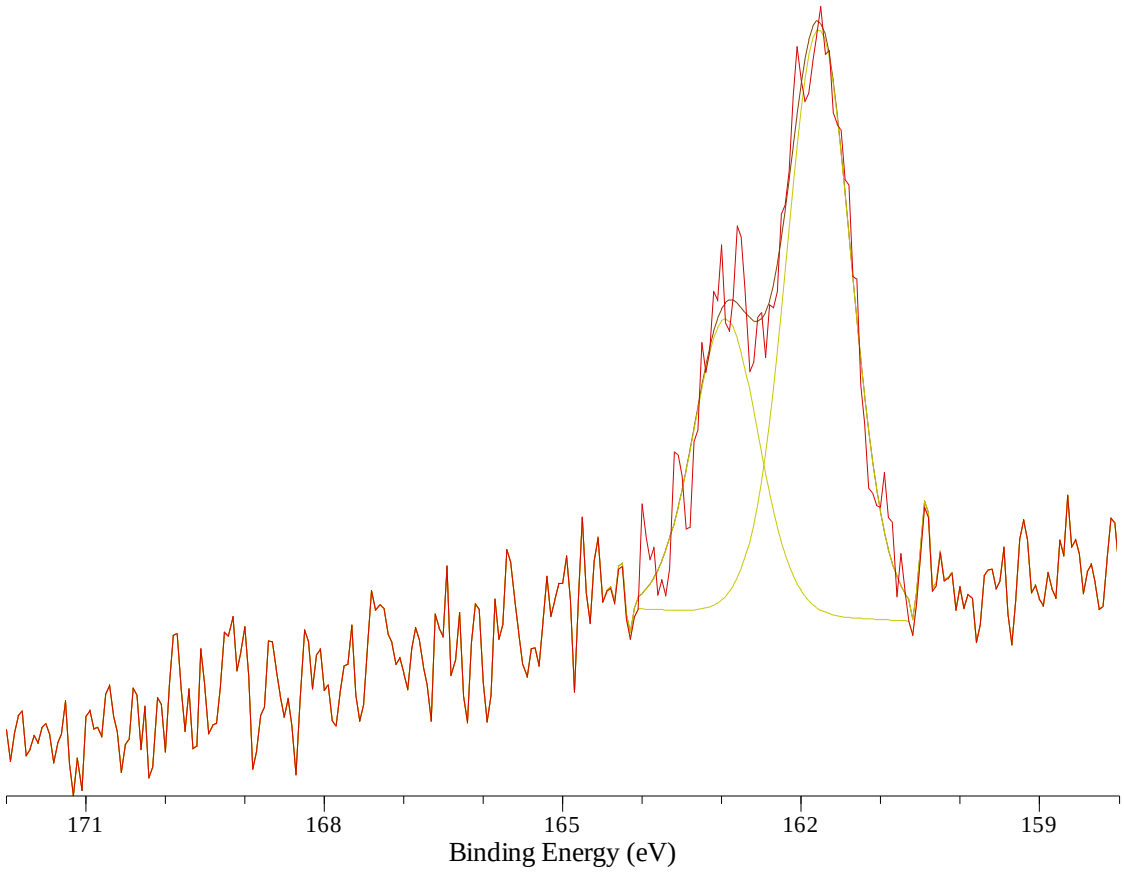

Figure 6.18. A high-resolution XPS spectrum in the S 2p region of a gold film immersed in a 5-mM solution of $[AgSCH_2CH_2COOH]_n$ in aqueous 0.397-M NaOH for 24 h.

higher than with that on a surface formed by adsorption of the thiol on a UPD-Ag/Au surface, though LEIS spectra of a similar film are consistent with the desired structure.

Results from gold exposed to the *tert*-nonyl polymer were similar to those of the diol polymer. High-resolution XPS spectra in the silver region indicated the adsorbed material was predominately thiolate-bound silver, however, a peak corresponding to silver metal or Ag_2S was also present, indicating some decomposition of the polymer. A high-resolution spectrum in the sulfur region confirmed the presence of thiolate, however, the Ag:S ratio was inconsistent with the formation of a SAM on UPD-Ag/Au, and indicated a large excess of silver. Contact-angle data for the gold film exposed to the *tert*-nonyl polymer, however, are consistent with that of adsorption of a monolayer on the surface.

The silver and sulfur XPS binding energies for films formed from the carboxylic-acid polymer on gold most closely matched those of a SAM on UPD-Ag/Au, however, the Ag:S ratio was inconsistent and the surface contained no oxygen (by XPS).

6.3.4 The Formation of Silver Nanoparticles from Silver (I)-thiolate Polymers

Given the evidence for the decomposition of silver(I)-thiolate polymers summarized above, we attemped to utilize this instability to our benefit. Therefore, the second focus of our interest in silver (I)-thiolate polymers was in their possible role as precursors to silver nanoparticles. We hypothesized that controlled decomposition of these polymers might produce of Ag^0 nanoparticles and dialkyl disulfides (equation 6.2).

$$AgSR \xrightarrow{\Delta \text{ or } \lambda\nu} RSSR + Ag^0 \text{ (NP)} \qquad (6.2)$$

The remaining thiolate polymer might then act as a capping agent for the nanoparticles and prevent uncontrolled growth of the nanoparticles in size. Some indication that this process might be viable was provided by the high temperature thermal decomposition of the silver containing metal-organic polymer, $[Ag(\mu_3\text{-malic acid})]_n$.[9] Our work indicated that low-temperature synthesis of soluble silver nanoparticles from silver(I)-thiolate polymers might be possible. We examined both thermolysis and photolysis of our polymers as possible routes to controlled decomposition.

6.3.4.1 Thermolysis of Silver (I)-thiolate Polymers

A 5-mM aqueous solution of the diol polymer, $[AgSCH_2CHOHCH_2OH]_n$ was heated at 90 °C. Over 5 h, the color of the solution changed from an initial pale yellow to olive green. Analysis by UV/vis spectrophotometry showed the growth of two absorbances, centered at ~460 nm and ~600 (Figure 6.19), as well as scattering of light at wavelengths below ~425 nm. These peak maxima are consistent with some literature examples of surface plasmon peaks for Ag nanoparticles,[27-29] though more commonly these peaks appear at shorter wavelengths (360 – 450 nm for particles with diameters of ~2 – 50 nm).[29,30] Filtration of these solutions through 200 nm syringe-tip filters did not significantly affect the spectra. Upon storage at room temperature, the spectra of these heated samples changed over the course of days, indicating that the products formed were not stable. The solutions were stable, however, when heated in the presence of the polyethylene glycol surfactant, Pluronic L62®. A sample (5-mM solution) of the diol polymer was thermolyzed for 30 min and analyzed by transmission electron microscopy (TEM) to confirm the presence of irregularly shaped nanoparticles with sizes ranging

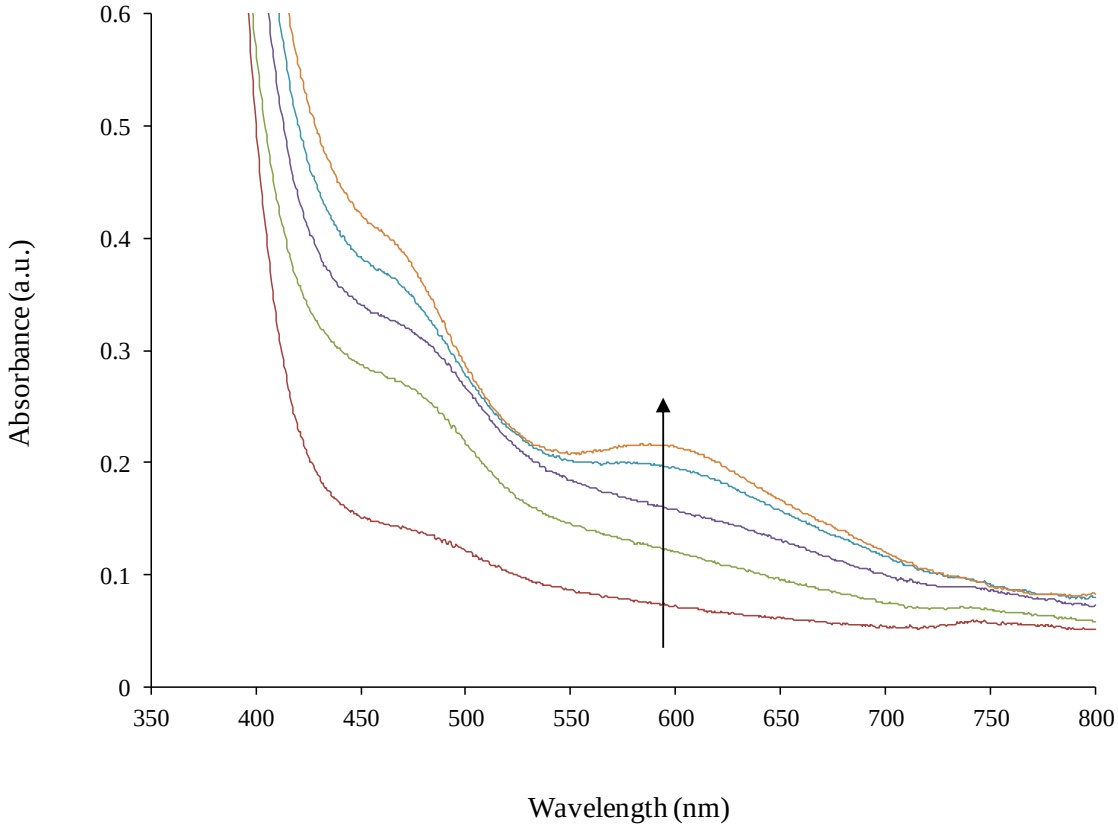

Figure 6.19. Time-dependent UV/vis spectra of a 5-mM aqeuous solution of $[AgSCH_2CHOHCH_2OH]_n$ heated in water at 90 °C. The arrow indicates the progression of spectra taken of samples heated for 12, 15, 20, 45, and 60 min, respectively.

from 2 – 20 nm (Figure 6.20). The range of sizes indicates that the decomposition of the diol polymer is not sufficiently controlled by the available thiolate groups or the disulfide byproduct.

Heating a 5-mM solution of the *tert*-nonyl polymer in refluxing toluene produced no visible color changes, and analysis by UV/vis spectrophotometry did not reveal the appearance of any absorbances. Heating a 5-mM aqueous solution of $[AgSCH_2CH_2COOH]_n$ in basic solution did produce color changes, from pale yellow to orange, over 1 – 3 h. If the solution were heated for a longer period, however, it became brown and a solid precipitated. When the concentration of OH^- was varied, the solution color after thermolysis would also vary, but no clear trend in this variance could be ascertained. Despite the color changes, UV/vis spectra of solutions that had been heated for 1 – 3 h revealed only scattering at short wavelengths (< 400 nm) and did not contain any peaks.

6.3.4.2 Photolysis of Silver (I)-thiolate Polymers

Photolysis of silver (I) salts is a well-established route to the formation of silver nanoparticles.[31-34] The process is similar to black-and-white photography in that silver salts, such as silver halides, silver nitrate, and silver perchlorate, are photoreduced to silver metal in the presence of an electron donor. The mechanism in solution is thought to occur by the electron transfer from a solvent molecule to a silver ion,[35] though this effect can be enhanced by the addition of electron donating species to the reaction mixture such as TiO_2 or ketones.[32,33,36] We attempted to use this process with our polymers as precursors. Photolysis of the carboxylic-acid and diol polymers in water (5

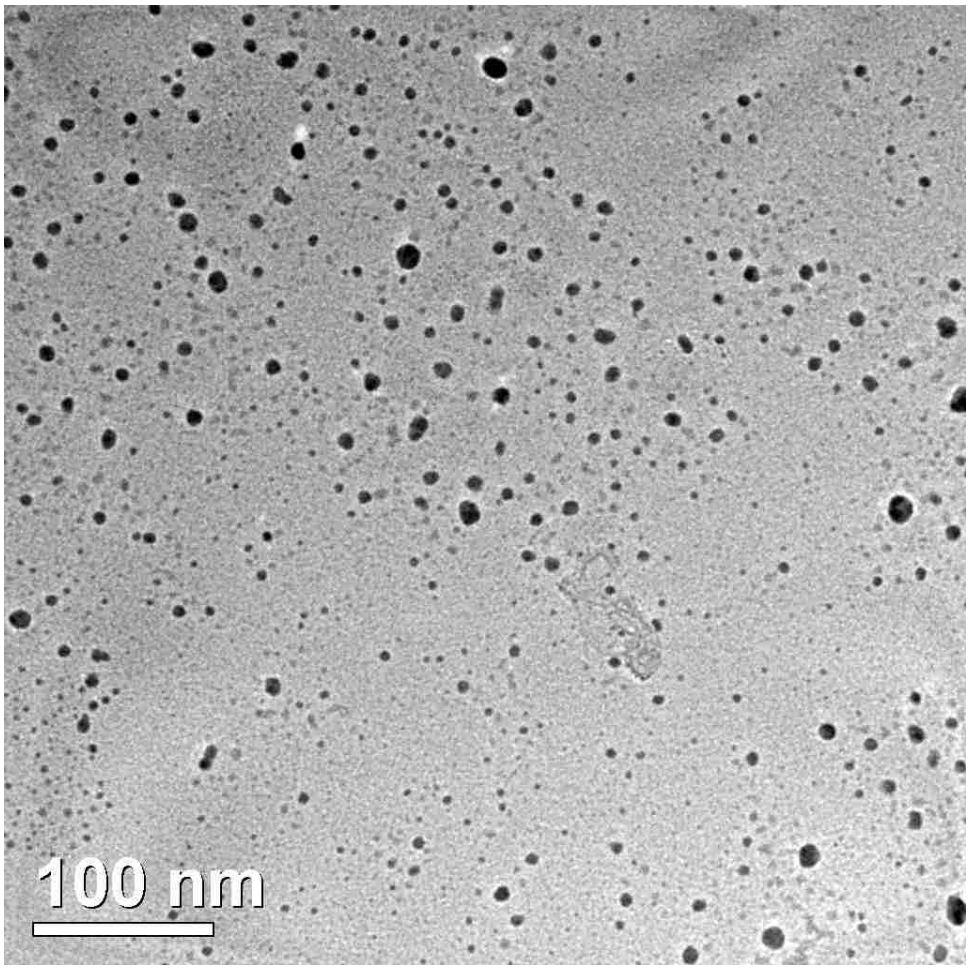

Figure 6.20. A TEM image at 250K magnification of nanoparticles formed by the thermolysis of $[AgSCH_2CHOHCH_2OH]_n$ in aqueous solution at 90 °C for 30 min.

mM) using a UV photoreactor with emission in the range of 300 – 415 nm and a λ_{max} at 350 nm generated little change in the color of the solutions.

Photolysis of $[AgSC(CH_3)_2(CH_2)_5CH_3]_n$ in hexanes (5 mM) in a glass roundbottom flask (λ cut-off of 275 – 320 nm) fit with a condenser for times ranging from 15 min to 5 h did, however, produce changes in the solutions. Hexanes was chosen as a solvent because it does not absorb between 300 and 415 nm. Analysis of these samples by UV/vis (Figure 6.21) revealed the growth of an absorbance near 500 nm, which shifted to longer wavelengths and became more intense with longer exposure, indicative of a plasmon reasonance shifting as particle size increases. Scattering above ~450 nm also became more prominent over time, consistent with the formation of large nanoparticles. The solution progressed from colorless, through yellow and orange, to deep red over 5 h. To explore the effect of higher-energy light provided by the photoreactor, a quartz flask was used to allow transmittance of light down to a wavelength of ~ 200 nm, compared to a cut-off of ~ 275 – 320 nm for a glass flask. Surprisingly, although a similar color and spectral progression proceeded, it did so at a slower rate. The effect of the silver(I)-thiolate polymer concentration on photolysis (in quartz) was also studied. The concentrations of photolyzed solutions were increased to 9.73 mM and 33.69 mM, which resulted in a more prominent absorbance near 525 nm for the polymers photolyzed in solution (Figure 6.22). The polymer was also photolyzed as a neat oil in a quartz cuvette, then suspended as a 16 mM solution in hexanes for UV/vis analysis, which showed a smaller absorbance near 510 nm (Figure 6.22).

We attempted to purify the polydisperse samples of nanoparticles, made from photolysis of samples in quartz flasks, to produce a more monodisperse composition.

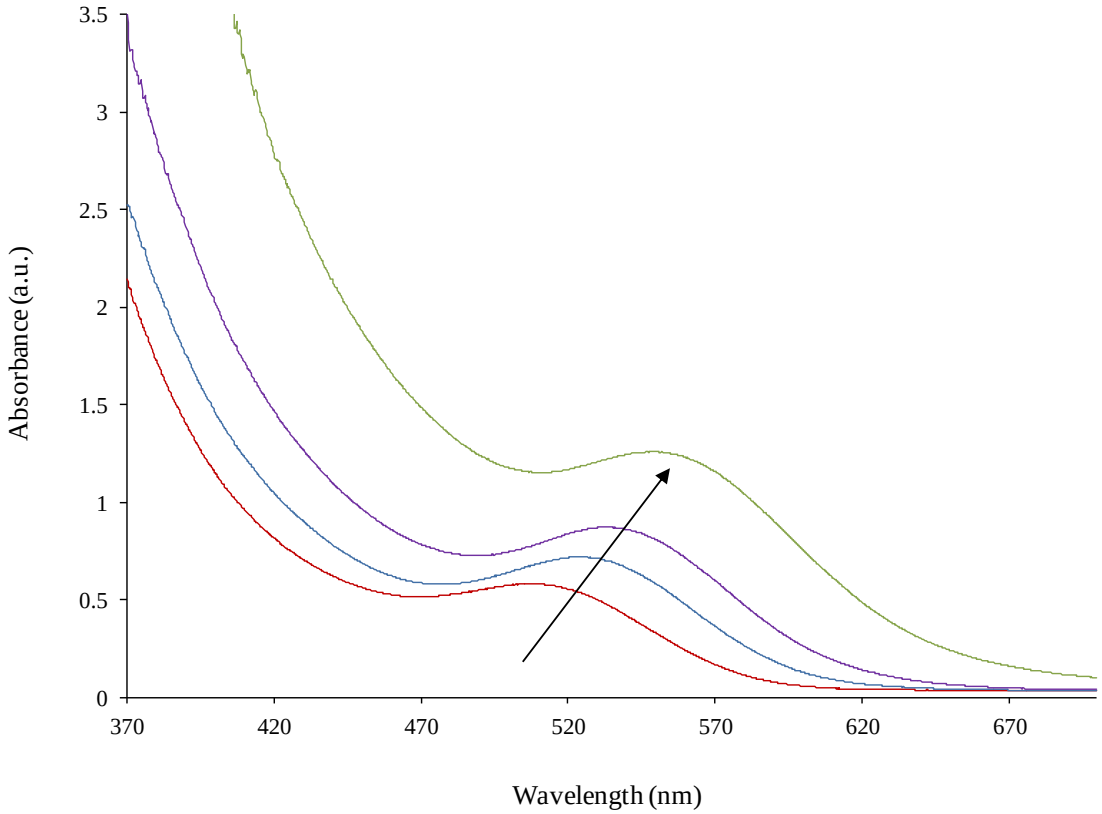

Figure 6.21. Time-dependent UV/vis spectra of a 5-mM hexanes solution of $[AgSC(CH_3)_2(CH_2)_5CH_3]_n$ photolyzed in a glass flask. The arrow indicates the progression of spectra taken of samples heated for 1, 2, 3, and 5 h, respectively.

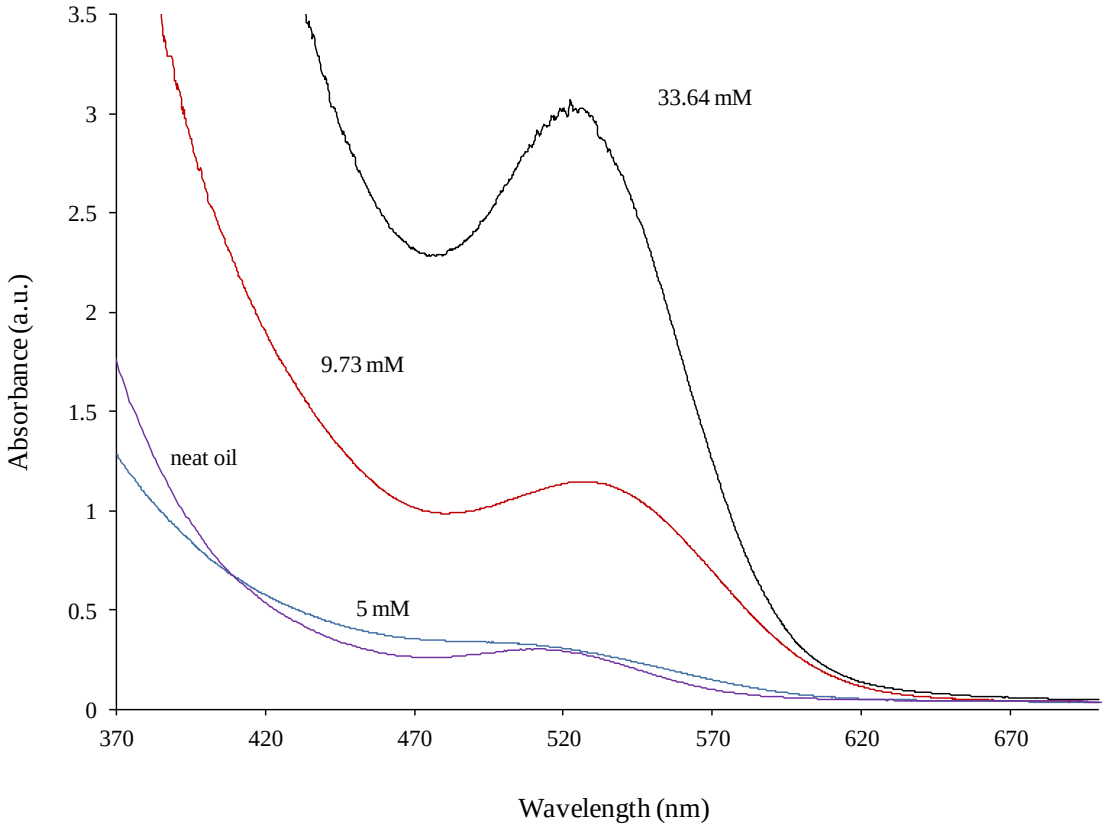

Figure 6.22. UV/vis spectra of hexanes solutions of $[AgSC(CH_3)_2(CH_2)_5CH_3]_n$ photolyzed in quartz for 2 h at different concentrations.

The solvent was removed from a 33.69-mM sample, leaving behind yellow oil spotted with red. The yellow color was similar to that of the unreacted polymer. The oil was stirred in warm (30 °C) methanol until the solvent picked up most of the red color, generating a pinkish solution, and leaving behind the yellow oil. This solution was decanted, then cooled in an ice bath, which resulted in the formation of a cloudy white precipitate, consistent with di-*t*-nonyl disulfide. The precipitate was removed by filtration through a 250-nm syringe-tip filter, giving a clear pink solution. The UV/vis spectrum of this solution displayed a large peak at ~ 535 nm, with considerably less scattering than previously seen (Figure 6.23). The reason for the red-shift in this spectrum is not immediately clear. Analysis by TEM confirmed the presence of nanoparticles, however, the sample was not monodisperse (Figure 6.24). Images indicate a bi-modal distribution of large particles (~ 10 – 50 nm) smaller (~ 2 – 5 nm) particles. From these images, it is not clear if the particles formed are composed of Ag metal or AgS_2, or if the particles are two- or three-dimensional. Although there is a literature example of ~ 25-nm Ag nanoparticles having an absorbance maximum near 535 nm,[28] typically, large particles around 100 nm have absorbances near 535 nm, and particles on the order of 2 – 50 nm absorb near 360 – 450 nm.[29,30] An attempt to purify this sample further by centrifugation at a speed of 50,000 rpm for 2 h, resulted in the separation of a similar red-spotted yellow oil, and leaving behind a pink solution. Analysis by UV/vis revealed little change across the wavelength region (Figure 6.23). Transmission electron microscopy images of the centrifuged sample (Figure 6.25) showed a gradated distribution of particle sizes, from large particles in the range of 10 – 15 nm to smaller particles around 2 – 5 nm.

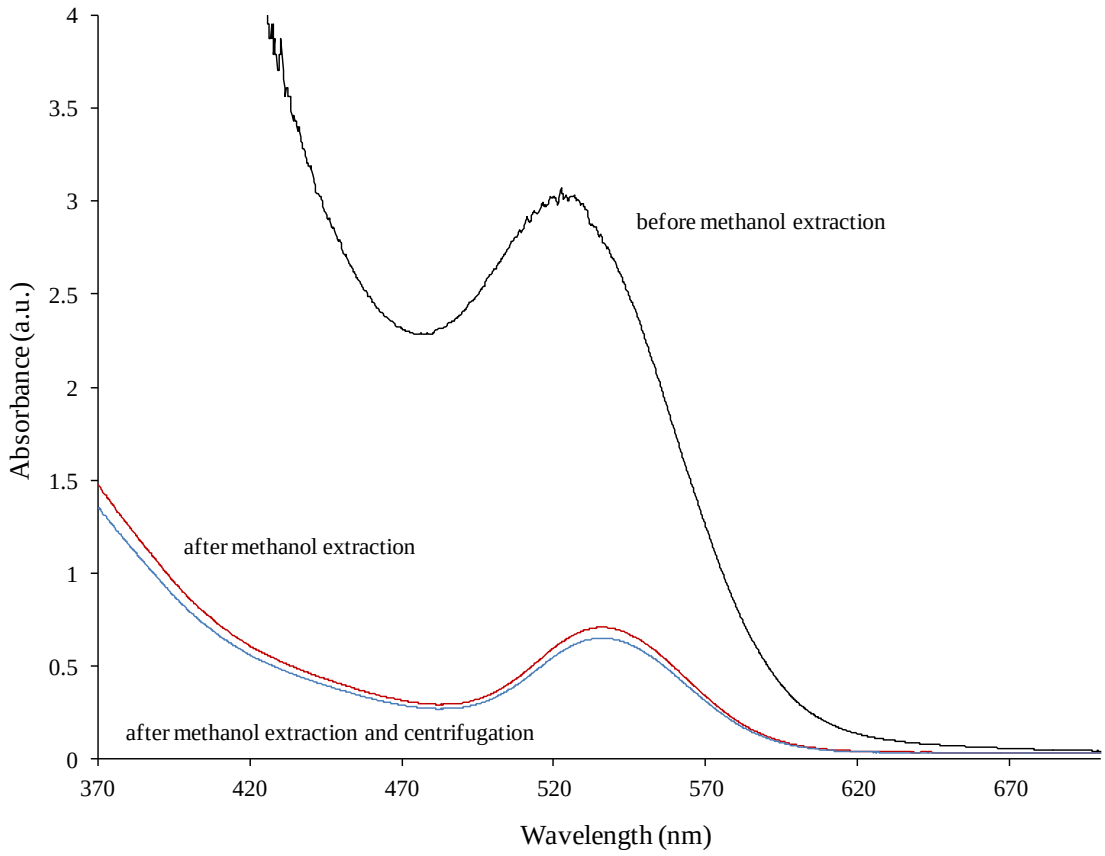

Figure 6.23. UV/vis spectra of a 33.69-mM solution of $[AgSC(CH_3)_2(CH_2)_5CH_3]_n$ photolyzed in a quartz flask for 2 h before extraction from methanol, after extraction from methanol, and after extraction from methanol and centrifugation at 50,000 rpm.

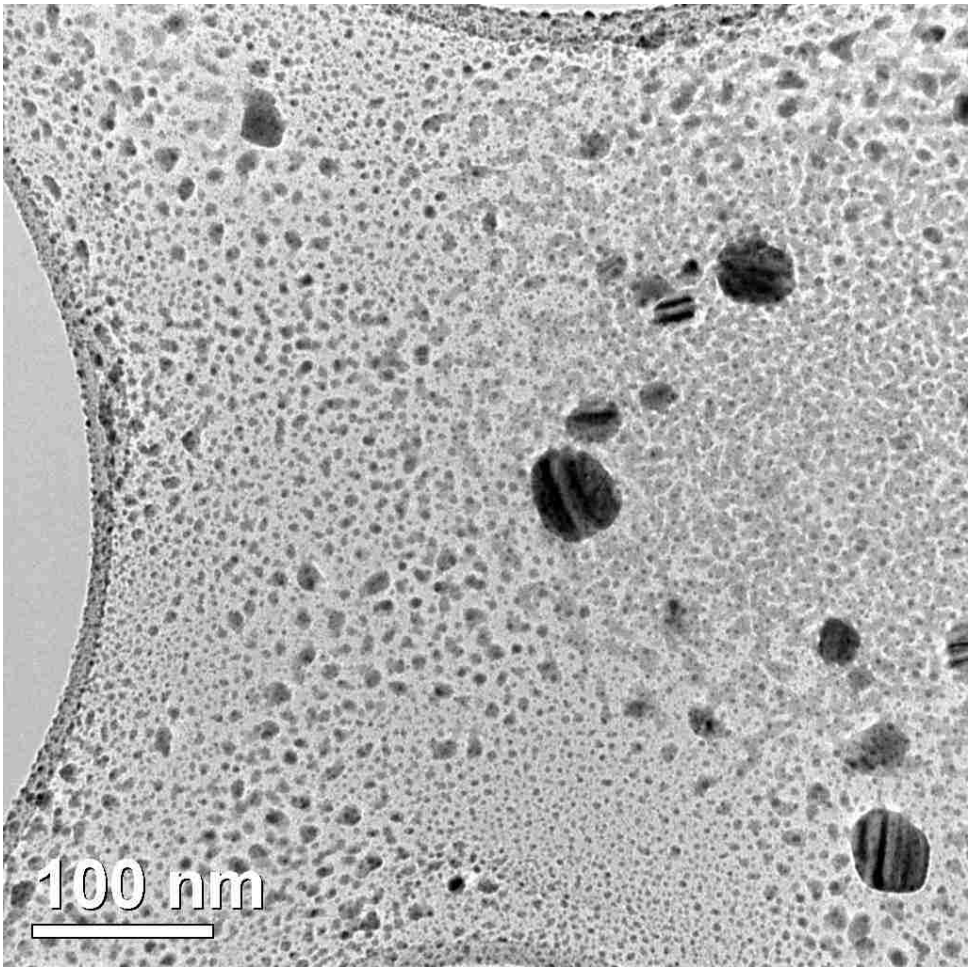

Figure 6.24. A TEM image at 250K magnification of nanoparticles formed by the photolysis in a quartz flask of a 33.69-mM solution of $[AgSC(CH_3)_2(CH_2)_5CH_3]_n$ in hexanes for 2 h.

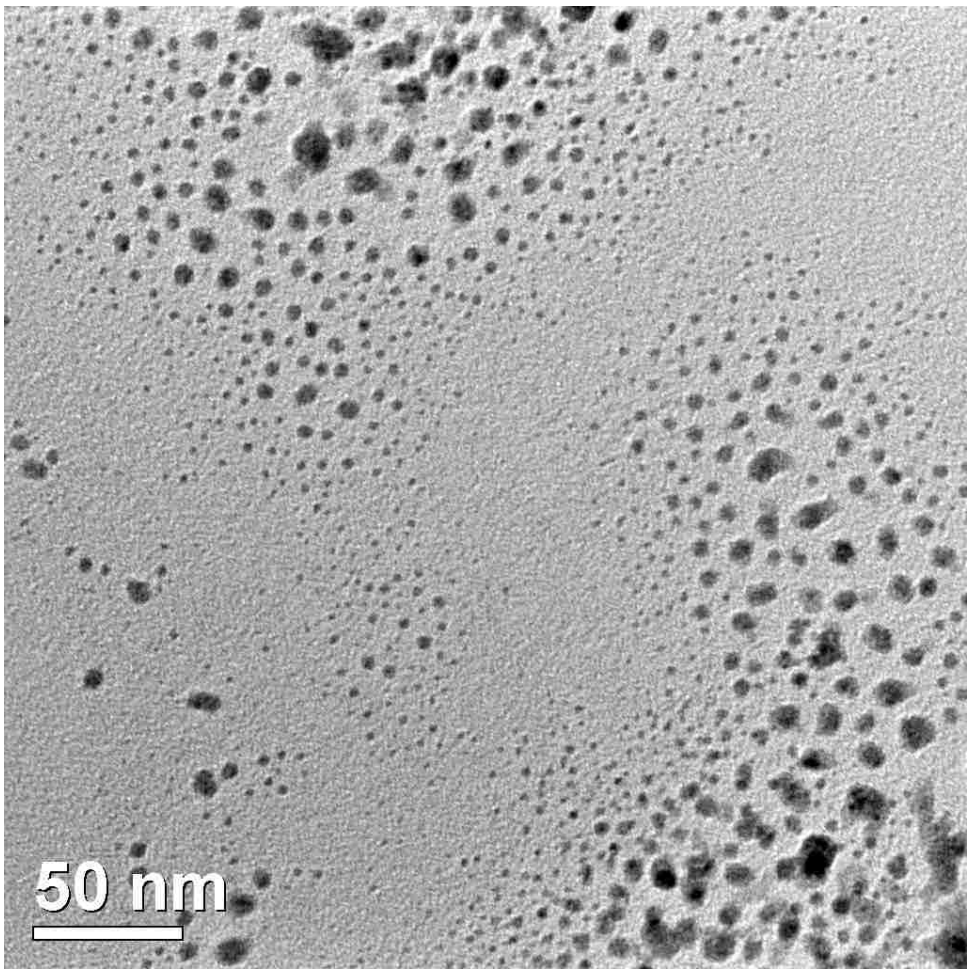

Figure 6.25. A TEM image at 500K magnification of nanoparticles formed by the photolysis in a quartz flask of a 33.69-mM solution of $[AgSC(CH_3)_2(CH_2)_5CH_3]_n$ in hexanes for 2 h and have been purified by extraction from methanol, filtration and centrifugation at 50,000 rpm.

6.4 Conclusions

The silver(I)-thiolate polymers described in this chapter adsorbed onto gold surfaces from solution, however, it is likely that decomposition of the polymers occurred during this process. Analysis by XPS indicated that the diol polymer decomposed significantly with no evidence for a thiolate-bound structure similar to a SAM on UPD-Ag/Au. High-resolution XPS spectra in the silver and sulfur regions indicated that silver metal or Ag_2S may have formed as the polymer decomposed. Analysis of films from the *tert*-nonyl and carboxylic-acid polymers, however, did confirm the presence of thiolate species for those systems, though decomposition of the polymers was also observed. High-resolution XPS spectra of the *tert*-nonyl polymer in the silver and sulfur regions indicated the adsorbed material was predominately thiolate-bound silver, however, some silver metal or Ag_2S was likely also present. High-resolution XPS spectra in the silver and sulfur regions for films formed from the carboxylic-acid polymer resembled that from SAMs on UPD-Ag/Au, however, an XPS survey spectrum did not reveal the precence of any oxygen, and a high-resolution spectrum in the carbon region was not consistent with a carboxylic-acid terminated surface.

Silver nanoparticles can be formed from these polymers by either thermolysis or photolysis, as shown by UV/vis spectra and TEM images. The UV/vis spectra contained peaks assigned to surface plasmon reasonances of silver nanoparticles, and TEM images show polydisperse distributions of nanoscale silver-metal particles. Thermolysis of the diol polymer in water resulted in spherical nanoparticles with a size distribution of 2 – 20 nm, but thermolysis of the other polymers was unsuccessful. Photolysis of the diol and carboxylic-acid failed to produce any silver nanoparticles,

photolysis of the *tert*-nonyl polymer in hexanes resulted in the formation of a bi-modal distribution of large (~ 10 – 50 nm) and small (~ 2 – 5 nm) particles after purification by extraction from methanol. Further purification of this sample by centrifugation reduced this particle size distribution to 2 – 15 nm.

6.5 Experimental

General. *Tert*-nonyl mercaptan (95.0% mixture of isomers) was purchased from TCI America and used as received. 3-Mercaptoproprionic acid (99+ %) and 3-mercapto-1,2-propanediol were used as purchased from Aldrich. Reagent grade acetone (99.9%), methanol (99.9%), and hexanes (95.8%) were used as purchased from Pharmco-AAPER and Commercial Alcohols. Ethanol (Anhydrous, J.T. Baker, 95%) was used as received. Acetonitrile (ACN, Acros, 99.8%) and tetrahydrofuran (THF, Mallinckrodt, 99%) were purified and dried using a PureSolv system (Innovative Technology, Inc.). Silver nitrate (99.8%) and chloroform (99.9%) were purchased from Fischer and used as received. Hexadecane (99%, Aldrich) was passed through activated alumina twice before use in contact-angle measurements. Gold (99.999%) was used as supplied by VEM Vacuum Engineering. Dichloromethane (99.5%), toluene (99.9%), hydrogen peroxide (30%), sodium hydroxide (97%), and sulfuric acid (95%) were used as received from EMD. Pluronic L62® surfactant was purchased from BASF and used as received.

Preparation of Gold Films. Gold films were prepared on piranha-cleaned glass slides. *Caution: Piranha solution, a 4:1 (v/v) mixture of concentrated H_2SO_4 and 30% H_2O_2, reacts violently with organic material and should be handled carefully.* Approximately 50 Å of Ti (as an adhesion promoter) and then 1000 Å of Au were

evaporated onto the substrates by e-beam vapor deposition. Electrodes were used soon after deposition, or cleaned prior to use by cycling its potential (-1.2 V to 1.5 V, 100 mV/s) seven times in 0.5-M aqueous sulfuric acid to remove any contaminants.

Synthesis of Ag(I)-thiolate Polymers. The starting thiol was dissolved in 25 mL of the acetonitrile (0.1 M). In another beaker, a 0.1-M solution of $AgNO_3$ was prepared in 25 mL of acetonitrile. The thiol solution was then added to the silver nitrate solution with stirring, and immediately a precipitate formed, or in the case of the *tert*-nonyl polymer, an oil. The solution was stirred for 24 h to allow the reaction to proceed to completion. In the case of the solid polymers $[AgS(CH_2)_{11}CH_3]_n$, $[AgSCH_2CHOHCH_2OH]_n$, and $[AgSCH_2CH_2COOH]_n$, the slurry was filtered to collect a crude product, which was then washed with acetonitrile and dried under vacuum. In the case of the oily *tert*-nonyl polymer, the solvent was decanted, and the oil was stirred in methanol for 24 h. The methanol was then decanted and remaining solvent was removed under vacuum. The soluble products, $[AgSCH_2CHOHCH_2OH]_n$, $[AgSCH_2CH_2COOH]_n$, and $[AgSC(CH_3)_2(CH_2)_5CH_3]_n$,were analyzed by NMR. The isolated yield of $[AgSCH_2CHOHCH_2OH]_n$ was 85%. ^{1}H NMR (in D_2O): $[AgSC\mathit{H}_2CHOHCH_2OH]_n$, 3.53 – 3.72 (br, 2H); $[AgSCH_2C\mathit{H}OHCH_2OH]_n$, 3.53 (br, obscured); $[AgSCH_2CHO\mathit{H}CH_2O\mathit{H}]_n$, 3.50 (br, obscured); $[AgSCH_2CHOHC\mathit{H}_2OH]_n$, 2.85 – 3.20 (br, 2H,). The isolated yield of $[AgSCH_2CH_2COOH]_n$ was 89%. ^{1}H NMR (in D_2O): $[AgSC\mathit{H}_2CH_2COOH]_n$, 2.72 – 3.22 (br, 2H); $[AgSCH_2C\mathit{H}_2COOH]_n$, 2.25 – 2.45 (br, 2H). The isolated yield of $[AgSC(CH_3)_2(CH_2)_5CH_3]_n$ was 85% for the mixture of isomers. ^{1}H NMR (in $CDCl_3$): $[AgSC(C\mathit{H}_3)_2\ C\mathit{H}_2\ (CH_2)_4CH_3]_n$, 1.38 – 1.52 (m, obscured by

isomers); $[AgSC(CH_3)_2\ CH_2\ (CH_2)_4CH_3]_n$, 0.92 – 1.38 (m, obscured by isomers); $[AgSC(CH_3)_2\ CH_2\ (CH_2)_4CH_3]_n$, 0.80 – 0.92 (m, obscured by isomers).

Contact-Angle Measurements. Advancing contact angles of water and of hexadecane were measured with a Rame-Hart NRL model 100 goniometer. A minimum of six measurements were made on three independent drops at various locations on each sample. To perform contact-angle titration measurements, solutions were prepared by combining phosphoric acid (14.7 M, pH -0.47) with 2.0-M aqueous NaOH to give solutions of pH 1.00, 1.99, 3.00, 4.00, 5.01, 6.00, 8.00, and 11.99. The solutions between pH 1.99 and 11.99 were buffered.

X-ray Photoelectron Spectroscopy (XPS). Spectra of gold films exposed to $[AgSCH_2CHOHCH_2OH]_n$, and $[AgSCH_2CH_2COOH]_n$ polymer solutions were collected using a Scienta ESCA-300 spectrometer with monochromatized Al Kα X-rays generated using a rotating anode. Photoemission was measured with a 300-mm-diameter hemispherical analyzer. Samples were grounded by placing screws in contact with both the electrode surface and the sample holder. The pressure in the sample chamber was $\sim 2\times10^{-9}$ Torr, and samples were analyzed at a 20° take-off angle between the sample surface and the path to the analyzer. Spectra of gold films exposed to $[AgSC(CH_3)_2(CH_2)_5CH_3]_n$ solutions were collected using a Thermo Scientific K-Alpha spectrometer with monochromatized Al Kα X-rays. Photoemission was measured with a 180° micro-focused hemispherical analyzer. The sample was grounded by placing screws in contact with the electrode contacts and the sample holder. The pressure in the sample chamber was $\sim 2\times10^{-8}$ Torr, and samples were analyzed at a 45° take-off angle between the sample surface and the path to the analyzer. Spectra produced by this

instrument had a lower signal-to-noise ratio than those produced by the Scienta ESCA-300. Spectra were collected within 1 h of removal from solution and analyzed using CASAXPS® software (version 2.3.15dev77). Survey spectra were taken at a 300-eV pass energy and with a step energy of 1 eV. The pass energy for high-resolution spectra in the Au, Ag, C, O, and S regions was 150 eV, and the step energy was 0.05 eV. The carbon 1s and oxygen 1s photoemission was fit with peaks whose full-widths at half-maximum (fwhm) were allowed to vary. The silver 3d photoemission was fit with peaks due to the $3d_{5/2}$ and $3d_{3/2}$ spin-orbit components, with the fwhm allowed to vary but constrained to be equal to one another, and areas in a 3:2 ratio, respectively. The gold 4f photoemission was fit with peaks due to the $4f_{7/2}$ and $4f_{5/2}$ spin-orbit components, with the fwhm allowed to vary but constrained to be equal to one another, and areas in a 4:3 ratio, respectively. The sulfur 2p photoemission was fit with peaks due to the $2p_{3/2}$ and $2p_{1/2}$ spin-orbit components, with the fwhm allowed to vary but constrained to be equal to one another, and areas in a 2:1 ratio, respectively.

Low Energy Ion Scattering (LEIS). Spectra of the gold sample bearing adsorbed $[AgSCH_2CHOHCH_2OH]_n$ were generated using an ION-TOF Qtac 100 instrument. An iridium filament was used to produce a beam of He^+ ions with 3000 eV of kinetic energy. The ion beam struck the surface of the sample at normal incidence, and scattered ions were collected at an angle of 55°. The energies of the scattered ions were measured using an azimuthal detector operating with a pass energy of 3000 eV. Samples were analyzed under an ion current of 1.22×10^{-2} μA, with the beam rastered over a square region 2000 μm across, to give a total ion dose of 1.88×10^{14} cm^{-2} for a single scan.

Transmission Electron Microscopy (TEM). Nanoparticle samples were analyzed by TEM using a JEOL JEM-2000FX microscope equipped with a tungsten filament and a background pressure of ~ $2.5x10^{-5}$ Pa. Samples were prepared by drop-casting solutions onto copper grids. Images were obtained at 180 kV and at various magnifications

Adsorption Studies of Ag(I)-thiolate Polymers. Polymers were dissolved in solution (1- or 5-mM, see text) prior to adsorption. Gold films were immersed in these solutions for 24 h. The samples were then removed from soliution, rinsed (see text) and dried under a stream of N_2. Samples were then analyzed by contact angle and XPS.

Thermolysis of Ag(I)-thiolate Polymers. Polymers were dissolved in solution and heated in a round bottom flask fitted with a condenser. The color of the solution was observed throughout heating. When a significant change in color had occurred, the samples were cooled in a room-temperature water bath and analyzed by UV/vis spectrophotometry.

Photolysis of Ag(I)-thiolate Polymers. Polymers were photolyzed in solution, or neat in a Rayonet Model 100 photorector. The reaction chamber has a diameter of 10 in, is 15-in deep, and contains twelve T-5 ultraviolet lamps that each produce ~ 35 W between 300 – 415 nm. Polymer solutions were contained in a glass or quartz round bottom flask fitted with a condenser to prevent loss of solvent. Neat polymers were placed in a quartz cuvette during photolysis. At various intervals, the UV lamps would be switched off for a few seconds in order to observe samples, and when a significant change in color occurred, the samples would be removed and analyzed by UV/vis spectrophotometry.

Ultraviolet/visible Spectrophotometry (UV/vis). Nanoparticle samples in solution were analyzed using a Shimadzu UV-2101 PC spectrophotometer equipped with a dual light source for a wavelength range of 190 – 900 nm and a resolution of 0.1 nm. Samples were analyzed within 1 h of formation and absorbance spectra were taken from 370 – 800 nm in a quartz cuvette.

6.6 Acknowledgements

We gratefully acknowledge Lehigh University for support of this research in the form of a Faculty Innovation Grant. We also thank Dr. Al Miller and Dr. Rob Pafchek for their assistance with acquisition of the XPS data, and Mr. Robert Keyse for his assistance in obtaining the TEM images.

6.7 References

1. Åkerström, S., Silver Alkylmercaptides. *Acta Chem. Scand.* **1964,** *18* (5), 1308.
2. Åkerström, S., Silver (I)alkanethiolates. *Ark. Kemi* **1965,** *24* (6), 505-518.
3. Dance, I. G.; Fisher, K. J.; Banda, R. M. H.; Scudder, M. L., Layered Structure of Crystalline Compounds AgSR. *Inorg. Chem.* **1991,** *30* (2), 183-187.
4. Baena, M. J.; Espinet, P.; Lequerica, M. C.; Levelut, A. M., Mesogenic Behaviors of Silver Thiolaters with Layered Structure in the Solid-state - Covalent Soaps. *J. Am. Chem. Soc.* **1992,** *114* (11), 4182-4185.
5. Levchenko, A. A.; Yee, C. K.; Parikh, A. N.; Navrotsky, A., Energetics of Self-assembly and Chain Confinement in Silver Alkanethiolates: Enthalpy-entropy Interplay. *Chem. Mater.* **2005,** *17* (22), 5428-5438.
6. Dance, I. G.; Fitzpatrick, L. J.; Rae, A. D.; Scudder, M. L., The Intertwined Double-(-AG-SR-)$_\infty$ -Strand Chain Structure of Crystalline (3-Methylpentane-3-thiolato)silver, in Relation to (AGSR)$_8$ Molecules in Solution. *Inorg. Chem.* **1983,** *22* (25), 3785-3788.
7. Dance, I. G., On the Molecularity of Crystalline Cylcohexanethiolatosilver(I). *Inorg. Chim. Acta* **1977,** *25*, L17-L18.
8. Liu, Y.; Ma, W. S.; Liu, W. W.; Li, C.; Liu, Y. L.; Jiang, X. Y.; Tang, Z. Y., Silver(I)-Glutathione Biocoordination Polymer Hydrogel: Effective Antibacterial Activity and Improved Cytocompatibility. *J. Mater. Chem.* **2011,** *21* (48), 19214-19218.

9. Akhbari, K.; Morsali, A.; Retailleau, P., Silver Nanoparticles from the Thermal Decomposition of a Two-dimensional Nano-coordination Polymer. *Polyhedron* **2010,** *29* (18), 3304-3309.
10. Schaaff, T. G.; Rodinone, A. J., Preparation and Characterization of Silver Sulfide Nanocrystals Generated from Silver(I)-thiolate Polymers. *J. Phys. Chem. B* **2003,** *107* (38), 10416-10422.
11. Bashiri, R.; Akhbari, K.; Morsali, A., Nanopowders of 3D Ag-I Coordination Polymer: A New Precursor for Preparation of Silver Nanoparticles. *Inorg. Chim. Acta* **2009,** *362* (4), 1035-1041.
12. Conte, P.; Carotenuto, G.; Piccolo, A.; Perlo, P.; Nicolais, L., NMR-investigation of the Mechanism of Silver Mercaptide Thermolysis in Amorphous Polystyrene. *J. Mater. Chem.* **2007,** *17* (2), 201-205.
13. Corbierre, M. K.; Lennox, R. B., Preparation of Thiol-capped Gold Nanoparticles by Chemical Reduction of Soluble Au(I)-thiolates. *Chem. Mater.* **2005,** *17* (23), 5691-5696.
14. Jennings, G. K.; Laibinis, P. E., Underpotentially Deposited Metal Layers of Silver Provide Enhanced Stability to Self-assembled Alkanethiol Monolayers on Gold. *Langmuir* **1996,** *12* (26), 6173-6175.
15. Jennings, G. K.; Laibinis, P. E., Self-assembled n-Alkanethiolate Monolayers on Underpotentially Deposited Adlayers of Silver and Copper on Gold. *J. Am. Chem. Soc.* **1997,** *119* (22), 5208-5214.
16. Oyamatsu, D.; Nishizawa, M.; Kuwabata, S.; Yoneyama, H., Underpotential Deposition of Silver onto Gold substrates Covered with Self-assembled Monolayers of Alkanethiols to Induce Intervention of the Silver Between the Monolayer and the Gold Substrate. *Langmuir* **1998,** *14* (12), 3298-3302.
17. Kaushik, V. K., XPS Core Level Spectra and Auger Parameters for Some Silver Compounds. *J. Electron Spectrosc. Relat. Phenom.* **1991,** *56* (3), 273-277.
18. Bain, C. D.; Troughton, E. B.; Tao, Y.-T.; Evall, J.; Whitesides, G. M.; Nuzzo, R. G., Formation of Monolayer Films by the Spontaneous Assembly of Organic Thiols from Solution onto Gold. *J. Am. Chem. Soc.* **1989,** *111* (1), 321-335.
19. Saliba, N.; Parker, D. H.; Koel, B. E., Adsorption of Oxygen on Au(111) by Exposure to Ozone. *Surf. Sci.* **1998,** *410* (2-3), 270-282.
20. Krozer, A.; Rodahl, M., X-ray Photoemission Spectroscopy Study of UV/ozone Oxidation of Au Under Ultrahigh Vacuum Conditions. *J. Vac. Sci. Technol., A* **1997,** *15* (3), 1704-1709.
21. Irissou, E.; Denis, M. C.; Chaker, M.; Guay, D., Gold Oxide Thin Film Grown by Pulsed Laser Deposition in an O_2 Atmosphere. *Thin Solid Films* **2005,** *472* (1-2), 49-57.
22. Laibinis, P. E.; Whitesides, G. M.; Allara, D. L.; Tao, Y. T.; Parikh, A. N.; Nuzzo, R. G., Comparison of the Structures and Wetting Propeteries of Self-Assembled Monolayers on Normal-Alkanethiols on the Coinage Metal-Surfaces, Cu, Ag, Au. *J. Am. Chem. Soc.* **1991,** *113* (19), 7152-7167.
23. Holmes-Farley, S. R.; Reamey, R. H.; McCarthy, T. J.; Deutch, J.; Whitesides, G. M., Acid-base Behavior or Carboxylic-acid Groups Covalently Attached at the Surface of Polyethylene - The Usefulness of Contact-angle in Following the Ionization of Surface Functionality. *Langmuir* **1985,** *1* (6), 725-740.

24. Bain, C. D.; Whitesides, G. M., A Study by Contact-angle of the Acid-base Behavior of Monolayers Containing Omega-mercaptocarboxylic Acids Adsorbed on Gold - An Example of Reactive Spreading. *Langmuir* **1989,** *5* (6), 1370-1378.
25. Lee, T. R.; Carey, R. I.; Biebuyck, H. A.; Whitesides, G. M., The Wetting of Monolayer Films Exposing Ionizable Acids and Bases. *Langmuir* **1994,** *10* (3), 741-749.
26. Cornella, J.; Sanchez, C.; Banawa, D.; Larrosa, I., Silver-catalysed Protodecarboxylation of ortho-Substituted Benzoic Acids. *Chem. Commun.* **2009,** *0* (46), 7176-7178.
27. He, S. T.; Yao, J. N.; Jiang, P.; Shi, D. X.; Zhang, H. X.; Xie, S. S.; Pang, S. J.; Gao, H. J., Formation of Silver Nanoparticles and Self-assembled Two-dimensional Ordered Superlattice. *Langmuir* **2001,** *17* (5), 1571-1575.
28. Nallathamby, P. D.; Lee, K. J.; Desai, T.; Xu, X. H. N., Study of the Multidrug Membrane Transporter of Single Living Pseudomonas Aeruginosa Cells Using Size-Dependent Plasmonic Nanoparticle Optical Probes. *Biochemistry-US* **2010,** *49* (28), 5942-5953.
29. Evanoff, D. D.; Chumanov, G., Synthesis and Optical Properties of Silver Nanoparticles and Arrays. *ChemPhysChem* **2005,** *6* (7), 1221-1231.
30. Zhang, Q. B.; Tan, Y. N.; Xie, J. P.; Lee, J. Y., Colloidal Synthesis of Plasmonic Metallic Nanoparticles. *Plasmonics* **2009,** *4* (1), 9-22.
31. Zhang, L. Z.; Yu, J. C.; Yip, H. Y.; Li, Q.; Kwong, K. W.; Xu, A. W.; Wong, P. K., Ambient Light Reduction Strategy to Synthesize Silver Nanoparticles and Silver-coated TiO_2 with Enhanced Photocatalytic and Bactericidal Activities. *Langmuir* **2003,** *19* (24), 10372-10380.
32. Scaiano, J. C.; Aliaga, C.; Maguire, S.; Wang, D., Magnetic Field Control of Photoinduced Silver Nanoparticle Formation. *J. Phys. Chem. B* **2006,** *110* (26), 12856-12859.
33. Maretti, L.; Billone, P. S.; Liu, Y.; Scaiano, J. C., Facile Photochemical Synthesis and Characterization of Highly Fluorescent Silver Nanoparticles. *J. Am. Chem. Soc.* **2009,** *131* (39), 13972-13980.
34. Sato-Berru, R.; Redon, R.; Vaquez-Olmos, A.; Saniger, J. M., Silver Nanoparticles Synthesized by Direct Photoreduction of Metal Salts. Application in Surface-enhanced Raman Spectroscopy. *J. Raman Spectrosc.* **2009,** *40* (4), 376-380.
35. Hada, H.; Yonezawa, Y.; Yoshida, A.; Kurakake, A., Photoreduction of Silver Ion in Aqueous and Alcoholic Solutions. *J. Phys. Chem.* **1976,** *80* (25), 2728-31.
36. Hada, H.; Yonezawa, Y.; Ishino, M.; Tanemura, H., Photoreduction of Silver Ion on the Surface of Titanium Dioxide Single Crystals. *J. Chem. Soc., Faraday Trans. 1* **1982,** *78* (9), 2677-84.

Chapter 7

Future Work

7.1 Future Work

7.1.1 Future Work with Regioselective SAM Formation from Dialkyl Disulfides

The formation of mixed dialkyl disulfide monolayers using the protection-deprotection technique should be explored. This preparation can be accomplished by including two dialkyl disulfide precursors in solution during potential-assisted SAM formation. Work with mixed monolayers should include disulfides of varying chain length (i.e., shorter alkyl chains mixed with longer alkyl chains) and with a wider range of functional groups. For instance, methyl ester-terminated and amide-terminated disulfides should be easily synthesized in the same manner as the disulfides in Chapters 4 and 5.

The attachment of nanoparticle assemblies to the surface of a SAM-coated gold electrode should also be attempted. For example, TiO_2 nanoparticles should attach to a carboxylic acid-terminated surface.[1,2] Assemblies such as these have been shown to hold promise for photovoltaic applications as well as photocatalysis.[1-3] The attachment of TiO_2 nanoparticles to a gold surface would allow for the creation of a photovoltaic cell by the collection and transfer of photocurrent (Figure 7.1). Another example of this process is the attachment of CdS particles to a thiol-terminated SAM, wherein a photovoltaic cell was created.[4,5]

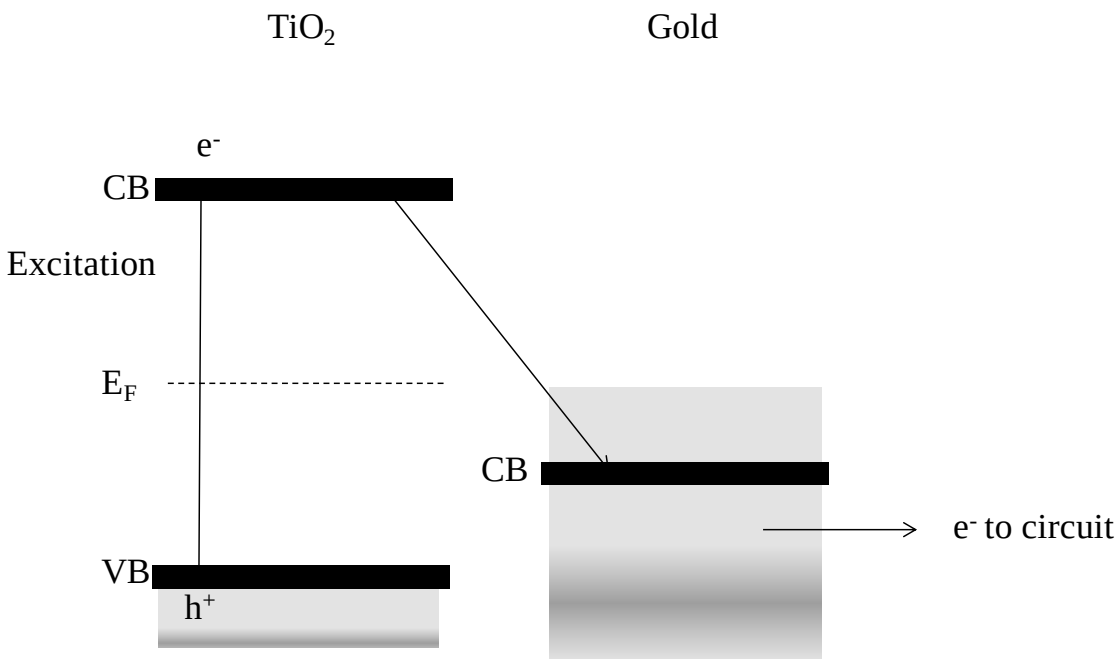

Figure 7.1. Schematic representation of the collection of photocurrent in a TiO_2 – Gold system.

7.1.2 Future Work with Silver (I)-thiolate Polymers

There remains much work to be done concerning the use of silver (I)-thiolate polymers as precursors for monolayer films and nanoparticles. The formation of films from solutions of $[AgSCH_2CH_2COOH]_n$ on gold should be repeated in order to rectify the contrasting results of the contact-angle and XPS studies with regards to the presence of the carboxylic-acid groups. As this system was the closest to that of a SAM on UPD-Ag/Au it deserves further study to determine if the polymer is decomposing during adsorption. With the understanding of the solution-phase species of this polymer gained from 2D-NMR studies, it should also be possible to suggest a mechanism for the association of this polymer with gold.

For future studies of these polymers as nanoparticle precursors, one should further develop the photolytic methodology. Specifically, a greater use of electron microscopy in addition to UV/Vis spectrophotometry can give a more direct indication of the conditions that allow for more uniform size distributions. The centrifugation of suspensions of Ag nanoparticles should be pursed as well. An improvement in particle size distribution was noticed after 2h of centrifugation, so longer centrifugation times should be explored as they may produce a more narrow size distribution of particles. Once well-defined synthetic parameters have been established, applications of these nanoparticles could include the synthesis of various core@shell structures. The creation of Ag or Au@TiO_2 structures would be especially interesting for the study of CO oxidation. This may be able to be achieved through the hydrolysis of titanium(IV) bis(ammonium lactato)dihydroxide (TiL_n), in the presence of Ag or Au nanoparticles. The hydrolysis of TiL_n results in the formation of TiO_2 which may nucleate and form on

the surface of the nanoparticles.[6,7] Controlling the conditions of hydrolysis may allow for control over the amount of TiO_2 formed, and thus the size of the Ag or Au@TiO_2 structures.

7.2 References

1. Nevins, J. S.; Coughlin, K. M.; Watson, D. F., Attachment of CdSe Nanoparticles to TiO_2 via Aqueous Linker-Assisted Assembly: Influence of Molecular Linkers on Electronic Properties and Interfacial Electron Transfer. *ACS Appl. Mater. Interfaces* **2011,** *3* (11), 4242-4253.
2. Dibbell, R. S.; Watson, D. F., Distance-Dependent Electron Transfer in Tethered Assemblies of CdS Quantum Dots and TiO2 Nanoparticles. *The Journal of Physical Chemistry C* **2009,** *113* (8), 3139-3149.
3. Hu, X.; Bürgi, T., Photoinduced Electron Transfer and Photodegradation of Malonic Acid at Au/TiO_2 Investigated by in situ ATR-IR Spectroscopy. *Appl. Catal. A* **2012,** *449* (0), 139-144.
4. Ogawa, S.; Fan, F. R. F.; Bard, A. J., Scanning-tunneling-microscopy, Tunneling Spectroscopy, and Photoelectrochemistry of a Film of Q-CdS Particles Incorporated in a Self-assembled Monolayer on a Gold Surface. *J. Phys. Chem.* **1995,** *99* (28), 11182-11189.
5. Nakanishi, T.; Ohtani, B.; Uosaki, K., Effect of Immobilized Electron Relay on the Interfacial Photoinduced Electron Transfer at a Layered Inorganic-organic Composite Film on Gold. *J. Electroanal. Chem.* **1998,** *455* (1-2), 229-234.
6. Moriguchi, I.; Maeda, H.; Teraoka, Y.; Kagawa, S., Preparation of TiO2 Ultrathin Film by Newly Developed Two-Dimensional Sol-Gel Process. *J. Am. Chem. Soc.* **1995,** *117* (3), 1139-1140.
7. Rouse, J. H.; Ferguson, G. S., Stepwise Formation of Ultrathin Films of a Titanium (Hydr)oxide by Polyelectrolyte-assisted Adsorption. *Advanced Materials* **2002,** *14* (2), 151-154.

Vita

Kevin M. Cook was born in Buffalo, NY on June 24th, 1986. He was raised in South Buffalo and graduated from Hutchinson Central Technical High School in 2004. He obtained his Bachelors of Science in chemistry from SUNY, the University at Buffalo in 2008. In 2008, he moved to Bethlehem, PA to attend Lehigh University and pursue his Ph.D. in chemistry.

Publications

Cook, K. M.; Ferguson, G.S.; "Gold Oxide as a Protecting Group for Regioselective Surface Chemistry," *Chemical Communications* **2011**, *47(46)*, 12550-12552

Cook, K. M.; Ferguson, G.S.; "Determination of the Wavelength-Dependent Refractive Index of a Gold-Oxide Thin Film," *Journal of Physical Chemistry C* **2011**, *115(46)*, 22976-22980

Cook, K. M.; Ferguson, G.S.; "Relative Lability of Gold-Oxide Thin Films in Contact with Air, Solvents, or Electrolyte Solutions," *Journal of Vacuum Science & Technology A* **2013**, *31*, 021508

Cook, K. M.; Nissley, D. A.; Ferguson, G.S.; "Spatially Selective Formation of Hydrocarbon, Flurocarbon, and Hydroxyl-terminated Monolayers on a Microelectrode Array," *Langmuir* **2013**, *29 (23)*, 6779–6783